Politecnico di Torino

Corso di Laurea Magistrale in Ingegneria Civile
A.a. 2020/2021
Sessione di Laurea Luglio 2021

Damage Detection and Monitoring in Buried Steel Pipelines

Relatori:
Prof. Rosario Ceravolo
PhD. Gaetano Miraglia
PhD. Marco Civera
PhD. Erica Lenticchia

Candidato:
Davide Di Nardo Di Maio

Table of Contents

LIST OF FIGURES

LIST OF REFERENCES

[1] Farrar & Worden, John Wiley & Sons Ltd (2013). Structural health monitoring; a machine learning perspective.

[2] Valivonis & Skuturna, Journal of Civil Engineering and Management (2007) . Cracking and strength of reinforced concrete structures in flexure strengthened with carbon fibre laminates

[3] Worden, Farrar, Mandon & Park, The Royal Society (2007). The fundamental axioms of structural health monitoring.

[4] Farrar, Worden and Park, Keith (2010). Complexity: a New Axiom for structural Health Monitoring?

[5] Catbas & Aktan, American Society of Civil Engineers (2002). Condition and Damage Assessment.

[6] Hua Peng Chen and Yi-Qing Ni, John Wiley & Sons Ltd (2018). Structural Health Monitoring of Large Civil Engineering Structures.

[7] Cawley & Adams, The Journal of Strain Analysis for Engineering Design (1979). The location of defects in structures from measurements of natural frequencies.

[8] Wolff & Richardson, Structural Measurement Systems Inc. (1989). Fault detection in structures from changes in their modal parameters.

[9] Lieven & Ewins, (1988). Spatial Correlation of Mode shapes, the Coordinate Modal Assurance Criterion COMAC.

[10] Rytter, A. (1993). Vibrational Based Inspection of Civil Engineering Structures. Dept. of Building Technology and Structural Engineering, Aalborg University.

[11] Rudolf Clausius, (1864). Treatise on the mechanical theory of heat.

[12] Shannon, Bell System Technical Journal (1948). A Mathematical Theory of Communication.

[13] Farrar, Leyasi, Mellos, Sheinker, Per, Lieven, The Society for Explerimental Mechanics (2020). Comparison of Complexity Measures for SHM.

[14] Farrar, West, Locke Andrews, Scheinker, The Society of Experimental Mechanics (2019). Applying Concepts of Complexity to SHM.

[15] Ceravolo, Lenticchia & Miraglia, Elsevier Ltd (2019). Spectral entropy of acceleration data for damage detection in masonry buildings affected by seismic sequences.

[16] Bandt & Pompe, Phys Rev Lett. (2002). Permutation entropy: a natural complexity measure for time series.

[17] Higgins, Stroebele & Zahidi, Pure Technologies (2021). Numbers don't lie: PCCP performance and deterioration based on a decade of condition assessment data.

[18] Rizzo, Adv. Civ. Eng. (2010). Water and wastewater pipe nondestructive evaluation and health monitoring: A review.

[19] Maruschak, Poberezny & Prentkovskis, J Fail. Anal. and Preven. (2018). Physical and Mechanical Aspects of Corrosion Damage of Distribution Gas Pipelines After Long-Term Operation.

[20] Pavan, Vikrant, Vimalan & Singh, Elsevier (2013). Case Studie in Engineering Failure Analysis.

[21] Kishawy & Gabbar, Int. J. Press. Vessel. Pip. (2010). Review of pipeline integrity management practices.

[22] Quarini & Shire, Proc. Inst. Mech. Eng. Part E J. Process Mech. Eng. (2007). A Review of Fluid-Driven Pipeline Pigs and their Applications.

[23] Sider, The Wall Street Journal (2014). High-Tech Monitors Often Miss Oil Pipeline Leaks.

[24] The University of Manchester, faculty of science and engineering PhD Thesys (2016). Simulation, Measurement and Detection of leakage and Blokage in Fluid Pipeline Systems.

[25] Bao, Hao & Li, Struct. Control Heal. Monit. (2013). Vibration-based structural health monitoring of offshore pipelines: numerical and experimental study.

[26] Liu & Kleiner, IEEE Sens. J. (2012). State-of-the-art review of technologies for pipe structural health monitoring.

[27] Glisic & Yao, Struct. Heal. Monit. An Int. J. (2012). Fiber optic method for health assessment of pipelines subjected to earthquake-induced ground movement.

[28] Golub & Underwood, Mathematical Software (1977). The Block Lanczos Method for Computing Eigenvalues.

[29] Gazetas, Journal of Geotechnical Engineering (1991). Formulas and Charts for Impedances of Surface and Embedded Foundations.

[30] Muraglia, Castellaro & Rossi, Bologna University. Effetti di sito e Vs30: una risposta alla normativa antisismica.

[31] Gutenberg, Journal of Geophysical Research (1958). Two types of microseisms.

[32] Asten & Henstridge, Geophysics. (1984). ARRAY ESTIMATORS AND THE USE OF MICROSEISMS FOR RECONNAISSANCE OF SEDIMENTARY BASINS.

[33] Ceravolo, Civera, Lenticchia, Miraglia & Surace, Elsevier Ltd (2020). Damage Detection and Localisation in Buried Pipelinies using Entropy in Information Theory.

[34] Posey, Johnson & Vohra, Electron Lett (2000). Strain sensing based on coherent Rayleigh scattering in an optical fibre.

[35] Kikuchi, Naito & Okoshi, IEEE J Quantum Elect (1988). Measurement of Raman scattering in single-mode optical fiber by optical time-domain reflectometry.

[36] Kurashima, Horiguchi & Tateda, Opt Lett (1990). Distributed temperature sensing using stimulated Brillouin scattering in optical silica fibers.

[37] Deng, Zhiyang et al. (2020). A Wall-thinning Measuring Method Based on Magnetic Permeability Perturbation.

[38] Abraham Mengesha Woldemariam, Walter O. Oyawa & Timothy Nyomboi, Cogent Engineering (2020). Experimental studies on the behavior of concrete-filled uPVC tubular columns under axial compression loads,

LIST OF TABLES

INTRODUCTION

Pipeline structures are the most convenient and fastest means of transport and supply of fuels and fluids in general.
Therefore, their correct and continuous functioning is of vital economic and social importance.

Nowadays, the most widely used Pipeline Integrity Management techniques involve fairly invasive monitoring methods as resorting to Pipeline Inspection Gauge devices.
The need to temporarily stop the lines and non-targeted inspections define the poor efficiency of the current monitoring techniques of Steel Pipelines which require the research of new investigation methods.
Looking at these premises, a Structural Health Monitoring approach for Damage Identification would seem the most suitable to fulfil the task of studying the health status of Pipelines, such as the Vibration Based Investigation which is one of the common methods used in the field of civil engineering monitoring.
The problem of these type of monitoring approaches is that they have been studied and widely used on structures such as bridges or towers, but they have not found a well-defined application in the field of Pipeline Monitoring.

In recent years, the concepts of information theory and more specifically spectral entropy measures have been increasingly investigated and applied in SHM.
Among the numerous existing forms of entropy, the intention of this work, which is the natural consequence of the studies carried out by Ceravolo et al. and transposed in publications [15] and [33], is to investigate a method founded on the use of Wiener Entropy as the damage-sensitive feature for the Buried Steel Pipelines Damage Identification.

The thesis is organized in order to initially introduce the main notions of Structural Health Monitoring and particularly entering into the specifics of the civil engineering applications.
Subsequently, the concept of complexity is studied and defined, linking it to the entropy measures proposed by information theory, focusing particularly on Wiener Entropy.
Once the theoretical approach and concepts related to the measure that will be used have been introduced, we move on to the description of the structures to be investigated.
In this part, materials, methods of construction and working are defined, as well as the definition of the damage modes useful for understanding the scenarios to be taken into consideration.

Then, the Finite Element Analysis by mean of the *Ansys Mechanical Apdl* software is introduced: not having available monitoring data on real structures, an analytical study was carried out on intact and damaged states of the structure.

In particular, it has been developed a Finite Element Model represented the structure on which the study is conducted (a Continuous Buried Steel Pipeline monitored through the support of distributed fiber optic sensors) and on which a Transient Analysis has been carried out.

The strain values obtained from the numerical monitoring simulation are then used as Input data within a *Matlab* algorithm to extrapolate and process the Wiener Entropy measure.

1. DAMAGE IDENTIFICATION

The discussion below is by no means an exhaustive survey of the subject and constitutes just an overview of the discipline on which this thesis is based. For a deepened treatment of this topic the reader is referred to the book of *Farrar and Worden* [1].

1.1 Damage

By defining damage as a variation of the system that negatively affects its characteristics, it is easy to understand how the concept of damage is only meaningful if a comparison is made between the damaged (final) and undamaged (initial) condition of the system.
The changes introduced within the system can affect geometric properties, material characteristics or constraint / boundary conditions. As already mentioned above, the damage can cause a change in the initial state of the system**,** for example:

- Geometry change and consequent alteration of stiffness due to the formation of cracks *(e.g. Figure 1.1)* which at the same time do not influence the constraint conditions.

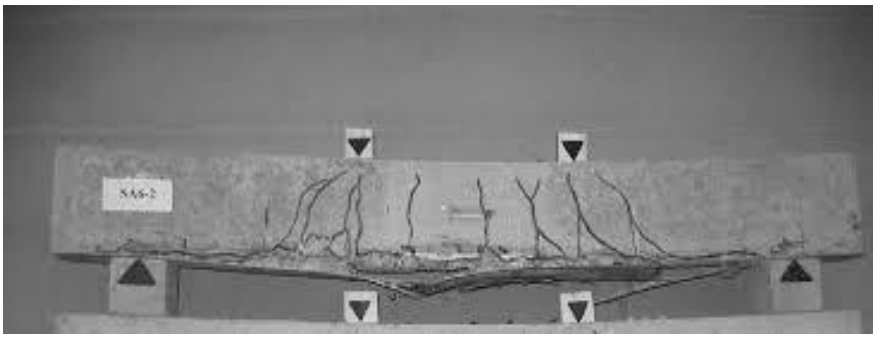

Figure 1.1 Cracked beam in experimental test *(Source: Journal of Civil Engineering and management)* [2]

- Variation of constraint conditions caused by, for instance, the erosion of the soil surrounding the bridge piers due to the increasing water flow *(e.g. Figure 1.2)*.

Figure 1.2 Pier bridge scour *(Source: Alchetron.com)*

- Collapse of a bolted connection that determines the variation (or rather the loss) of the connection between two or more elements.

Etc.

Regarding the construction material, considering that ideal conditions are not realizable in real life and the damage can be considered as an imperfection, although with different degrees, all real materials can be considered damaged.
The problem is not the presence of these defects, but their position and degree of severity which can influence the behaviour of the structure in service condition due to their evolution and consequent loss of efficiency up to the collapse in extreme cases.
A further problem is linked to the possible evolution over time, as the damage can increase as in the case of corrosive processes or fatigue phenomena.

1.2 SHM discipline for the identification of the damage

Structural monitoring is the fundamental tool to guarantee the health of structures and allowing optimal management from both a practical and an economical point of view.
One of the main objectives of structural monitoring is the so-called *"identification of the damage" (Rytter, 1993)* [10], structured on several levels which, with the progress of the analysis, are characterized as follows:

- **Level 1: Damage detection**.
  This level is limited to the understanding of the presence of any type of damage, without investigating its characterization.

- **Level 2: Localization of the damage.**
  The presence of the damage is investigated to the point of identifying its position. This level represents a necessary condition to understand where to go to carry out a possible maintenance operation, but it is not sufficient to understand if the intervention is actually necessary to realize.

- **Level 3: Quantification of the damage**.
  This step allows to understand if the structure is compromised in such a way as to require maintenance by the characterization of the damage severity (for example the percentage of mass or stiffness lost by the material).

- **Level 4: Damage prognosis.**
  The study is extended to the evolution of the damage during the time, in order to understand if and how the damage will compromise the health of the structure.

Damage identification is closely linked to several disciplines including the Structural Health Monitoring (SHM) which consider a series of global methods used in the civil, aeronautic and mechanic field in order to monitoring the health status of large structures by studying their dynamic behaviour.
The strategy provides the observation and periodic measurement of the dynamic response of the structure over the time, the identification of the damage-sensitive features and finally the statistical analysis of the features to determine the damage status of the system.
The measurements are continuously updated so that the results highlight any changes in the system indicating a damage process.

For example, one of the most used monitoring approaches in civil field are defined Vibration-Based Investigation (VBI) as the Vibration-Based Damage Detection Methods (VBDDM) which consist in to investigate the modification of modal forms and the variation of eigenvalues.
In fact, a reduction of stiffness (and consequent increase in damping) due to damage, involves an obvious reduction of the natural frequencies.
Then, the collection of recorded data allow to trace the characteristics of the damage through the dynamic characterization.

1.2.1 Procedure of SHM

The SHM can be summarized in a series of steps, presented in [1], that define a general procedure to be followed for the success of the monitoring project:

- **Operational evaluation**: it constitutes the phase preceding the actual monitoring operation and serves to lay the foundations of the entire process.
  In particular, the following are defined:
  - The justifications, in terms of safety and cost-effectiveness, in order to proceed with the monitoring;
  - The most likely damage scenarios for the type of structure;
  - The structural and environmental conditions of the system to be analyzed;
  - The limitations on data acquisition due to the operating conditions.

- **Data acquisition**: series of decisions concerning the choice, positioning and number of sensors to be used; on data storage system; on the type of excitement to which the system is subjected and on monitoring intervals according to the type of damage to be characterized.

- **Data normalization**: because the systems to monitoring are often subject to a strong variability of the operating conditions, especially in the civil field (for example the variation of the stiffness properties of the bridges due to thermal excursions), the normalization it become necessary because it allows to distinguish changes due to the variability of operating conditions to those due to damage.
  Often, the choice of the normalization to be adopted, together with the choice of the damage-sensitive features, is the most delicate issue to face in order to create a solid SHM system.

- **Data cleansing**: operation aimed to identify and eliminating all those data that can be considered fallacious due to, for example, an incorrect positioning of the sensors.

- **Data compression**: a large amount of data is extrapolated from the measurements taken. If we also consider the fact that monitoring is prolonged for long periods of time, the number of data available grows dramatically and therefore a data compression operation is required to allow an easy management of the same.

- **Data fusion**: operation aimed to fuse together data (in vector or matrix form) coming from differently distributed sensors or to combine data of different nature for an easier identification of the damage.

- **Feature extraction**: it consists in the most delicate phase of the whole operation and is still a subject of discussion in the research field. The so-called "damage-sensitive features" correspond to those quantities extrapolated through the processing of the data obtained from the monitoring and which help to characterize the damage.
  The processing corresponds in a series of mathematical operations or transformation aimed to obtain the parameters representative the health condition of the structure.
  Taking the example of VBDDM, features extraction leads to the identification of modal shapes as the damage-features parameter.

- **Statistical modelling for feature discrimination**: this is the last phase of the SHM process and is the one in which the result of the monitoring is defined.
  In this moment the statistical models to be applied in the algorithms which operate on the previously extracted features are defined.
  This process is used to find a correlation between what are the damage-features parameters and the damage status of the structure. These statistical models are defined through machine learning techniques which can be of two types:
  - *supervised learning algorithms* that arise from tests carried out from available data on both the damaged and undamaged structure
  - *unsupervised learning algorithms*, typical of the SHM, in which data are available only from the undamaged structure.

  Statistical models are used to minimize the possibility of damage evaluation errors and are also used to distinguish two types of SHM: *protective monitoring* to evaluate the current state of safety of the structure and *predictive monitoring* that looks at what is the evolutionary state of the damage, identifying a trend within the collected data and thus elaborating a predictive model.

1.2.2 Approaches for the dynamic identification

As mentioned previously, the dynamic identification aims to identify the dynamic characteristics of the structure such as natural frequencies and modal shapes in VBDDM.
This type of operation can be tackled by following an analytical or experimental approach.
In the first, we start from the knowledge of the characteristics of the structure (geometry, materials, boundary conditions, mass distribution, stiffness and damping). Then, It is possible to determine the modal parameters from the eigenvalues resolution of the stiffness, mass and damping matrices.

Moving on the experimental approach, the starting point is the dynamic excitation on the structure and the observed structural response.
Starting from these data, the frequency response functions are extrapolated and the dynamic parameters of the structure are estimated.

1.2.3 Axioms of SHM

Given the economic and safety advantages that can be obtained thanks to damage identification techniques, since the beginning of the twenty-first century the research and publications on this topic have strongly grown and the progress of technology has led to an ever deeper knowledge of the same.
This knowledge is reflected in the production of the so-called axioms or fundamental principles generally recognized and on which SHM is based *(Worden et al., 2007)* [3] :

Axiom I. All materials have inherent flaws or defects.

Axiom II. Damage assessment requires a comparison between two system states.

Axiom III. Identifying the existence and location of damage can be done in an unsupervised learning mode, but identifying the type of damage present and the damage severity can generally only be done in a supervised learning mode.

Axiom IVa. Sensors cannot measure damage. Feature extraction through signal processing and statistical classification are necessary to convert sensor data into damage information.

Axiom IVb. Without intelligent feature extraction, the more sensitive a measurement is to damage, the more sensitive it is to changing operational and environmental conditions.

Axiom V. The length and time scales associated with damage initiation and evolution dictate the required properties of the SHM sensing system.

Axiom VI**.** There is a trade-off between the sensitivity to damage of an algorithm and its noise rejection capability.

Axiom VII. The size of damage that can be detected from changes in system dynamics is inversely proportional to the frequency range of excitation.

Axiom VIII. Damage increases the complexity of a structure *(added in 2010 by Farrar, Worden and Park)* [4]. This crucial aspect is the foundation of this thesis and will be discussed in the chapter 2.

1.2.4 Feature extraction

As already mentioned in the previous paragraphs, a damage-sensitive feature is a quantity derived by transformation or mathematical operations from the data obtained in the monitoring phase performed by sensors placed on the structure.
The extrapolation of this quantity is aimed to identify an useful quantity to grasp the differences between the undamaged (or initial) and damaged (or final) state by means of machine learning algorithms.

The choice of the damage-sensitive feature is made according to the type of damage to be analyzed, the type of structure and the level of knowledge to be obtained of the state of damage.
For this reason it is possible to affirm that there is no universally usable feature for any damage scenario and its choice varies case by case.
The basic principle to follow for the most correct choice is that for which the feature adopted must be such that the identification of damage scenarios, or in any case of variation between initial and final state, from machine learning must be as simple as possible (the ideal condition would be to grasp just visually a variation of the system indicative of the damage).

On the other hand, the feature should be such as to be sensitive only to the presence of damage and not to any environmental and operational alterations, which unfortunately practically never happens in reality and that is why the data must always be subject to normalization.
Moreover, in the case that multiple damage scenarios are possible, it is inevitable to adopt more features in such a way to capture the presence of all types of damage.

An useful method to identify a suitable feature can be to apply defects congruent to those expected on the structure and studying the parameters sensitive to the expected damage.
For this purpose, the use of analytical tools such as Finite Element Models can be a valid choice.
In particular, numerical experiments are carried out where the model is created faithfully following what is the real structure and subsequently the most probable damage scenarios for the specific situation are applied analytically.
In this way it is possible to experiment which are the best features which allow to describe the various damage cases.

1.3 SHM in Civil Engineering

The SHM system is used in the civil field in order to monitoring large structures such as bridges, towers, dams, tunnels and pipelines.
The deterioration of these structures, despite the optimization of the design methodologies, is inevitable and is due to the environmental and operational conditions to which the facilities are subjected. This deterioration can be caused by cyclic loads from traffic, environmental factors (corrosion of steel and carbonation of concrete), aging of the materials used or by extraordinary events such as impacts, explosions, earthquakes or floods.
Structural health will inevitably be affected by these factors (in addition to normal condition loads) characterized by uncertainty and variability.
For these reasons it is not possible to establish a priori the real useful life of the structure from the design stage and monitoring becomes the best technique to overcome economic and structural problems.

1.3.1 Vibration-Based Damage identification methods

The Vibration-Based method is one of the most commonly methods used for damage identification in the civil field, as already introduced in *chapter 1.2.*
The key principle on which the method is based is the identification of the modal parameters or the frequency response function as damage-sensitive features.
In fact, once the damage has occurred, the variation of the structural parameters such as stiffness, flexibility and deformation energy also implies the variation of the modal parameters (natural frequency and modal shapes). Both variations are used as indicators of damage.
The modal parameters are obtained from the vibrational measurements of the structure linked to the modal analysis.

Another parameter often used as damage feature in the context of Vibration Based Identification VBI is the strain energy which, as already happens in the simplest case of beam, undergoes a change once the damage has occurred.
Depending on the damage indicators chosen, two types of damage identification methods can be distinguished: one based on the study of modal parameters and its derivatives (modal forms, FRF and natural frequencies) and the other, instead, which presupposes the use of structural parameters (stiffness matrix or strain energy).

1.3.2 Structural modelling

As already introduced in *chapter 1.2.4*, one of the methodologies for identifying the most correct damage-sensitive feature consists in the creation of a model that is as consistent as possible with the real structure and analytically applying the damage case expected for the specific case.

The complexity of the model depends on the type of structure to be analyzed and the type of damage expected. In fact, in the case of a cracked beam, the damage can be modelled as a reduction of stiffness at the expected position of the crack.
A state of damage corresponding to a cracked beam from fracture mechanics, on the other hand, presupposes a much more detailed model.
Furthermore, the model to be created depends above all on the operational characteristics of the monitoring procedure, such as the quality and type of data measured. In fact, in the case of vibration modal measurements of the lower frequency modes, only coarse models can be used.

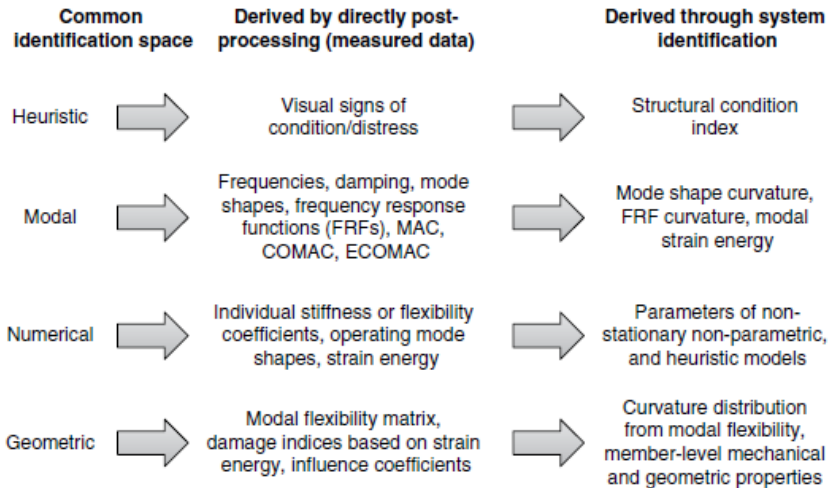

Figure 1.3 Possible global structural damage indices for civil engineering structures *(Source: American society of Civil Engineers)* [5]

Considering the highly redundant structures, the classification of the structural elements and the evaluation of the different modes according to the sensitivity to damage are useful tools to simplify the problem and avoid the redundancy of physical parameters.
This information is obtained through modal analysis which assumes a fairly accurate modelling. The procedural process has the ultimate goal of simplifying the identification of the damage, whose complexity is proportional to the model one.

The requirements that structural modelling for damage identification must respect *(Hua Peng Chen and Yi-Qing Ni, 2018)* [6] are:

- The computed modal parameters predicted by the structural model are well correlated with the measured data from the intact structure;
- Modal parameter uncertainty due to modelling errors is less than modal parameter changes caused by actual damage;
- the size of the finite element model is appropriate so that the number of the model DOFs is not significantly larger than that of measured DOFs in the modal testing;
- the structural model is accurate enough not to mask the damage location in the modelling process.

1.4 Examples of damage-sensitive features in VBI

The purpose of this chapter is to illustrate the theory on which the use of the most common damage-sensitive features of Vibration-Based Investigation is based.

1.4.1 Natural frequencies

Natural frequencies have the advantage that they can be measured easily and are independent of the measurement location.
The basic concept is that for which the variation of stiffness due to damage, both local and distributed, leads to a consequent variation of the natural frequencies of the structure.
In this way the presence of the damage is easily identifiable, but this does not happen to its localization. Then, the level 1 of structural monitoring (damage detection) is reached, differently to the level 2 (damage localization).

The variation of natural frequency of structure is linked to the variation of stiffness by means of the expression proposed by *Cawley and Adams (1979)* [7]:

$$\Delta\omega_i^2 = \hat{\omega}_i^2 - \omega_i^2 = \frac{\boldsymbol{\phi}_i^T \Delta\mathbf{K}\boldsymbol{\phi}_i}{\boldsymbol{\phi}_i^T \mathbf{M}\boldsymbol{\phi}_i} \tag{1.1}$$

In the previous expression, the variation of the squared frequency that corresponds to the difference between those of the damaged and undamaged state is directly proportional to the variation of stiffness matrix that the system undergoes during the damage process.

Everything is referred to the i-th modal shape.

Considering the variation of stiffness equal to a percentage of the initial stiffness of the system and when the damage concerns e-element of the structure,, we can rewrite the expression as follows:

$$\Delta\omega_i^2 = \alpha_e \frac{\boldsymbol{\phi}_i^T \mathbf{K}_e \boldsymbol{\phi}_i}{\boldsymbol{\phi}_i^T \mathbf{M} \boldsymbol{\phi}_i} \tag{1.2}$$

α is a non-dimensional coefficient referred to e-element and which represent the percentage of stiffness lost.

Considering that the modal forms of the undamaged structure are normalized respect to the mass matrix, we can identify the reduction coefficient of the stiffness matrix, reaching the knowledge of the severity of the damage afflicting the element:

$$\alpha_e = \frac{\Delta\omega_i^2}{\boldsymbol{\phi}_i^T \mathbf{K}_e \boldsymbol{\phi}_i} \tag{1.3}$$

The use of natural frequency as a damage-sensitive feature is not able to identify the location of the damage.

At the most, in fact, it is possible to understand which element of the structure is damaged but not the precise position. The problems also arise with symmetrical structures, which make the problem even more complex because the damage would result on two elements.

1.4.2 Direct mode shape comparison

Good results can be obtained from this method in terms of damage detection and localization.

The key concept is the quantification of the correlation between the modes of the initial / undamaged and final / damaged state by the resource of an index.

The most used indices are the modal assurance criterion MAC and the coordinate modal assurance criterion COMAC.

The first is defined as follows *(Wolff and Richardson 1989)* [8] and compares the i-th modal form of the undamaged structure with the j-th modal form of the damaged structure:

$$MAC\left(\boldsymbol{\phi}_i^u, \boldsymbol{\phi}_j^d\right) = \frac{\left|\boldsymbol{\phi}_i^{uT} \boldsymbol{\phi}_j^d\right|^2}{\left|\boldsymbol{\phi}_i^{uT} \boldsymbol{\phi}_i^u\right| \left|\boldsymbol{\phi}_j^{dT} \boldsymbol{\phi}_j^d\right|} \tag{1.4}$$

As already mentioned, this index is a variable quantity between zero and one. In the event that the MAC assumes a very small value, it means that there will be a strong correlation between the two modes and then a possible presence of damage.

The problem is that the localization is based on the simplified assumption that moving towards DOF near the damage, the correlation increases.

This statement is not necessarily valid and for this reason the COMAC index is introduced *(Lieven & Ewins, 1988)* [9]:

$$COMAC(j) = \frac{\sum_{i=1}^{Nm}\left[\phi_i^u(j)\phi_i^d(j)\right]^2}{\sum_{i=1}^{Nm}\left[\phi_i^u(j)\phi_i^u(j)\right]\sum_{i=1}^{Nm}\left[\phi_i^d(j)\phi_i^d(j)\right]} \tag{1.5}$$

The characteristics are similar to those of the MAX but, unlike before, we now try to investigate the correlation between equal modes corresponding to the j-th DOF and different damage status.

If the i-th modal form of the damaged state is uncorrelated from the i-th modal form of the undamaged structure at the j-th DOF, it means that just in the proximity of the considered DOF there would be damage.

Understanding the severity of the damage remains unknown.

1.4.3 Damping

While damping is often referred as a damage-sensitive feature, its validity is questionable.

In fact, despite the fact that even small damage has been shown to significantly affect the modal damping ratios *(Rytter 1993)* [10], these remain strongly influenced by other factors that differ from the state of damage (environmental and aging conditions).

The strong sensitivity to these factors makes the use of this feature poorly valid and its normalization is of complex evaluation.

1.4.4 Frequency response function

Another parameter that can be used in the field of damage detection is the frequency response function and, in particular, the sensitivity of slope and curvature towards the presence of cracks. The methods based on the use of the FRF differ from those that use the modal forms because they assume only the processing of the measured data, without resorting to any modelling or modal extraction and includes all the frequencies present in the measurement range and not only the modal ones.

Once the frequency range has been detected, it is easy to evaluate the variation of FRF curvatures between damaged and undamaged structure and this is the indicator of the presence of damage.

The problems related to the localization of the damage still remain and the evaluation of damage severity becomes difficult to understand, because the correlation between the variation in FRF curvature and the degree of damage is complex to identify. The advantage over the previous method is that we have not to realize an analytical model.

2. ENTROPY AS DAMAGE SENSITIVE FEATURE IN SHM

As introduced in *1.2.3*, in 2010 an axiom of SHM which concerns the increase in complexity within the system due to the state of damage is defined.

The term complexity is not easy to define because it can be explained from several points of view ranging from the simplest methods based on the qualitative vision to those related to the more complex quantitative measures.

2.1 Congruence between damage and complexity

In general, complexity can be understood as the difficulty of a system to be described, organized and reproduced or as the number of internal and external elements and connections that compose it. Looking at what the investigated field is, the complexity can take on various meanings from the geometric point of view, material and information intended as data collection and management.

2.1.1 Qualitative definition

Searching the simplest way to explain the concept of complexity by correlating it to the damage, it is certainly useful to make a visual comparison between two distinct situations.

In fact, if we asked any person to make a comparison and explain the differences between the two structures represented in *figure 2.1*, they would surely reply that the one on the left is in perfect condition while the building on the right is in critical one.

Figure 2.1 Comparison between undamaged and damaged building

The natural understanding of these differences is certainly given by experience, which allows us to reconnect the images with others previously seen and classified. But it is equally true that the

difference between the two situations can be captured by the feeling of order that the structure on the left gives compared to that of disorder given by the image on the right.
Disorder is implicitly linked to the concept of complexity because what is disordered and chaotic is obviously complex. Then, we can affirm that by comparing two images that represent the same subject in two distinct situations of order (integrity) and disorder (deterioration), the intrinsic nature of complexity allows us to immediately distinguish the damaged from the undamaged.
The example shown in *figure 2.2* is useful to expand the concept of complexity.
In fact, if in *figure 2.1* the sense of complexity is given by a geometric perception of the structure and looking at the global complexity of the system, in *figure 2.2* the disorder regard a smaller system, in which the damage concerns the corrosion of the material.
As before, the two situations of order and disorder are clearly distinguishable.

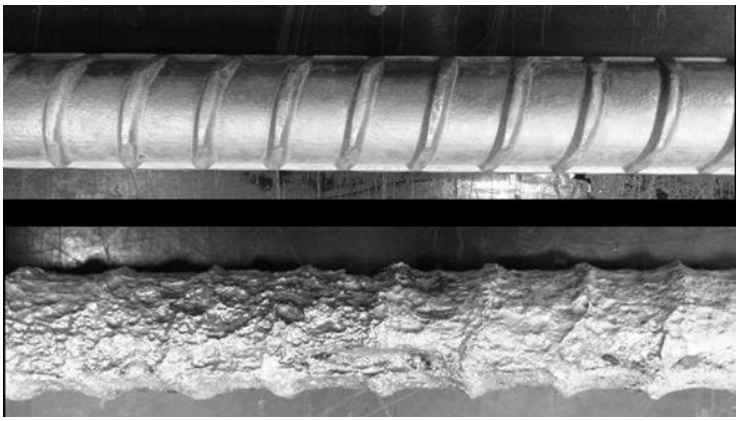

Figure 2.2 Comparison between uncorroded and corroded steel bars.

2.1.2 Quantitative definition

Now we want to look for the definition of congruence between damage and complexity by means measurable and objective parameters. It is chosen to analyze the simulation of the dynamic behaviour of a structure in the undamaged and damaged conditions.

The following example is taken from the publication of *Farrar, Worden and Park* [4] and the characterization of the experiment can be found in [13].
The test structure illustrated in *figure 2.3* is defined by 3 floors and a single span. A shaker is connected to the base to allow the excitation of the structure by means of a harmonic base input.
The damage is simulated between second and third floor by placing a bumper at the base of a column connected to the third floor and disconnected from the second one.

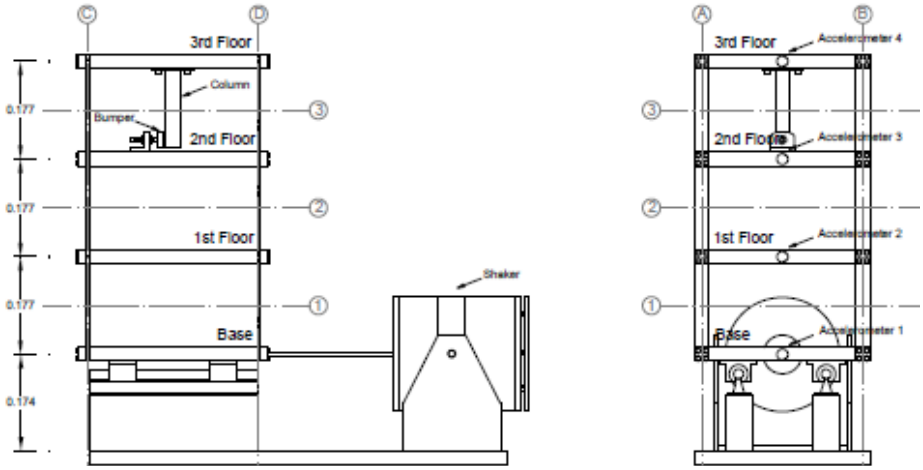

Figure 2.3 Test structure [4]

Figure 2.4 illustrates the acceleration time history responses measured on the top floor without and with the presence of bumpers.

It is easily noticeable how the response in case of bumper presence increases in complexity from the regular one without bumper.

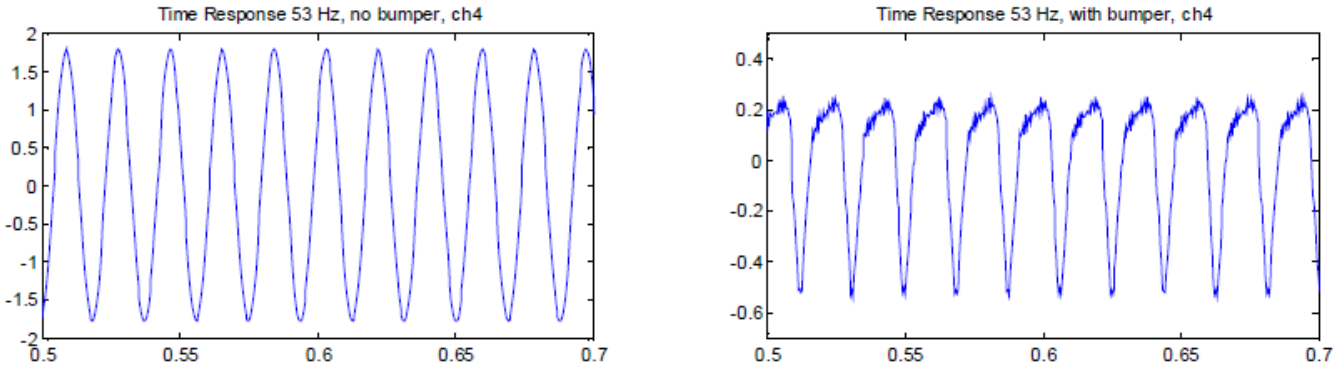

Figure 2.4 Acceleration time history responses of undamaged (left) and damaged (right) structure [4]

2.2 Entropy: the measure of complexity

Explained the connection between damage and complexity, it becomes useful to investigate how to quantify the increase of complexity of measured data in structures which suffer damage.
The extent of this complexity falls within the information theory and, in particular, the concept of entropy is considered.

2.2.1 Definition of Entropy and Information Theory

The concept of entropy was coined in the 19th century by *Rudolf Clausius* [11] in the field of thermodynamics.
In statistical mechanics, entropy is interpreted as a measure of the disorder present in any physical system and it is identified with the letter S. The term has become popular for the large amount of phenomena it can interprets and has been adopted in several disciplines, including the Information and Signals Theory which we are going to investigate because the developed work is based on the collection and manipulation of data *(chapter 1.2.1 Procedure of SHM)*.

The birth of information theory corresponds to *Shannon's publication in 1948* [12] in which it is defined as *"the mathematical elaboration of phenomena related to the measurement and transmission of information on a physical communication channel"*. The quantity that measures the amount of data is called entropy.
The entropy measures developed over the years are various and it is necessary to investigate which of these measures is the most suitable to respond to the problems inherent the Structural Health Monitoring.
As will be pointed out in the following paragraphs, in which the entropy measures are introduced, there is not a measure capable of fulfilling the role of damage-sensitive feature in all possible cases, but depending on the type of structure, material and damage, there will be a measure with which it is possible to get the best results.
The observations regarding the use of the different entropy measures are based on the information provided in the publication of *Farrar et al.(2020)* [13] in which *Shannon (2.2.2), Rényi (2.2.4), Spectral (2.2.5), Approximate (2.2.6), Sample (2.2.7) and Permutation (2.2.8)* entropies are tested by means the *Naive Bayes classifier (2.2.10) and K-means clustering (2.2.11)* on 3 different test models: bearing defects in rotating machine, 4DOF impact oscillator and impact oscillator with bearing damage.

2.2.2 Shannon Entropy

This measure of entropy is statistically defined as the probability distribution function of a random variable to approach a uniform distribution *(Shannon, 1948)* [11]. It was investigated in the context of determining how many bits are needed in order to quantify information.
Considering the Shannon entropy, this constructs a probabilistic distribution *P (x)* using the time-frequency distribution TFD of a signal *x (t)*.

$$P(q) = \frac{\sum_r S(r,q)}{\sum_q \sum_r S(r,q)} \tag{2.1}$$

Where *S(r,q)* is the spectrogram of the signal *x (t)*.

The Shannon's entropy is expressed as follow:

$$H(x) = -\sum_{i=1}^{N} p_i(x) * \log_2(p_i(x)) \tag{2.2}$$

H (x) aims to measure the uncertainty related to the succession of results for a group of N random variables. These variables are the *x* and *p (x)* is the PDF of the variable.
In the case of uniform distribution there would be complete uncertainty on what result will be achieved and therefore, in this case, Shannon's entropy would give high values.

Data obtained in [13] show how the Shannon entropy is strongly affected by errors compared to the other measurements regarding the experiment of rotating machine and impact oscillator with bearing damage.
Regarding the 4DOF impact oscillator, the results can be considered satisfactory and this means that the Shannon entropy is capable of detecting damage simulated by non-linearity, introduced within the initial linear system, such as cracks which tend to open and close under different load conditions.

The use of Shannon entropy is also investigated in a previous publication by *Farrar et al. (2019)* [14] in which two systems with different damage were investigated.
As regards the first non-linear system, the presence of cracks inside a framed structure was simulated and the increase in entropy from the moment of initialization of the damage proved evident.

On the other hand, considering the second linear model, the simulated damage was related to the corrosion of the material of an aluminium plate and the results were not as satisfactory as those obtained from the first one. In order to make valid the use of Shannon entropy, it was necessary to implement an image processing technique in order to reduce the increase in material complexity due to corrosion (decrease in stiffness) to an increase of geometric complexity.

Summarizing the conclusions extrapolated from [14] and also considering what was explained for the tests in [13], it can be said that Shannon's entropy offers valid results in the case of materials affected by uncertainty (for example concrete) and in damage scenarios involving an increase in geometric complexity such as cracks.

Another proof in favour of this thesis is given by the publication of *Ceravolo, Lenticchia & Miraglia (2019)* [15] in which the use of the Shannon entropy, on a finite element model represent a linear elastic plane masonry wall and then validated on real cases, was experimented.
Also in this case it is specified that the Shannon entropy is a good damage-sensitive feature as regards structures with great uncertainties (as indeed masonry structures, referring to [15]).

2.2.3 Wiener Entropy

The Wiener Entropy, denoted by *Hw*, is defined as the ratio between the geometric mean and the arithmetic mean of the signal power spectrum:

$$H_w = Q \frac{\sqrt[Q]{\prod_q S(q)}}{\sum_q S(q)} \tag{2.3}$$

Q is the total number of frequency bins and *S(q)* is the discrete power spectrum of the recorded vibration time history.
This measure is the one that will be employed in this thesis as damage-sensitive feature within the simulation of a Damage Identification process for a Buried Steel Pipeline.
The choice of the use of this measure is justified in a separate subsequent chapter *(2.3 Wiener Entropy application in SHM)*.

2.2.4 Rényi entropy

The Rényi entropy is nothing more than the generalization of the Shannon's one.

With this type of entropy we aim to define the quantity of information useful for the realization of random processes with a given precision and with a known PDF of the variables.
The order of entropy (defined a priori) is of great importance and serves to scale the PDF in order to bring out the values with greater probability.
The order of entropy can take values from 0 (maximum entropy for a discrete variable) to alpha (> 0). As the order of entropy increases, the difference in terms of probability is amplified.
With order equal to 1 we obtain the Shannon entropy.

$$RE_{\alpha}(x) = \frac{1}{1-\alpha} \log \left(\sum_{i=1}^{N} {p_i}^{\alpha}(x) \right) \tag{2.4}$$

The results obtained in [13] regarding the Rényi entropy are, albeit slightly more precise, very similar to those obtained with the Shannon entropy and then, we can say that this measure is also useful for identifying damage attributable to cracks.

2.2.5 Spectral entropy

The spectral entropy consists in a particular application of Shannon entropy in which the uniform distribution is replaced with a power density function.
This function $p_i(f)$ corresponds to the energy of the single frequency band $f(i)$ which is normalized respect to the total energy of the signal.

$$p_i(f) = \frac{f(i)}{\sum_{J=1}^{N} f(i)} \tag{2.5}$$

Once the probability distribution function $p_i(f)$ and the distribution $f(i)$ of the signal frequencies are defined, the expression for the calculation of the spectral entropy is defined:

$$SE(f) = -\sum_{i=1}^{N} p_i(f) * \log\left(p_i(f)\right) \tag{2.6}$$

In general, the spectral entropy is one of those that shows the best average results in [13].
Going into detail, as regards the Rotating Machinery, good results are obtained at any speed test while; for the 4DOF impact oscillator there are minimum errors compared to the Shannon entropy only in the case in which the sensors are positioned close to the damage.
The same goes for the impact oscillator with bearing damage test.

This means that the measure is a valid alternative if there are sensors in the proximity of the damage location and this implicitly means that it is necessary to know or predict the location of the damage within the structure. However, it remains one of the best solutions.

2.2.6 Approximate entropy

This measure of entropy serves to give a measure, over the time, of the regularity of a succession of data by defining the unpredictability of the observations. Considering a time series *S* with a maximum value of points *N*, we define the procedure for calculating the entropy of this series:

a) Let's start by considering the time series S_N:

$$S_N = \{x(1), x(2) \ldots x(N)\} \tag{2.7}$$

b) From the series we extrapolate vectors as follows (*m* is the length of the vector):

$$\begin{gathered} X(1) = \{x(1), x(2) \ldots x(m)\} \\ X(2) = \{x(2), x(3) \ldots x\,(m+1)\} \\ X\,(N-m+1) = \{x\,(N-m+1)\,, x(\,N-m+2\}\ldots x(N)\} \end{gathered} \tag{2.8}$$

c) It is now specified that the difference between two vectors *X(i)* and *X(j)* is defined in this way:

$$d\,(X(i), X(j)) = \max_{k=1,2\ldots m}\,(|x\,(i+k-1) - x\,(j+k-1)\,|) \tag{2.9}$$

d) The previous expression is inserted within the similarity criterion which is used to compare each vector extrapolated from the series with the others, in order to identify the maximum differences encountered bv the set r.

$$C_i^m(r) = \frac{1}{N-(m-1)} \sum_{i=1}^{N-m+1} \Theta\,\{r - d\,[X(i), X(j)]\} \tag{2.10}$$

$$\Theta\,\{x\} = \begin{cases} 1, x \geq 0 \\ 0, x < 0 \end{cases} \tag{2.11}$$

e) We can now define the approximate entropy *ApEn* of the time-series data:

$$\phi^m(r) = \frac{1}{N-m+1} \sum_i \ln\left[C_i^m(r)\right], \quad i = 1, 2, \ldots . N-m+1 \tag{2.12}$$

$$ApEn\,(m, r, N) = \phi^m(r) - \phi^{m+1}(r) \tag{2.13}$$

Data regarding the approximate entropy obtained in [13] are among the most variable.

As for the rotating machine, the best results are obtained at high speeds and as the velocity decrease, the error values increases. In the 4DOF, the measure is more precise with the Naive-Bayes classifier and, in general, with respect to sensors close to damage. In the impact oscillator with bearing damage the error obtained by using the approximate entropy is the minimum one.
We can affirm that this measure is suitable for describing damage in simple systems.

2.2.7 Sample entropy

This entropy measure is a modified version of the Approximate one. The difference between the two measures is that self-similar patterns are not considered when comparing vectors in Sample entropy.
Therefore, the procedure in order to identify the sample entropy is similar to the previous one up to *expression (2.10)* with the difference that no comparisons are made between vectors with i = j.
Thus we arrive at the definition of sample entropy as follows:

$$SampEnt\,(m,\,r,\,N) = -\ln\frac{\phi^{m+1}}{\phi^{m}} \tag{2.14}$$

The trend of the results obtained by using the Sample entropy in [13] is comparable with that of the approximate one, even if the latter proves to be affected by lower errors.

2.2.8 Permutation entropy

The permutation entropy has the purpose of identifying a trend in the data. For a thorough understanding of this measure, the reader is referred to the book of *Bandt & Pompe* [16].

$$PE_{m.\mathrm{norm}} = \frac{-1}{\log_2(m!)}\sum_{i=0}^{m!}\pi_i * \log_2(\pi_i) \tag{2.15}$$

The experimental tests in [13] have shown that permutation entropy, even if it is slightly more affected by errors than spectral entropy, is the measure that best distinguishes the "damaged" from the "undamaged" case.

2.2.9 Mutual information

By the use of this measure we try to identify the number of information that can be deduced from a signal *X* using that of a second one *Y*. In the expression appear the joint probability distribution $p_{xy}(x, y)$ and the marginal distributions $p_x(x)$ and $p_y(y)$.

$$I(X;Y) = \sum_y \sum_x p_{XY}(x, y) \ln\left(\frac{p_{XY}(x, y)}{p_X(x) * p_Y(y)}\right) \tag{2.16}$$

Mutual information tends to be more precise in terms of fewer errors when used within a Naive-Bayes classification process and it is more effective when information from sensors close to damage is taken into account.

2.3 Wiener Entropy application in SHM

The application of Wiener Entropy in SHM is treated in this paragraph because, as previously mentioned, it corresponds to the measure that will be used in the simulation of damage identification described in the following chapters.
Resuming [15], in addition to the evaluation of the efficacy of the Shannon Entropy introduced in *2.2.2*, the Wiener Entropy is also studied in order to understand how and in which cases it is of justified use.
For more detailed information, the reader is referred to the publication.

What has been developed in [15] is a study aimed to identifying which measure, between the Wiener Entropy and the Shannon Entropy, is the most suitable to constitute a valid damage-sensitive feature in a SHM process for the identification of the damage to masonry structures.
The work began by developing a FEM defined as a linear elastic plane masonry wall that implements plane stress theory. A progressive damage was applied to the model with the formation of a symmetrical diagonal crack in the centre of the wall.
The data obtained from the Finite Element full dynamic analysis, and through which the entropy of the system was defined, are the acceleration response along X axis at four extreme points of the model.
A disturbance component was added to these data to simulate the presence of white noise, according to a Gaussian distribution.
The analysis conducted on the FEM was then validated on real cases concerning structures in central Italy affected by earthquakes.

The results obtained from the experimentation regarding the Wiener Entropy are the following:

a) Wiener Entropy is very sensitive to variations in structural conditions.
b) As uncertainty about the material increases, Wiener Entropy becomes an increasingly unstable indicator.
c) The instability of Wiener's entropy in uncertain structures is linked to its ability to detect even low levels of damage.
d) White noise lower than 10% - 20% of the signal power has positive effects on the stability of the entropy measure.

For the reasons listed above, it is possible to establish that Wiener Entropy is a valid indicator of damage if used in cases involving the SHM of structures with little uncertainty, such as those made up of steel elements.
In fact, the strong sensitivity of this indicator towards structural changes would allow to identify even the smallest damage.
It could not happen in materials with more uncertainty such as masonry or concrete because the instability of the indicator would be due to the intrinsic nature of the material, such as the presence of imperfections just from its undamaged state.

Having defined which are the most favourable situations for the adoption of one or the other entropy measure, the use of the Wiener Entropy in the Damage Identification for a Steel Pipeline, developed in the following chapters, is justified.

3. CONTINOUS BURIED STEEL PIPES

A description of the structural types, types of damage and inspection methods of existing pipelines is useful to have a general overview of the problems related to these structures in the field of structural monitoring. The discussion is mainly focused on buried "flexible" pipes made of steel material, as object of study for the numerical simulation of SHM.

3.1 Overview

Today, pipelines correspond to one of the most used and efficient transport systems for the both off-shore and on-shore transport of liquids and gas. The movements may concern fuels such as oil and hydrocarbons (famous for their extension that cover distances between continents), transport of chemical products from industrial processes up to also including inter- and extra-urban transport of gas and water (Water Distribution Systems WDS).
The adoption of these systems in the context of short distribution is linked to the great safety that this type of structure can guarantee. In the case of long-distance transport, on the other hand, pipelines make it possible to have an advantage from the point of view of environmental and economic sustainability compared to other methods of handling such as sea, air or road means of transport.
Transport times are also to be considered, which are drastically reduced.

From the point of view of the environmental conditions in which the pipelines operate, we can distinguish 3 distinct cases:

- Pipelines placed above ground in dry conditions;
- Underwater pipelines;
- Buried pipelines.

3.2 Buried Pipeline

The choice to opt for the burying of the pipelines is linked to several advantages such as avoiding the occupation of space and creating obstacles, from the environmental point of view not affecting the landscape aspect and above all from a technical point of view in which the exposure to external environmental factors changes.

This thesis will deal with large diameter buried pipelines (d. > 60 cm) and from these we can distinguish two types of structures, considering the material point of view:

- Pre-stressed Concrete
- Steel

Obviously, according to the type of material, there will be different methods of construction, laying, use and various damage scenarios which structures can undergo.

3.2.1 Pre-stressed Concrete Cylinder Pipes (PCCP)

A simple introduction of this structural typology is given, without going into too much detail because they are not an object of interest in the work carried out, but they will certainly be subject to future studies. For more information the reader is referred to [17].
The PCCP, also called "rigid" pipelines since the loads are mainly carried by their own structure (low soil-structure interaction), are defined by a prestressed reinforced concrete core with high resistance strands or wires, in contact with a thin steel cylinder and coated externally with mortar.
The concrete core defines the supporting structure of the pipeline and the steel serves as protection against water. Prestressing is useful to compensate the tensile stresses induced in the pipe by internal flows and the mortar has the function to protect the prestressing threads from corrosion and physical damage.

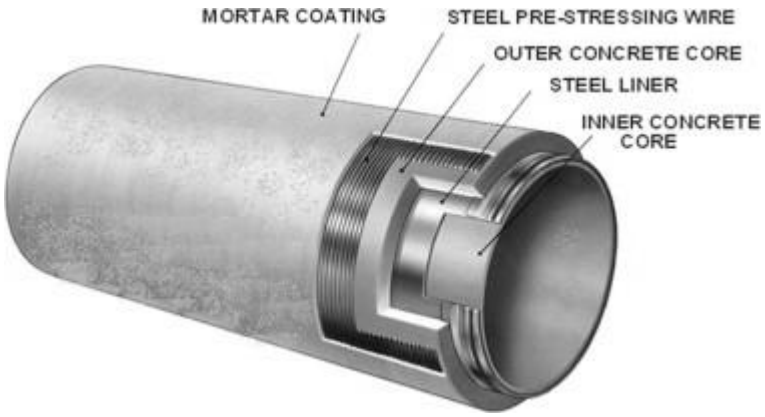

Figure 3.1 Showing PCCP elements *(Source: ScienceDirect.com)*

The laying of these pipelines is called "segmented" because it consists in connecting the adjacent prefabricated elements by means of mechanical joints which are subsequently sealed.

This type of pipelines is mainly used in urban fluids distribution because its apply on large stretches (e.g. transport of fuel) is inconvenient from the construction point of view (laying the concrete in contact with the steel, maturation, prestressing, etc.) and for their strong tendency to crack.

3.2.2 Steel Pipes (SP)

Steel pipes, also called "flexible" pipelines for their ability to define an integrated soil-structure system to support mechanical loads, are the most used type of pipeline in the WDS field.

Widely used also in the supply field of natural gas and oil, although much more expensive than other types, they hold their reputation for the advantages related to resistance to high pressure, their very adaptable shape, their light-weight and their possibility to deform without breaking.

Figure 3.2 Shape adaptivity in welded Steel Pipes *(Source: Citygasdistribution.com)*

Other advantages, compared to the previous PCCP case, are linked to the easier and cheaper transportability of the elements (less fragile than those in prestressed concrete) and the possibility of making solid connections with the adjacent elements in a simple way by welding (Continuous pipelines are equipped with highly rigid and constrained connections).

Obviously the advantages are countered by disadvantages concerning the need to adopt particular protections against the numerous corrosion scenarios that may occur; thermal conductivity and the more difficult repairs or replacement of steel welded element.
In addition to the continuous connection of the elements, also in this case it is possible to resort to a segmented laying, as in the PCCP, through bolted connections.

3.3 Damage and Failure Modes for continuous buried SP

At this point it is necessary to introduce all the possible damage and failure scenarios foreseen for SP. The scenarios we are about to describe define high risk frameworks for various reasons and all linked to the loss of fluid transported inside.

In fact, the loss of fluid, in addition to the obvious problems related to the lack of supply and economic loss, would also entail a very serious environmental impact and risk for the safety of people and infrastructures.

3.3.1 Failure Modes

a) **Tensile failure:** Nowadays, the most modern SP have ductility characteristics such as to be able to undergo large tensile deformations with high yielding before the collapse begin.
The tensile strength is useful because of the strong internal pressures that the internal fluids cause. The problem of the presence of these pressures, together with other problems linked for example to seismic actions, does not concern the pipeline itself but the connections.
In fact, the welded joints are very rigid, unlike the steel pipe element, and consequently a breakage by traction in the continuous SP is predictable in correspondence of joints.
Naturally, the scenario just described is influenced by corrosion (described later) which can affect part of the steel element or the welded joint itself.

b) **Local buckling:** High axial forces which tend to compress the steel pipe elements can cause local instability of the structure. Once the instability has occurred, in correspondence of the formed plastic hinge, all the effects of external actions (e.g. pressure of the fluids) will tend to concentrate in correspondence of the deformation occurred.

Figure 3.3 Shape Local buckling test on SP element. *(Source: Local buckling during bending tests in the STRESS lab at Northeastern University of a spirally welded thin-walled steel tube. Image courtesy Angelina Jay and Andrew Myers))*

c) **Beam buckling:** It occurs in the case of buried SP subjected to compression and bending due, for example, to seismic actions.

d) **Shear failure:** The shape of the deformation is similar to the one due to Local buckling.

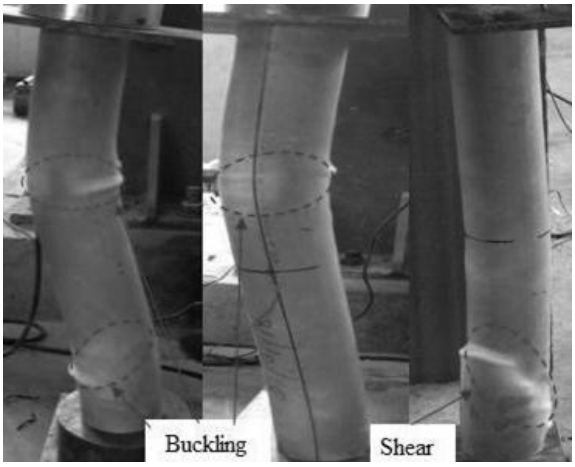

The cause of the shear failure is linked to relative movements between blocks of soil, such as in the case of pipelines that necessarily have to cross faults.

Figure 3.4 Comparison between shear failure and local buckling.
(Source: Cogent Engineering [38])

3.3.2 Damage Modes

Depending on the shape of the damage, a geometric classification can be defined: (a) circumferential cracking; (b) Longitudinal cracking; (c) Bell Splitting; (d) Pitting corrosion; (e) Blowout hole; (f) Spiral cracking. All illustrated in *Figure 3.5* [18].

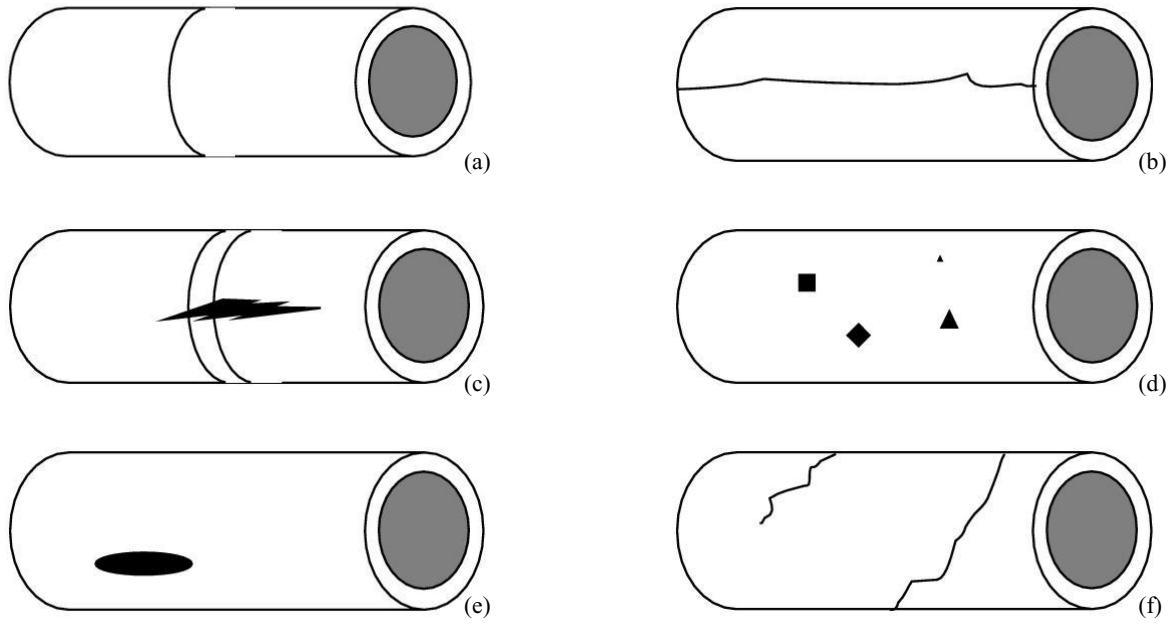

Figure 3.5 Geometry classification of damage in Pipelines [18]

The forms of damage that most commonly afflict the continuous buried SP, which can be traced back to the damage simulation developed in *chapter 4*, are described below.
To investigate the other cases of damage, the reader is referred to [19] and [20].

a) **Pitting corrosion:** Pitting corrosion corresponds to a particular form of corrosion which involves the formation of holes in metal surface such in SP.

Figure 3.5 Pitting corrosion on Steel Pipes *(Source: Case Studies in Engineering Failure Analysis[20])*

The creation of the hole is often accompanied by the covering with corrosion products which statically does not give any contribution of resistance to the structure, consequently the material can be considered lost.
Formed pit can be of hemispherical or cup-shaped.

This form of damage, albeit very small, can cause serious problems inside the Pipeline structure as initialization and evolution of cracks due to traction and consequently tensile failure.

Referring back to *paragraph 3.3.1 (a)*, it is noticeable how the presence of pitting corrosion can change the scenario of tensile failure since, by weakening the steel pipe element, this becomes the first candidate to break under traction effects while the welded joint can remain intact.

The pitting corrosion can be caused by several scenarios as the damage of the protective oxide film due to environmental factors (e.g. water acidity or strong presence of chloride); poor application of the protective coating or inclusions that undermine the quality of the metal.

b) **Stress-corrosion cracking:** The problem of stress-corrosion cracking mainly concerns the welded joints between steel elements. The cause of this damage condition is linked not only to the environmental conditions but also to the nature of the weld itself, which we know how to modify the microstructure of the steel in correspondence of the joint with a stiffening effect. Without going into too much detail, this stiffening is due to the formation of martensite in the microstructure of the iron-carbon alloy, an element that hardens the material and makes it more fragile. Brittleness implies a lower propensity to deformation under load which, together with particular environmental conditions favourable to corrosion, involves a loss of mass and stiffness in correspondence of the welded area.

With the simultaneous development of these processes, it is defined a pipeline with a cross section (whole or partial), of length depending to the weld condition, with mass and stiffness lower than the rest of the structure.

c) **Pipeline Thinning:** Thinning pipelines is caused to uniform corrosion or nothing more than a secondary effect of pitting corrosion.

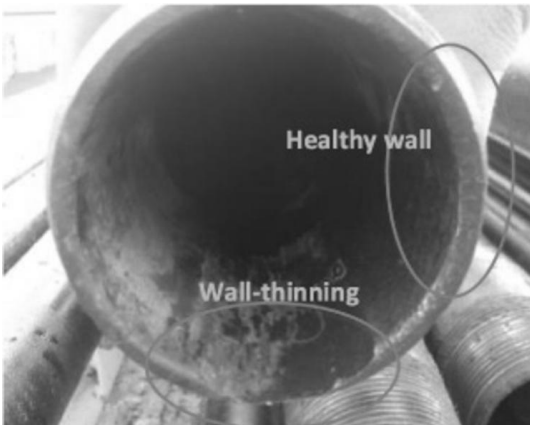

Figure 3.6 Demonstration of wall-thinning in pipelines.
(Source: International Journal of Applied Electromagnetic and Mechanics [37])

In this last case the corroded element, which has a point of maximum thinning due to pitting, is characterized by an area around the hole which has a thickness lower than the nominal one. Then, we pass from an intact and constant thickness to a variable one with increasing thinning towards the area of maximum pitting.
As can be seen from *Figure 3.6*, the loss of material is evident over a relatively large portion of the wall.

In the case of uniform corrosion, the thinning is not as evident as in the case of pitting because the thickness apparently remains constant, but in truth the intact material is progressively replaced by the product of corrosion causing a decrease in effective thickness.

3.4 Pipeline Integrity Management (PIM)

Pipeline Integrity Management (PIM) [21] corresponds to the set of operations regarding pipeline assessment, inspection, defect and repair, and maintenance.
With this approach we want to identify those phenomena of fatigue, corrosion, ground or anthropogenic movements that can define damage scenarios, also considering factory defects that can define weaknesses within the structure. The PIM also defines what are the foreseeable damage scenarios according to the type of pipeline considered (for pipelines that work at other pressures, bursts are foreseeable, for those at low pressures there is a risk of sedimentation etc.).
One of the main problems relating to the monitoring of Buried Pipelines is that concerning their reaching in order to allow accurate visual inspections. In fact, even if the pipelines are designed so that they can be inspected through the presence of maintenance holes (inspections physically possible), human-made surveys are not efficient from the time and economic point of view due to the length of the networks. Below some examples of PIM techniques are described.
For a more complete discussion of the topic the reader is referred to [21].

3.4.1 Pipeline Inspection Gauge (PIG)

Pigs are a type of devices, forced into the pipeline from a launcher (chamber of slightly larger diameter than the pipeline and connected to that) [22] having the function to guarantee a summary maintenance by removing material deposits and deformation issues.
The operation is based on propulsion through the flow of fluids which allows the movement of the devices along the development of the pipeline.

Figure 3.7 PIG insertion inside a pipeline *(Source: Intero integrity service B:V:)*

As can be guessed from *Figure 3.8*, the problem that afflicts the method based on the use of this type of device is linked to the possibility that, during the movement of the PIG along the pipeline, it gets stacked inside it, remaining trapped and blocking the transport of fluids.
In the event that this scenario occurs, the injection of pressure inside the duct is usually carefully increased, in order to prevent a structure burst from occurring.
If it is not possible to remove the device, it is inevitably necessary to carry out an excavation of the ground, exportation of the part of the pipeline (difficult in the case of continuous SP) and proceeding with the removal of the PIG or replacement of the element, with a consequent increase in operations cost.

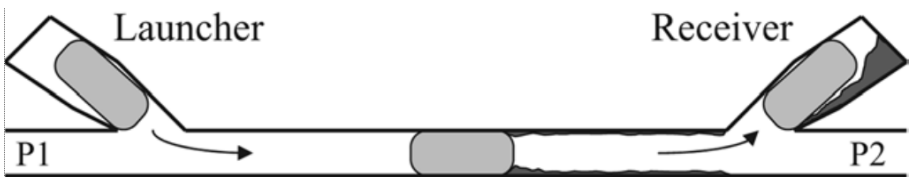

Figure 3.8 PIG driven by pressure difference across the pipeline [21]

These evidences make it clear that the use of the PIG is not always convenient and since they are devices of standardized dimensions, they cannot be used on all pipelines, in particular with small diameters.

3.4.2 Smart PIGs

As can be understood from the name, the working of the "Smart Pigs" devices remains the same as that described in *paragraph 3.4.1*.
The expression "smart" is linked to the fact that this type of device is able not only to solve the same problems as the classic PIG, but also to provide data regarding the integrity of the pipeline such as the location of damage.
There are various types of Smart Pigs and they differ according to the tools [21] equipped:

a) *Corrosion Tools*. They are used to identify the position of damage linked to corrosive actions such as thinning of the walls. On the basis of the principle used for data extrapolation, the following can be distinguished:
   - *Magnetic flux leakage (MFL);*
   - *Ultrasonic (UT).*

b) *Crack detection tools.* These are the most recently integrated tools in the PIM field. They aim to envy the position and extension of the cracks and are defined as:
   - *Ultrasonic crack detection;*
   - *Transverse magnetic flux leakage;*
   - *Elastic wave tool.*

c) *Geometry tools.* They are those devices that allow to define the geometry of the structure, investigating if there are any deformations such as to be attributable to phenomena of instability or action of external forces.
   - *Caliper tools*
   - *Pipe deformation tools*

Despite the wide range of useful information that Smart Pig devices are able to provide, the problems relating to the size and possible interruptions in the functioning of the pipelines remain, and for this reason in recent years less invasive methods which aim to achieve the same if not better results, have been developed and used.

3.5 SHM for Pipeline Integrity Management

The use of Structural Health Monitoring in pipeline monitoring is useful for solving the problems related to the invasiveness of traditional approaches. In fact, SHM, also defined as non-destructive monitoring, allows to extrapolate data regarding the health of the structure without interfering with its functioning. The techniques that define SHM in the Pipeline Integrity Management are Local-based and Global-based methods.

Into local ones, we can identify a series of techniques [23] as: Ultrasonic, radiographic, magnetic particle inspection (MPI), dye penetrant and electro-magnetic methods.
They are defined local techniques because the monitoring of the structure is done by looking at the local inspection of the same, without considering the entire global system.
The use of these techniques involves a large amount of time, resources and costs for the equipment to be used, for example, in data collection.

Explaining the global methods, unlike before, the identification of the damage occurs by considering the behaviour of the structure as a whole.
Among the most used techniques there are the acoustic wave one [24] which involves injecting into the operating pipeline (therefore filled with fluid) a small pressure pulse that generates pressure fluctuations of the fluid molecules. Along the longitudinal direction of the pipelines, microphones are mounted and used to capture the acoustic waves generated by the impulse. In fact, once the injection is carried out, pressure fluctuations of the fluid molecules will be generated with consequent propagation of acoustic waves through the pipeline.
The use of these data allows to identify any discontinuity indicating damage inside the structure, in particular thanks to the reflection and transmission of the acoustic waves in correspondence of these areas.

As already seen in *paragraph 1.3.1*, among the global methods of Structural Health Monitoring, one of the most used is the Vibration-Based Identification VBI which, however, as regards pipelines is not applied as much as other types of structures such as bridges.
Among the studies which aim to identify a damage-sensitive feature useful for the identification of damage in pipelines through VBI, those conducted by Bao et al. (2013) [25] concerning the use of the Autoregressive Moving Average (ARMA) model or more generally [26] are cited. Other researches concerned strain measurements through the use of fibre optic sensors distributed along the development of the pipelines [27].

3.5.1 Wiener Entropy as Steel Pipes damage-sensitive feature

In this circumstance we want to introduce the Wiener Entropy, already described in *chapter 2.3 "Wiener Entropy application in SHM"*, as a possible damage-sensitive feature of a Structural Health Monitoring in the context of Pipelines Integrity Management.

In fact, recalling that Wiener Entropy as a very sensitive measure to the variability of the conditions of the structure, it could be a possible valid indicator of damage in the Steel Pipes, object of study of this thesis.
Its use can be justified not only from the point of view of the material. Actually, if we want to base the monitoring operations of Buried Steel Pipes on a SHM approach with Wiener Entropy analysis, the data to be used for the extrapolation of the complexity measure would correspond to the strains which the pipelines undergoes under the action of seismic noise, the generic name for persistent vibrations of the ground due to various causes (ground movements, anthropogenic actions etc).
This aspect is made possible by the strong sensitivity of the Wiener Entropy which, even using deformations due to humanly imperceptible external actions, could reach the identification of the damage that includes the first and second level of the Rytter hierarchy [10] (detection and localization damage).

Therefore, the advantages of using this measure (and which still remain to be validated in the following chapters) would be:

- No invasive operations on the structure;
- No use of artificially induced actions;
- Continuous monitoring of the structure.

This technique, in order to be possible, requires the use of fibre optic sensors capable along the longitudinal development of the pipeline. The inherent problems concern the economic aspect and durability of the sensors in the expected environmental conditions.

The issues to be resolved are also the variability of the seismic noise over time which can lead to fallacious results, the pressure and movement of the fluids inside the pipeline and the percentage of white noise respect to the signal.

4. NUMERICAL MONITORING SIMULATION

Getting to the heart of the thesis, the work carried out can be divided into two main steps.

The first phase concerns the development of Finite Element Models FEMs and their numerical analysis for data extrapolation, thus defining a monitoring simulation on a continuous Buried Steel Pipe through the use of the software *ANSYS-Mechanical APDL 19.2.*

On the other hand, in the second phase we dealt with the manipulation of data obtained from the numerical simulation, in order to proceed with the damage identification.

Therefore, a damage identification process is defined according to a Structural Health Monitoring approach in which the part concerning the monitoring of the real structure is replaced by the study of a numerical model.

In this chapter we will talk about the first phase, in which we will describe all the steps that led to the creation of the models and the setting up of the analysis.

4.1 Materials and Geometry

Through the finite element models we want to represent a 19 meters longitudinal portion of a continuous Pipes in stainless steel UNS S31803.

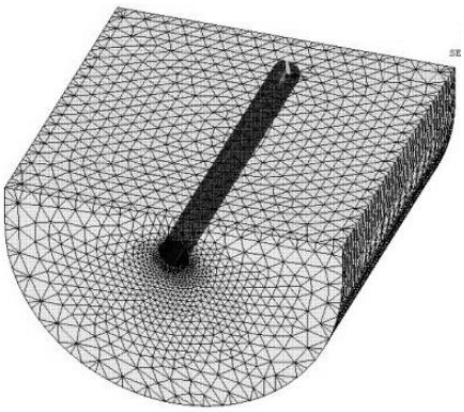

Figure 4.1 Case study geometry

The pipeline is buried within a loose sand ground and the its cross-section centroid location is 2.25 meters below ground level.

The outer radius of the cross section is 0.5 meters with a pipeline wall thickness of 0.02 meters. The surrounding soil to be considered was evaluated through a sensitivity analysis in order to identify the minimum value that the radius of the ground *(Re)* must assumes to eliminate any calculation error relating to the presence of the model boundary [33].

In particular, the longitudinal deformations of the pipeline were evaluated as the radius changed and it was found that for *Re* greater than 9.5 meters, the deformations considered due to the self-weight remain unchanged. On points at 0 °; 90 °; 180 °; 270° of the section (*Figure 4.9)* are positioned optical fibres (cross section area of $5*10^{-4}$ square meters) running along the entire longitudinal direction. The reference geometry is shown in *Figure 4.1* and the characteristics of materials are defined in *Table 4.1*.

	Steel	Soil	Optical fibre
Density [kg/m^3]	7850	1850	2480
Young's Modulus [MPa]	210.7*10^3	24	90*10^3
Poisson's Ratio [-]	0.3	0.2	0.2
fy [MPa]	490		
fu [MPa]	690		
ε_y	0.0023		
ε_u	0.025		

Table 4.1 Mechanical properties of materials

4.2 Finite Element Model

Once the characteristics of the system to be studied have been defined, it is necessary to go back to an equivalent analytical modelling.

A first study carried out on the model shown in *Figure 4.1*, in which the volume of soil was defined by means of the SOLID185 element and embedded along the boundary, led to incorrect results.
The reason was that that type of modelling did not take into account various aspects of fundamental importance such as:

- Multi-scale effects on the pipeline;
- Soil-structure interaction;
- Soil with only compressive resistance;
- It is therefore necessary to define an open system, in which the energy does not remain "trapped" inside the model, but has the possibility to be transmitted to the outside.

For the reasons listed above, it was not possible to use the initial model and a different approach had to be adopted for the realization of the analytical representation.
Specifically, the modelling process followed a series of steps in which, from simple 2D models useful for the extrapolation of the parameters, we were brought back to the equivalent 3D model in which the land surrounding the pipeline was replaced by a series of springs, simulating a scenario similar to the Winkler theory.

4.2.1 2D Static Analysis - Springs Stiffnesses

In this first 2D model, only an area of land is considered, corresponding to a section of the block represented in *Figure 4.1*, without taking into account the presence of the pipeline. The geometry is defined in *Figure 4.2*.

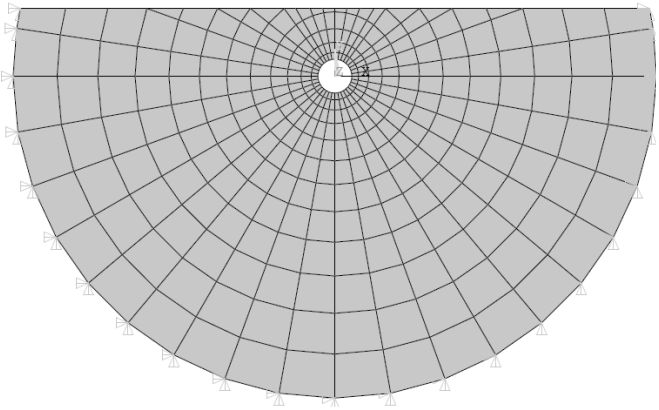

Figure 4.2 2D Soil Model geometry

The soil is defined by PLANE182 element, used for 2D models of solid structures and useful for describing plane-strain behaviours.

The associated material is the same as described in *Table 4.1 - Soil*.

A mapped Mesh is used for the discretization with refinement in correspondence of the hole due to the presence of the pipeline.

The boundary of the soil, excluding the upper part which corresponds to the ground free level, has been constrained in order to avoid any displacement and rotation (embedded constraint condition).

This 2D model is designed to define the stiffness of the ground at the contact points with the pipeline. In particular, 72 static analyzes were carried out (36 for each X and Y direction, 2 different analysis for each shared node) in which, in each of the analyzes, the single contact node (36 in total) between the ground and pipeline along one of the main directions was loaded *(e.g. Figure 4.3)*.

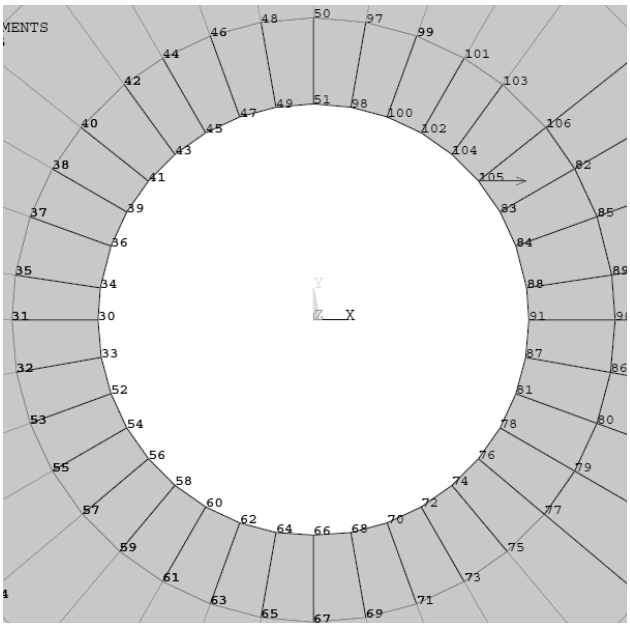

Figure 4.3 Detail of the nodes in common between the ground and the pipeline with node 105 loaded along the X direction.

From each of the 72 analyzes the displacement of the loaded node was extrapolated and putted as denominator of the applied force, led to the definition of the stiffness *(see the expression 4.1)* of the soil along the two directions for each ground-pipeline node.

$$K = \frac{F}{D} \tag{4.1}$$

The resulting stiffnesses correspond to the ones to be applied to the material of the springs that will replace the ground in subsequent models.

4.2.2 2D Modal Analysis (1) - Control Frequencies for Participant Modal Mass of the Soil

The base geometry remains the same as the previous 2D model. Unlike before, however, the 2D section of the pipeline inside the hole is also introduced *(see Figure 4.4)*.

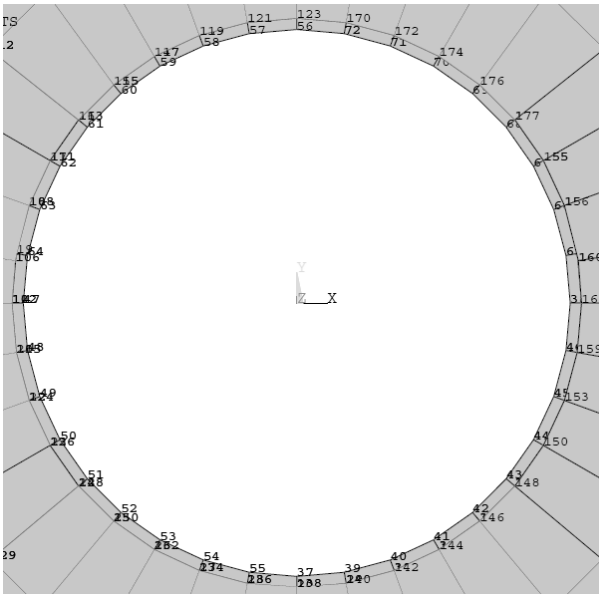

Figure 4.4 Detail of the model with the adding of the pipeline element.

The placing of the pipeline was carried out by creating an additional area inside the hole with a thickness corresponding to the thickness of the pipeline (0.02 meters).

The PLANE182 element has also been assigned to the pipeline area and the material is the one defined in *Table 4.1 - Steel.*

A modal analysis (Block Lanczos Method) [28] is set up in order to identify the natural frequencies to be compared with those extrapolated from the 2D model in which the ground is replaced with springs. This operation is necessary in order to be able to identify the participating ground mass.

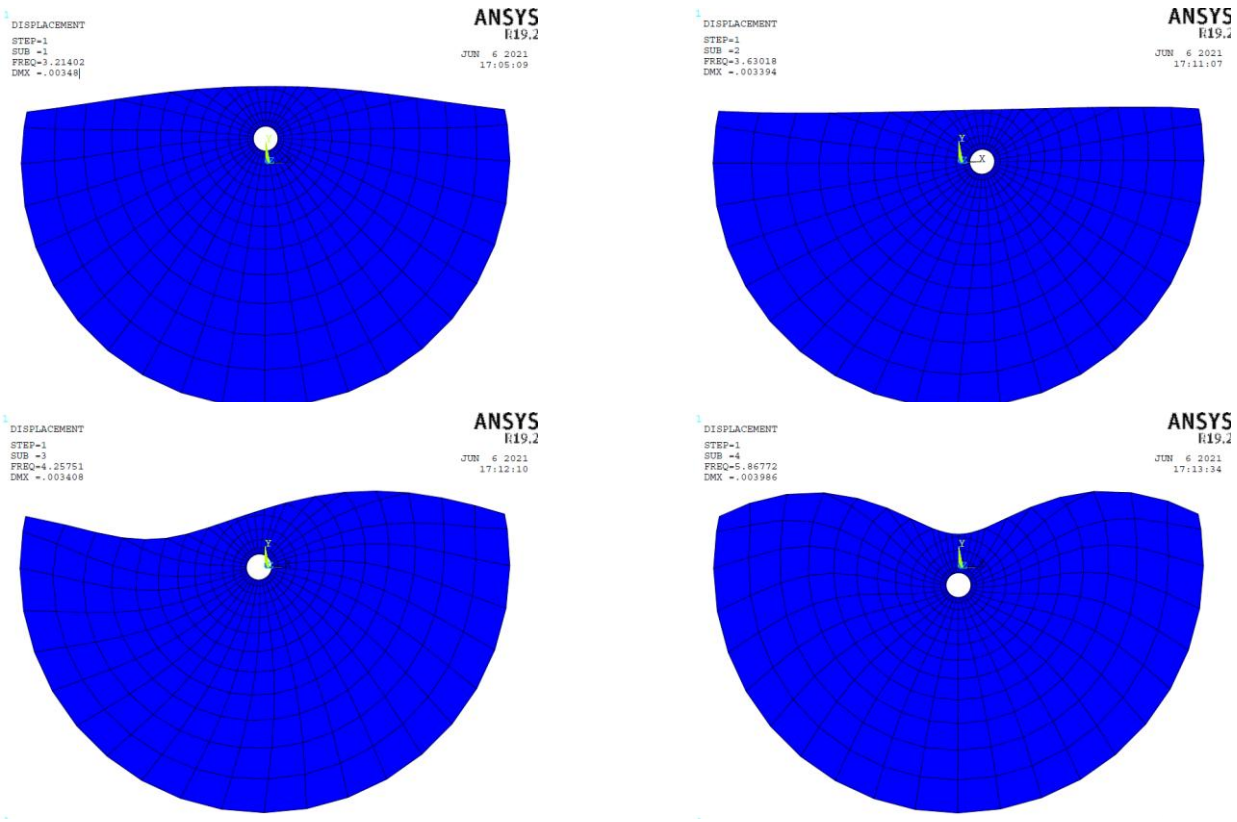

Figure 4.5 First 4 modal shapes of the 2D soil-pipeline system.

4.2.3 2D Modal Analysis (2) - Frequencies to Scale for Participant Modal Mass of the Soil

In this model, for the first time the ground surrounding the pipeline is replaced with a bed of springs independent from each other *(see Figure 4.6).* The springs are placed along the two main directions X and Y and the connection to the pipeline occurs at the nodes that in the previous models were shared with the ground.

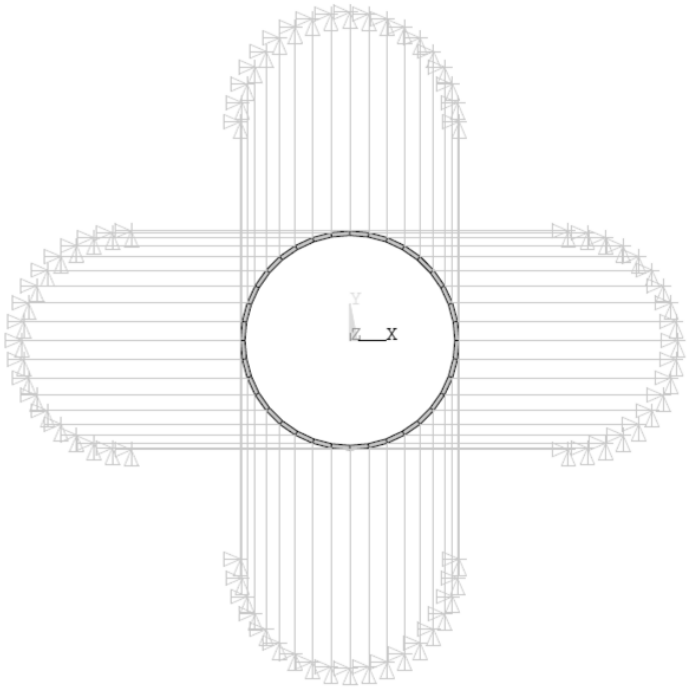

Figure 4.6 2D Pipeline-Springs geometry model

The discretized PLANE182 ground element is then replaced with 72 LINK180 elements (2 elements, each along one of the two main directions, for each node) rigidly constrained at the free end and with a mesh without discretization. In the definition of the material of the springs the density is not set, the Poisson's Ratio remains the same defined for the ground (0.2) and the value of the Young's modulus of the single spring corresponds to the ground stiffness calculated at the point and along the corresponding direction in the *model 4.2.1.*

The section of the spring is set in such a way as to have a compression-only behaviour *(see third point in chapter 4.2)* and unitary area. The value of the area equal to 1 is justified by *expression (4.2),* taking into account the length of the elements which is equal to 1 meter and that Young's modulus is set equal to the stiffness.

$$K = \frac{E * A}{L} \tag{4.2}$$

Once the modal analysis is completed and modal forms and corresponding natural frequencies have been identified *(see Figure 4.7)*, through the participation factors of the individual modes in the *model 4.2.2 and 4.2.3*, it is understood that the torsional one (third modal shape for the *4.2.2* and second modal shape for *4.2.3*) is the main mode and is the one on which to compare the frequencies between the two models.

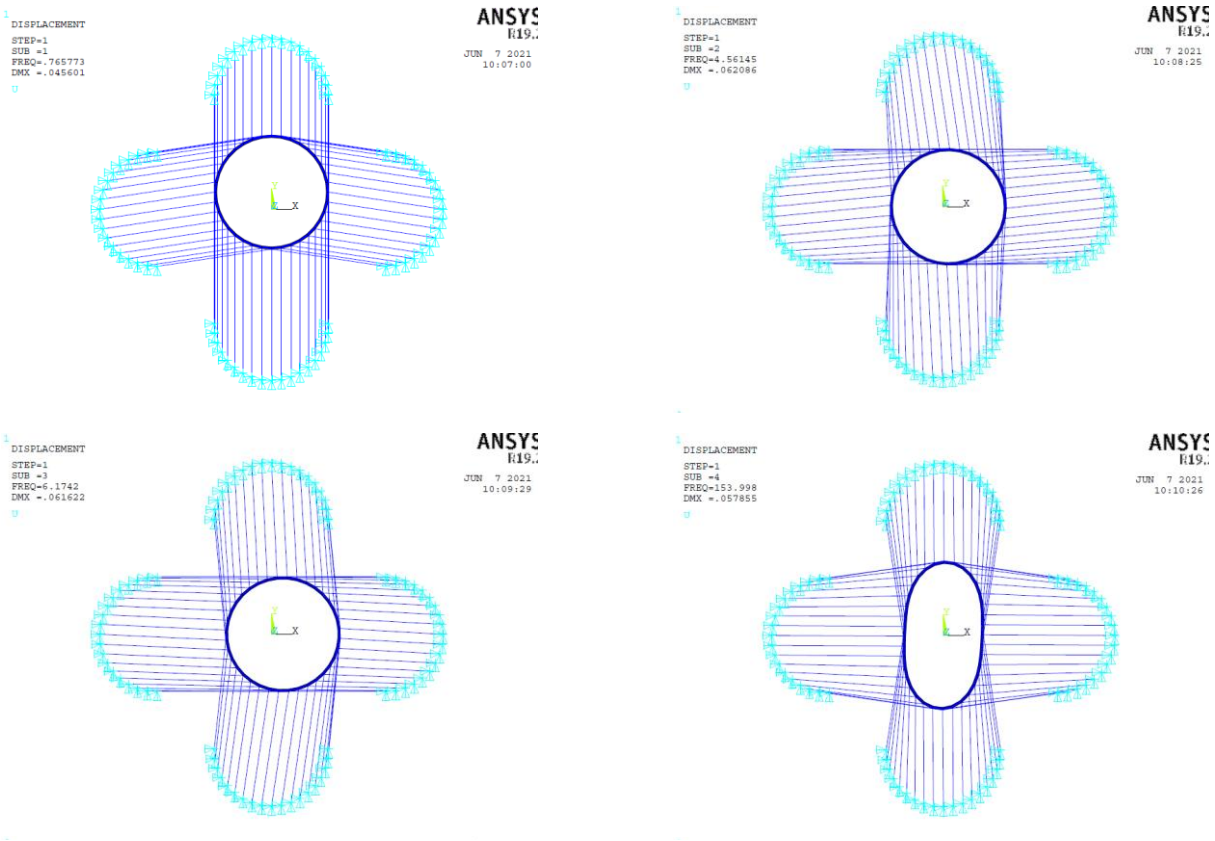

Figure 4.7 First 4 modal shapes of the 2D springs-pipeline system with no scaled density.

By dividing the second frequency of the current model (4.5614 Hz) with the third of the previous one (4.2575 Hz), we obtain a ratio equal to 1.0714. This value corresponds to the coefficient with which to scale the density of the pipeline, in order to take into account the participating mass of soil inside the model with the springs.

The new density value, to be used instead of the one indicated in the *Table 4.1 - Steel,* is equal to 9010.66 kg/m^3 .

4.2.4 3D Springs-Pipeline Model

This paragraph describes only the construction of the 3D finite element model without considering the creation of the acting forces and the setting of the analysis which will be dealt with separately in the following chapters.

Once the springs stiffnesses and the new density to be applied to the pipeline material in order to take into account the presence of the soil have been identified, it is possible to pass from the preliminary 2D models to the final 3D one, on which the analysis for the extrapolation of the data will be set.

The 3D Spring-Pipeline model is realized by the extrusion along the Z direction of the 2D model with a pitch of 10 centimetres up to an overall length of 19 meters. In this way a discretized area representing the Pipeline has been defined, caged inside the Springs Network and on which the mesh will be set.

Regarding the Springs, the definition of elements, sections, materials and restraints remains the same described in the previous model.

As regards the pipeline, the parameters to be changed are the density which must assume the value of 9010.66 kg/m^3 identified at the end of *paragraph 4.2.3* and the definition of the element that will no longer be a PLANE180 (we are no longer in the flat case) but a SHELL181, useful for meshing areas representing structures with a given thickness.

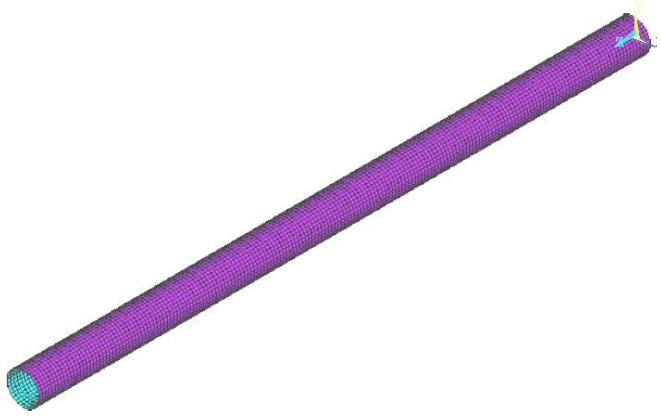

Figure 4.8 3D meshed geometry of SHELL181 element

For the first time, Optical Fibres sensors appear, positioned along the entire development of the pipeline and in correspondence of the points defined in *Figure 4.9*. The sensors are represented by means the BEAM188 element, the material parameters are those defined in *Table 4.1 - Optical Fibres* and the section is described by the area equal to 0.0005 square meters.

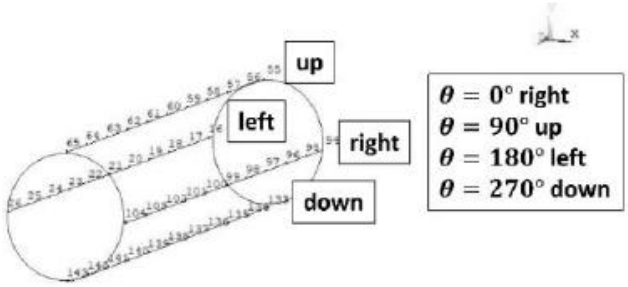

Figure 4.9 Location of BEAM188 elements

A fundamental aspect to consider and which has not been taken into account in 2D case (obviously) is the three-dimensionality of the system which presupposes the constraint of the Z direction.

For this purpose, a further network of springs has been created (added to the pre-existing ones in X and Y) along the Z free direction and which has the same characteristics of the springs along the X-axis, imposing then a congruence between the two horizontal stiffnesses (X and Z).

In order to obtain a more correct value of the springs stiffness (i.e. of the soil) along Z, it is advisable to deepen the study based on the Gazetas formulas [29] which refer to foundations and therefore not easy to apply to the specific scenario.

However, this approximation does not affect the final result.

- **Damage representation:** Important note must be made regarding the damage.
  As already explained in the first chapter, the definition of damage within a structure is useful if a comparison is made between an initial (undamaged) and final (damaged) situation of the system. The damaged state of the structure has just been defined, now it is necessary to understand how to model the damage from a physical-mechanical and geometric point of view.

  For this purpose it can be considered the concepts introduced in *chapter 3.3.2-Damage Modes* and carry them in the context of the Finite Element Model: to simulate the damage scenario, reductions in Pipeline (SHELL181) Stiffness are introduced through the adoption of multiplicative coefficients whose value depends on the severity of the damage to be investigated.
  The studied damage geometries correspond to situations of Corrosion-Thinning in correspondence of the welded joints and corrosion by Pitting, respectively represented by applying the reductions of Stiffness in correspondence of an entire cross-section or to a single discretized element.

4.3 Definition of the Acting (Seismic) Noise

Once the geometry definition and characterization of the elements that compose the system have been completed, we move on to the force application on the nodes of SHELL181 element.
We remind that this phase, together with the modelling one, it is not foreseen in real cases because the structure to be monitored and subjected to Seismic Noise is already given, without having to resort to any Finite Element modelling.
Since we want to simulate a continuous monitoring without the aid of artificially applied forcing *(see chapter 3.5.1)*, we must look for a representation as true-similar as possible of the so-called seismic noise, i.e. those persistent vibrations of the soil resulting from natural processes or anthropogenic actions (movement of vehicles, vibrating machines etc).

4.3.1 Displacements magnitude

Firstly, we need to identify the order of magnitude of these actions. For this purpose we take as reference the publication by Muraglia et al. [30] in which the Power Spectrum Density PSD of the

soil was measured as the signal (seismic noise) frequency changed. The result is represented in *Figure 4.10.*

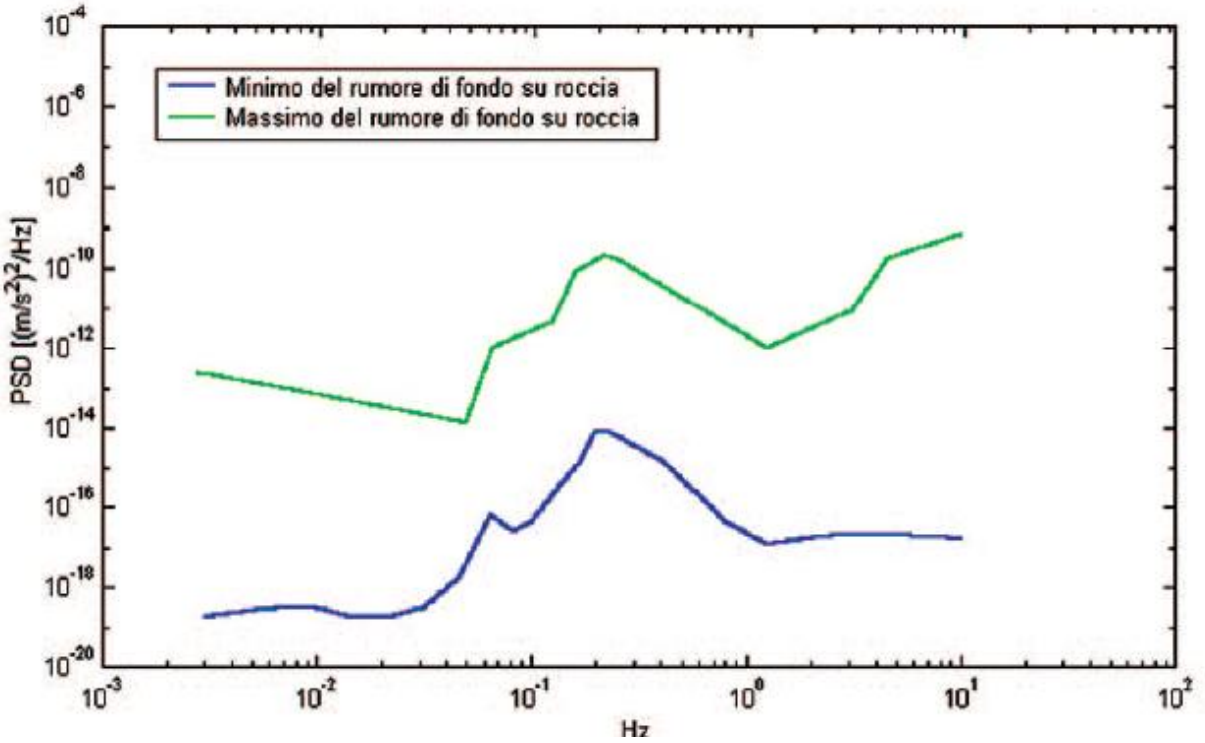

Figure 4.10 Maximum (Green) and Minimum (Blue) expected PSD value in soils when the signal frequency changes. [30]

At this point it is necessary to define the frequency range to be considered. These frequencies, as described by Gutenberg (1958) [31] and subsequently by Asten (1984) [32], depend strictly on the nature of the signal, ie on its origin. The frequency ranges according to the signal origin are defined in *Table 4.2.*

	Gutenberg (1958)	Asten (1978-1984)
Waves striking the coast	0.05-0.1 Hz	0.5-1.2 Hz
Moonson / large scale meteorological perturbations	0.1-0.25 Hz	0.16-0.5 Hz
Cyclones over the ocean	0.3-1 Hz	0.5-3 Hz
Local meteorological conditions	1.4-5 Hz	
Volcanic tremor	2-10 Hz	
Urban	1-100 Hz	1.4-30hz

Table 4.2 Frequency ranges according to Gutenberg and Asten Theories . [30]

Once the frequencies have been identified and used into the *Figure 4.10* graph, we are able to extrapolate the relative PSDs.

From the square root of the PSD relative to the reference frequencies, we identify the spectral accelerations A of the ground system. By dividing the spectral accelerations with the square of the natural pulsation of the system (identified by modal analysis of the 3D FEM) we extrapolate the spectral displacement D of the Springs-Soil system associated to the Seismic Noise.

f_sm [Hz]	f_fem [Hz]	A [m/s2]	V [m/s]	D [m]
5	16.501	3.72236E-03	3.62764E-05	**3.5356E-07**
50	16.501	1.29653E-03	1.25112E-05	**1.2073E-07**
100	16.501	8.64673E-03	8.51981E-05	**8.3112E-07**

Table 4.3 Deriving System Displacement from the Signal Frequencies

What interests it is not the absolute value but, as already said, we are looking for the magnitude of the Spectral Displacement which is in the order of 10^7 meters.

4.3.2 Time Variability of the Seismic Noise

Once the reference value has been obtained, a variability over time is assumed, defined by a Uniform Continuous Probability Distribution in the interval [1E-07; 9E-07].
The number of extracted values corresponds to the number of Time-Steps (defined in *chapter 4.4 Transient Analysis Settings*) considered in the development of the Finite Element Analysis. The values can assume a completely random positive "+" or negative "-" sign (the Seismic Noise has no preferential direction on which acts). This operation is performed three times, one for each direction X, Y and Z. The aim is to have a complete independence of the action along the three main axis of the Model.

In this way, what have been obtained are three vectors composed of T Displacement values (T=number of time-steps) extracted in a completely random way from the Uniform Distribution.
In particular, the single value is the displacement that the entire system undergoes.
From these displacements, we want to lead back to a formulation of Seismic Noise in terms of force.

4.3.3 From Seismic Noise Displacements to Forces

To carry out this step, the accelerations extrapolated previously in *Table 4.3* can be considered or better, we obtain three Acceleration vectors (X,Y,Z) from the Displacement ones multiplied to the square of System Natural Pulsation w *(4.3)*.

$$|A|_{Tx1} = |D|_{Tx1} * w^2 \tag{4.3}$$

The vectors obtained, multiplied by the mass of the Pipeline-Soil System, allows to get the forces acting on the System in each temporal step due to Seismic Noise along the three main directions *(4.4)*.

$$|F|_{Tx1} = |A|_{Tx1} * M \tag{4.4}$$

4.3.4 Space Variability of The Seismic Noise

Once the acting forces and the temporal variability of the action have been defined, the last step to be undertaken is to clarify the spatial variability of the Seismic Noise.
Considering that the portion of land studied is relatively limited, in the single time-step the sign of the action can be maintained but the values are necessarily subject to variability.
What it will get it is a matrix whose rows represent the temporal variability and the columns the spatial one. While the number of rows is equal to the number of time-steps T, the number of columns is equal to the number of nodes N that define the Pipeline element.

Retaking the force-vector $|F|_{Tx1}$, each element which composes this vector represent the total force acting on the system in the specific time-step (the first value is the total force acting in the first time-step, the second value is the total force acting in the second time-step, etc).
In order to define a matrix of space-time variability, the single element of the vector must be divided by the number of nodes of the Pipeline.

$$|f|_{Tx1} = |F|_{Tx1} * 1/N \tag{4.5}$$

Then, we pass from the value of the force acting on the total system to the value of the force applied to the single node in each time-step. This values will be used as the means of T Gaussian Distribution. From these T Distributions, N values are extrapolated for each T-ith time-step and the loads Matrix $|f|_{TxN}$ to use inside the Analysis is obtained.

4.4 Transient Analysis Settings

4.4.1 Solution Method

To study the response of the structure subjected to time-varying loads, a Transient Dynamic Analysis is set up.

Talking about the type of analysis chosen, it corresponds to a Small Displacement Transient, in which large deformation effects are neglected. The choice is justified by the fact that the models in the undamaged and damaged state are studied separately, therefore under the action of the loads the mechanical characteristics of the structure are not expected to change and the behaviour remains linear.

The equation used by the software to identify the dynamic response of the model is the general equation of motion *(4.6)*:

$$[M]\{\ddot{u}\}+[C]\{\dot{u}\}+[K]\{u\}=\{F(t)\} \tag{4.6}$$

For the resolution of *(4.6)* a Full Implicit Direct Integration is chosen. This means that there is no reduction of [K], [C] and [M] matrices, all nonlinearities are allowed and the equation of motion is directly integrated step by step over the time. In this way, at each temporal step (iteratively), a series of static equilibrium equations *(F = m*a)* are solved simultaneously.

The algorithm used to obtain the solution is the Newmark's one *(4.7; 4.8; 4.9)*:

$$\dot{u}_{n+1} = \dot{u}_n + (1-\gamma)\Delta t\, \ddot{u}_n + \gamma \Delta t\, \ddot{u}_{n+1} \tag{4.7}$$

$$u_{n+1} = u_n + \Delta t\, \dot{u}_n + \frac{\Delta t^2}{2}\left((1-2\beta)\ddot{u}_n + 2\beta \ddot{u}_{n+1}\right) \tag{4.8}$$

$$M\ddot{u}_{n+1} + C\dot{u}_{n+1} + f^{\text{int}}(u_{n+1}) = f^{\text{ext}}_{n+1} \tag{4.9}$$

This algorithm is part of Direct Time Integration Methods useful for the solution of the dynamic equation *(4.6)* by means of the acting force discretization.

Once the force has been sampled, displacements, velocities and accelerations of the system are obtained at each discrete time instant by using:

- equations of motion in the present and in the future (4.6; 4.9);
- initial conditions of the system;
- expressions to the differences (4.7; 4.8).

Entering into the specifics of the Newmark's method, this is nothing more than the generalization of the Implicit Methods, that is the family of algorithms that express future states as a function of the state parameters in the past, present and future (differently from the explicit ones, e.g. Method of Finite Differences, which use only the state parameters in the past and present).
The definition of the Newmark's algorithm as a generalization of the Implicit Algorithms is due to the fact that, by varying the values of γ and β, it can obtained methods such as, for example, the Average Acceleration one (γ = 0.5; β = 0.25) or the Linear acceleration one (γ = 0.5; β = 0.167).
The chosen parameters remains the default one of the Software (Method of the Average Acceleration).
This setting is maintained since this method is considered unconditionally stable: even in the case of accidental errors such as the presence of noise or signal truncation errors, the result does not change regardless of the length of the time-step.

4.4.2 Sampling Time

The importance of choosing the Integration Time Step Δt is linked to the fact that it affects the accuracy of the analysis and then its ability to strive for the exact solution.
Δt should be small enough to be able to capture the response frequency: different types of loads excite different natural frequencies of the structure and the response frequency is the weighted average of all the excited frequencies.
To define the Δt, the reference is made to the frequency on which the fiber optic sensors work.
In particular, their function is based on the introduction of light inside the fiber and takes place at certain frequencies around 1000 Hz. From this frequency, we obtain the Δt to be used in the analysis and which reflects the real case (Δt=0.001s).
Since it was decided to use the Newmark algorithm for carrying out the analysis, the procedure for validating the Δt value is based on the Stability Criterion for Newmark Method *(4.10):*

$$\frac{\Delta t}{Tn} = \frac{1}{(\pi * \sqrt{2})} * \frac{1}{\sqrt{\gamma - 2\beta}} \tag{4.10}$$

In this case, as can be proved, by inserting the γ and β values adopted in the analysis (respectively 0.5 and 0.25), for any Δt value the method remains stable and therefore 0.001s can be considered acceptable.

Regarding the total duration of the simulation, this must be chosen so as not to lose useful information and therefore not to run into problems of sub-sampling.
For this purpose the Nyquist Theorem, which defines the frequency with which a limited-band signal must be sampled in order not to lose information, is used.
This frequency, also called "Nyquist" frequency, must be at least double the signal band *(4.11):*

$$f_s > 2B_f \tag{4.11}$$

Resuming *Table 4.2*, it is clear that in order to not incur any type of error, it is necessary to consider the lowest expected frequency (0.05 Hz) which leads to obtaining a total time of 20 seconds.
This means that in carrying out the analysis, the Software approaches a number of 20000 iterations (20s/0.001s).

4.4.3 Damping Coefficients

Giving an approximate form to the damping matrix of the system is necessary since, in addition to a complex evaluation of this, not being diagonalizable, it does not allow to decouple the equations of motion in MDOF systems.
Ansys Mechanical APDL uses as the form of the Viscous Damping Matrix the approximate one defined in the Rayleigh- or Proportional Damping- Method *(4.12):*

$$[C]= \alpha[M] + \beta[K] \tag{4.12}$$

Where [M] and [K] are the Generalized Mass and Stiffness Matrices, respectively.
Consequently the matrix [C] (Generalized Damping Matrix) is nothing more than a linear combination of the other two matrices. In order to define the multiplicative coefficients α and β we refer to *(4.13; 4.14)* where the first two vibrating modes are compared:

$$\alpha= \zeta\,(2w_i w_j)/(w_i+w_j) \tag{4.13}$$

$$\beta = \zeta\,/(w_i+w_j) \tag{4.14}$$

Where the Relative Damping ζ (0.03) is considered constant for the first two modes of the system.
The identified values correspond to α = 0.449317 and β = 0.001995.

4.5 Output

Everything contained in this chapter concerns the analysis of the structure both in the undamaged condition and in the various expected damage scenarios.
As already mentioned, the analyzes of the different health conditions of the structure and the relative results have been studied separately, correlated just later in the Post-Processing phase *(chapter 5 - Data Processing).*

4.5.1 Data Acquisition by Fiber Optic Sensor

As already introduced in *chapter 4.1 - Materials and Geometry*, in this thesis work a monitoring using fiber optic sensors is being simulated.
In particular, the monitoring of Buried Pipeline through this type of sensors was studied in [27] and here we limit ourselves to introducing the general concepts.

The use of distributed optical fibers is justified by the type of structure and in particular by its geometry which, having a preponderant dimension (longitudinal) compared to the others and considering the uncertainty linked to the location of the damage, needs to be monitored continuously as well as from a temporal point of view, also in terms of spatiality.

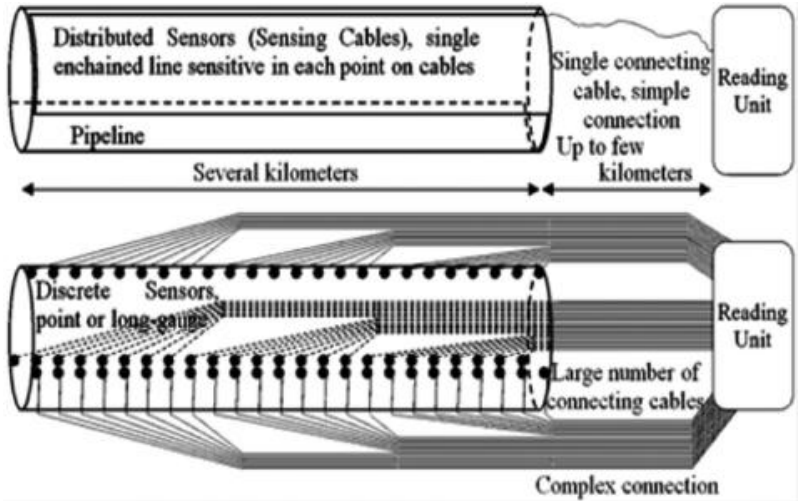

Figure 4.11 Schematic drawing of distributed and discrete monitoring [27]

The advantage of using this type of sensor is given by the fact that it perfectly replaces the discrete ones, but needs a single cabbage in order to transmit information (unlike the discrete ones that need a mean for data transfer for each single sensor).

In general, fiber optic sensors exploit variations in the propagation of light within them. These variations can be correlated with the elastic deformation of the fiber and can concern delays in propagation or wavelength.
There are three operating principles of optical fiber sensors: Rayleigh scattering [34]; Raman scattering [35] and Brillouin scattering [36]. The latter is the type of function that is preferable to

adopt for monitoring the damage status of the Buried Pipeline because it is able to evaluate the deformation of the fiber with a spatial resolution of less than one meter over distances of several kilometres, depending on the "step" between frequencies. Furthermore, it is also possible to correlate the deformation of the fiber with that of the monitored body through the introduction of a corrective factor identified by measuring the temperature.

The accuracy of the sensors strictly depends on the type used [37] and can range from estimated error limits between ±20 με in "Tape" Sensors up to errors greater than 50 με in "Cord" Sensors.

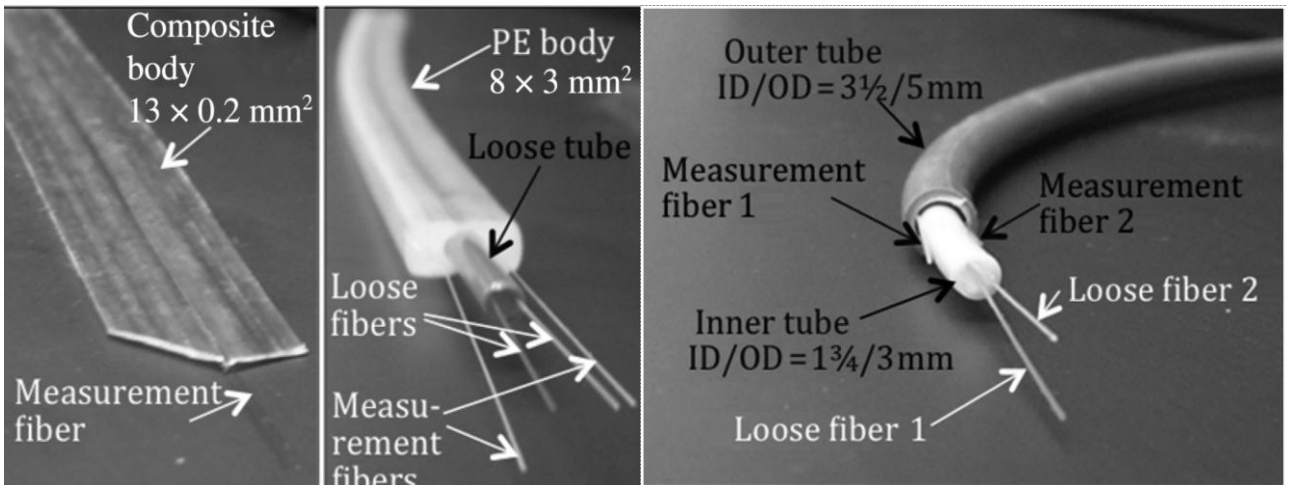

Figure 4.11 Tape sensor (left); Profile sensor (centre) and Cord sensor (right) [27]

The one just described corresponds to the real scenario that in this work, through finite element modelling and analysis, we tried to simulate.
The data obtained from the simulation correspond to the values of displacements in the longitudinal direction of the BEAM188 element (Fiber Optic) points.

In the real case, these sensors, distributed along the entire extension of the structure and positioned as shown in *Figure 4.9*, allow to identify the deformation values of the structure.
Consequently it may seem that there is a contradiction between the output of this monitoring simulation (Displacement) and what is obtained in the real monitoring (Deformation).
This discrepancy can be easily overcome by deriving the displacements in the Post-Processing phase.

4.5.2 Data Fusion

Once the analysis is finished, the Data Acquisition phase can be considered completed and the Data Fusion phase can be defined (*1.2.1-Procedure of SHM*).
In a real Structural Health Monitoring procedure, the Data Fusion phase is foreseen in the post-processing of data obtained during the monitoring operations. In particular, once the data are obtained, they are assembled in order to get the optimal shape to be processed.
In this case study, on the other hand, since there is no real monitoring but just a simulation through Finite Elements Analysis, we can organize the format of the output even before its extrapolation.

What it is obtained is a matrix whose columns correspond to the result on the individual monitored points and the rows define the variability of these results over time.
Each analysis carried out on the damaged models and the undamaged one allows to obtain a matrix of results relating to the specific state of health studied.
These matrices, identified separately, will be compared in the Post-Processing phase.

5. DATA PROCESSING

Once the displacement values have been obtained from the monitoring simulation by means of FEM analysis, the Data acquisition and Data fusion phases are concluded.

Leaving aside the steps related to Data Normalization and Data Cleansing, given that it is studied an analytical model not affected by problems related to uncertainties, and also Data Compression because it is superfluous in the case study; it can be considered directly the phase concerning the Feature Extraction.
Everything described in this chapter was developed using the *MATLAB R2019b* programming and numerical calculation platform.

5.1 Wiener Entropy - Feature Extraction

The first main step after the Monitoring and Data Acquisition phase is to calculate the Damage-Sensitive Feature through which we try to understand the damage characteristics.
In the specific case, the Feature to be extracted is the Wiener Entropy, of its *formula (2.3)* is re-proposed:

$$H_w = Q \frac{\sqrt[Q]{\prod_q S(q)}}{\sum_q S(q)} \tag{2.3}$$

5.1.1 Editing of Input data

In this preliminary phase, the Input data (which correspond to the Output matrices obtained from the analyzes in Ansys) inserted in Matlab are manipulated in order to obtain values that are congruent with those that would be obtained in real monitoring by optical fibers.

The Input matrices, which represent respectively the undamaged situation and the damaged one, have a dimension T x N with T = 20000 (number of iterations) and N = 200 (number of points from which the solution was extracted).
The matrices, named *"Disp_pre_damage_Z"* and *"Disp_post_XXdamage_Z"* (in which XX corresponds to the reduction of stiffness applied to the elements of the Pipeline that we wanted to simulate damaged), undergo an operation of derivation with respect to the space.

This manipulation of the values serves to pass from the displacement values (obtained by Ansys) to the deformation values (which would be obtained from a real monitoring process with fiber optic sensors):

```
Disp_pre = load('Disp_pre_damage_Z.txt');
Disp_post = load('Disp_post_XXdamage_Z_.txt');

Strain_pre = gradient(Disp_pre);
Strain_post = gradient(Disp_post);
```

Where dz is the distance between two adjacent acquisition points.
The new matrices *"Strain_pre"* and *"Strain_post"* have always a dimension of T x N.

5.1.2 Addition of White Noise

Subsequently, in order to obtain results comparable with those obtainable with real monitoring, a Gaussian white noise is added to the values of the new matrices:

```
for pnne = 1:length(noisV)
nois = noisV(pnne);
Strain_t0 = [Strain_pre-nanmean(Strain_pre) ; Strain_post-
nanmean(Strain_post)];
Strain_t = Strain_t0 +  (nois/100)*( min(Strain_t0) + (max(Strain_t0)-
min(Strain_t0)).*rand(size(Strain_t0)) );
Z = (0:NpF-1)*dz;
Strain_t_dx = Strain_t(:,1:NpF);
Strain_t_up = Strain_t(:,NpF+1:2*NpF);
Strain_t_sx = Strain_t(:,2*NpF+1:3*NpF);
Strain_t_do = Strain_t(:,3*NpF+1:4*NpF);
end
```

In the code above it is found:

- NoiseV: indicates the standard deviation of Gaussian white noise, expressed as a percentage of the Input signal. Values for 0% / 3% / 5% / 10% are investigated;
- NpF: Number of points (50) for each of the 4 optical fibers positioned on the Pipeline;
- dz: Step between acquisition points (0.1 m).

In this way, 4 deformation matrices are obtained, respectively measured on the points of the 4 sensors distributed in optical fiber (see Figure 4.9):

- Strain_t_dx: displacements measured by the sensor placed at 0 ° of the cross section;
- Strain_t_up: displacements measured by the sensor placed at 90 ° of the cross section;
- Strain_t_sx: displacements measured by the sensor placed at 180 ° of the cross section;
- Strain_t_do: displacements measured by the sensor located at 270 ° of the cross section.

Therefore, starting from the two initial displacement matrices, we are brought back to a single "Strain_t" matrix containing the two initial matrices and having a dimension of 2TxN.
The values of this last matrix differ from the two initials for its values which can be considered "dirty" respect to the starting ones. The "Strain_t" matrix is finally divided into four sub-matrixes of size 2Txn in which n is the number of acquisition points for the single optical fiber (50).

5.1.3 Calculation of the Wiener Entropy

Once obtained the undamaged and damaged state data for the four separate sensors, we can move on to the evaluation of the Wiener Entropy by mean the power spectrum of the time-domain signal which is the distribution of power contained within the signal over frequency, based on a finite set of data.. This operation is made possible thanks to the Matlab dsp.SpectrumAnalyzer System Tool.

```
ISF_dx = [];
ISF_up = [];
ISF_sx = [];
ISF_do = [];
for ii = 1:NpF
    [P,~,~] = pspectrum(Srain_t_dx(:,ii),fs,'spectrogram');
    ISF_dx(:,ii) = (geomean(P)./nanmean(P)).';
    [P,~,~] = pspectrum(Srain_t_up(:,ii),fs,'spectrogram');
    ISF_up(:,ii) = (geomean(P)./nanmean(P)).';
    [P,~,~] = pspectrum(Strain_t_sx(:,ii),fs,'spectrogram');
    ISF_sx(:,ii) = (geomean(P)./nanmean(P)).';
    [P,~,T] = pspectrum(Srain_t_do(:,ii),fs,'spectrogram');
    ISF_do(:,ii) = (geomean(P)./nanmean(P)).';
end
```

The P matrix contains the values that define the Power Spectrum of the signal *(5.1)* while the ISF are the matrices containing the Wiener Entropy values for each acquisition point at any instant of integration time defined in T.
T is a vector of time instants corresponding to the centers of the windowed segments used to compute short-time power spectrum values.

$$E_s = \|\mathbf{s}\|^2 = \int_{-\infty}^{\infty} s^2(t)\,dt \tag{5.1}$$

The power spectrum can be defined as the energy of the signal and can be interpreted as the sum of infinite contributions of the signal at different frequencies.

5.2 Feature Discrimination

Feature Discrimination is that phase of data processing in which the algorithm to treat the damage-sensitive feature (in this case the Wiener Entropy) is defined in order to make the result clear.
In particular, we try to give a shape / representation of the feature such as to be able to easily grasp any damage scenarios by defining at least their presence and position (first two levels of the Rytter hierarchy).

In order to obtain a clear view of the damaged state of the structure, also defining the differences between the initial undamaged state and the final damaged one, it was decided to represent the trend of the Wiener Entropy function (ISFs in the code) in a three-dimensional space whose axes are represented respectively by the absolute value of WE; time and space (position with respect to the structure).
The construction of the ISF is such as to allow in the representations to have a fictitious monitoring of 40s: this means that the trend of the WE is not defined on a time axis equal to that defined in the single FEM analysis (20s) but two analyzes relating to the initial and final state of the Pipeline are merged in succession. The purpose of this operation is to make clear the difference between the structural condition before 20 seconds (first Finite Element Analysis for undamaged state) and after 20 seconds (second FEA for damaged structure).
In this way, by manipulating the input data of two separate analyzes, it is possible to simulate a single analysis in which, at the instant immediately following the twentieth second, the damage occurred.

First of all, a for loop is set up. There, the *ISF_2* matrices which contain the Wiener Entropy values to be inserted in the graphs are constructed: in each iterative loop, defined on the centre T-ith of the windowed segments used to compute short- time power spectrum values, an *ISF_temp* vector is created containing the WE values for each time step; then we move on to the function with which to correlate the values of WE in the *ISF_temp* to the *Z* position, defined Smoothing Spline *(5.2):*

$$p\sum_i w_i(y_i-s(x_i))^2+(1-p)\int(d^2s/dx^2)^2dx \qquad (5.2)$$

This function is used in case the data is noisy. The smoothing spline s is constructed for the specified smoothing parameter p and the specified weights wi. If the weights are not specified, they are assumed to be 1 for all data points. $p = 1$ produces a cubic spline interpolant.

Once the smoothing spline has been identified (*fitresult* in the code), the *ISF_2* matrix is constructed. The values contained in the matrix are obtained by intersecting the interpolating function with the values of *Zfit* (vector containing a number of positions equal to the number of integration time windows T, expressed as a function of T and Z).

```
ISF_dx2 = [];
ISF_up2 = [];
ISF_sx2 = [];
ISF_do2 = [];
Zfit = (0:length(T)-1)/(length(T)-1)*Z(end);
parfit = 1;
for ii = 1:length(T)
    ISF_temp = ISF_dx(ii,:);
    [xData, yData] = prepareCurveData( Z, ISF_temp );
    ft = fittype( 'smoothingspline' );
    opts = fitoptions( 'Method', 'SmoothingSpline' );
    opts.SmoothingParam = parfit;
    [fitresult, ~] = fit( xData, yData, ft );
    ISF_dx2(ii,:) = feval(fitresult,Zfit);
    [...] %Also for ISF_up2
    [...] %Also for ISF_sx2
    [...] %Also for ISF_do2
end
```

The one described in the code above is repeated ([...]) inside the for loop for all the remaining data *(ISF_up; ISF_do; ISF_sx).*

The last step before setting up the representations is to define normalized ISF values. In this way it is possible to represent both the WE in absolute value and the variation of the WE values.

```
ISF_norm = [];
ISF_norm(:,:,1) = 100 * ( ISF_dx2 - ISF_dx2(1,:) ) ./ ISF_dx2(1,:);
ISF_norm(:,:,2) = 100 * ( ISF_up2 - ISF_up2(1,:) ) ./ ISF_up2(1,:);
ISF_norm(:,:,3) = 100 * ( ISF_sx2 - ISF_sx2(1,:) ) ./ ISF_sx2(1,:);
ISF_norm(:,:,4) = 100 * ( ISF_do2 - ISF_do2(1,:) ) ./ ISF_do2(1,:);
```

6. RESULTS

This chapter illustrates the results obtained by the previously defined algorithm.
An attempt is therefore made to carry out an Identification of the Damage by means of a graphical support and the results have been commented to understand what are the observations that can be drawn from it.
The Output Data regarding the comparison between undamaged structure and various damage scenarios applied analytically will be viewed. The damage conditions that we wanted to simulate are congruent to the real ones defined in *3.3.2 - Damage Modes* and in all cases, different reductions in stiffness of the elements was studied.

The results obtained are presented by illustrating the trend of the Wiener Entropy in time and space. In particular, the same three-dimensional graph (WE; t; z) is shown from 4 different views: the first, top left, shows the graph from the top and is the most representative one because it defines a clear view of where the entropy tends to decrease in value due to damage.
The second, top right, is a view of the entropy trend of the point affected by stiffness reduction over time and serves to highlight the decrease of entropy after the application of the damage.
The third view, bottom left, serves to highlight the position in which the entropy tends to vary in value (the entropy values over time, and referred to the single point, overlap so as to determine a "crest" in correspondence of the damage).
Last view of the results, bottom right, is an overview of the three-dimensional graph which is used to visually display the "crest" of entropy variation over time at the damaged points. In particular, it helps to understand how the points affected by damage have entropy values that differ a lot from those of the points that have remained intact ones.

6.1 Cross Section Completely Damaged

In this case we attempts to simulate the damage suffered by the Pipeline at the welded joint in the event of a Stress-Corrosion concomitance.
Below, the results regarding the damage centered in 2.4m of the longitudinal direction of the Pipeline are shown. In particular, the reduction of stiffness concern the entire cross section and therefore the damage affects all four sensors placed on the structure.

6.1.1. 5% Stiffness Reduction

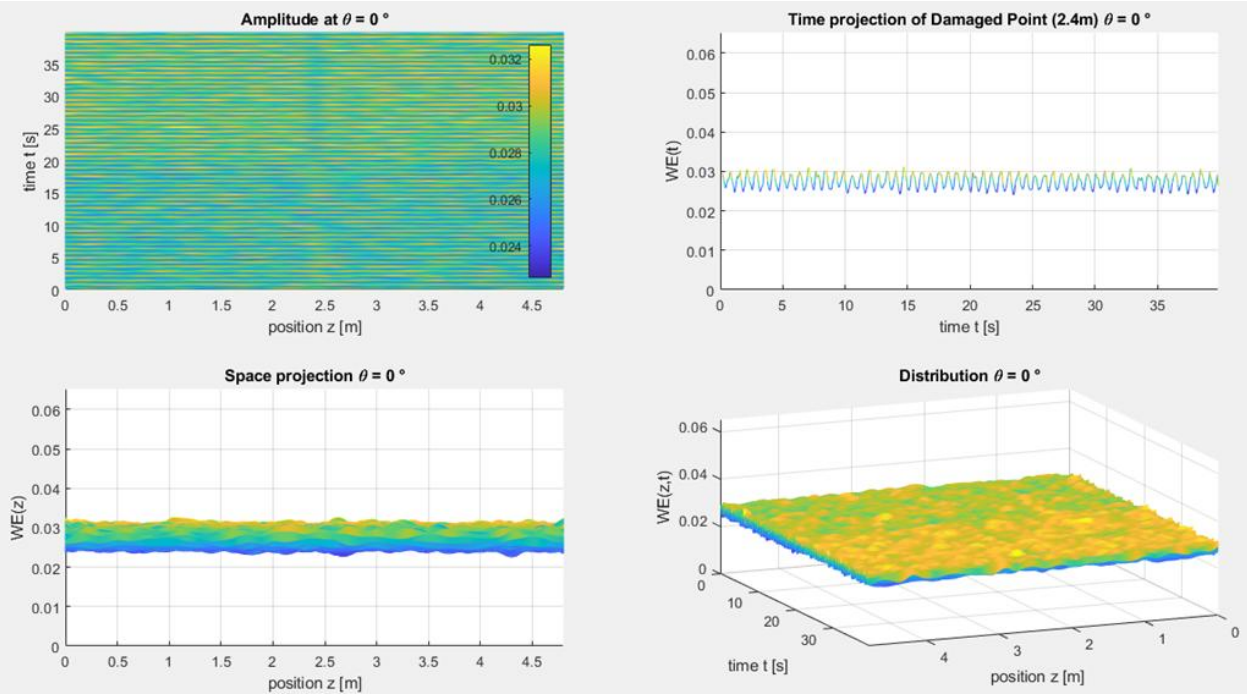

Figure 6.1 Comparison of 0° results (WE) for undamaged- and 5% damaged- cross section with 5% white noise

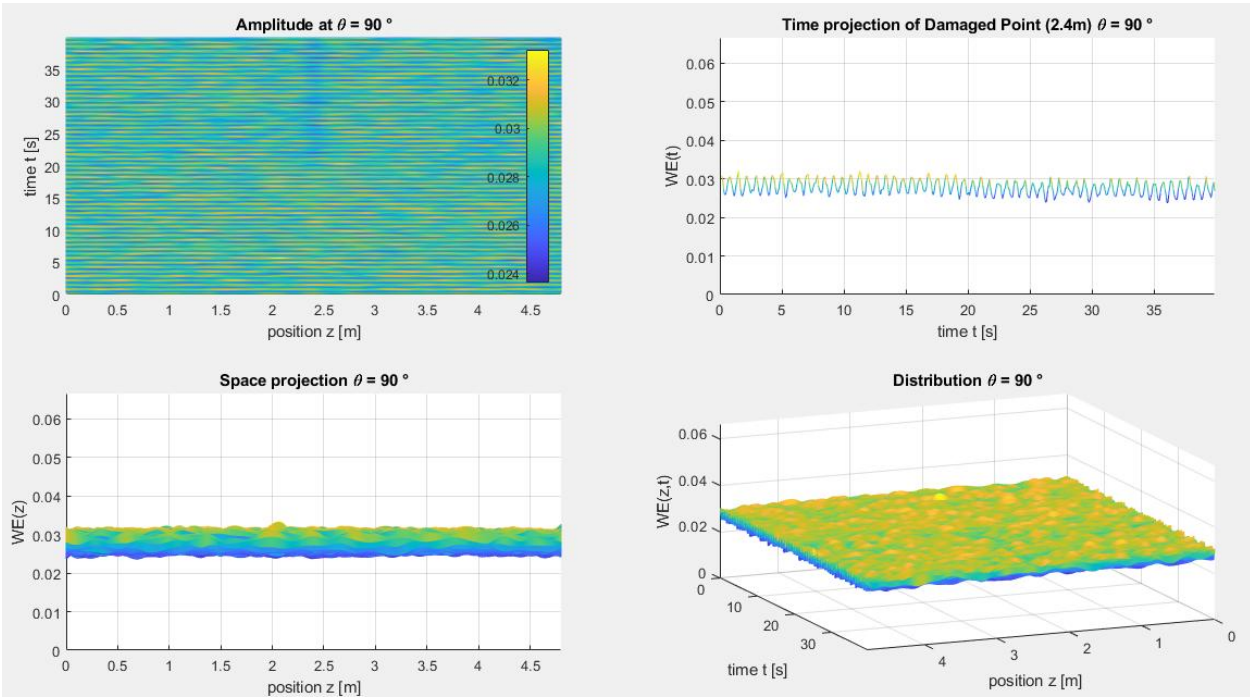

Figure 6.2 Comparison of 90° results (WE) for undamaged- and 5% damaged- cross section with 5% white noise

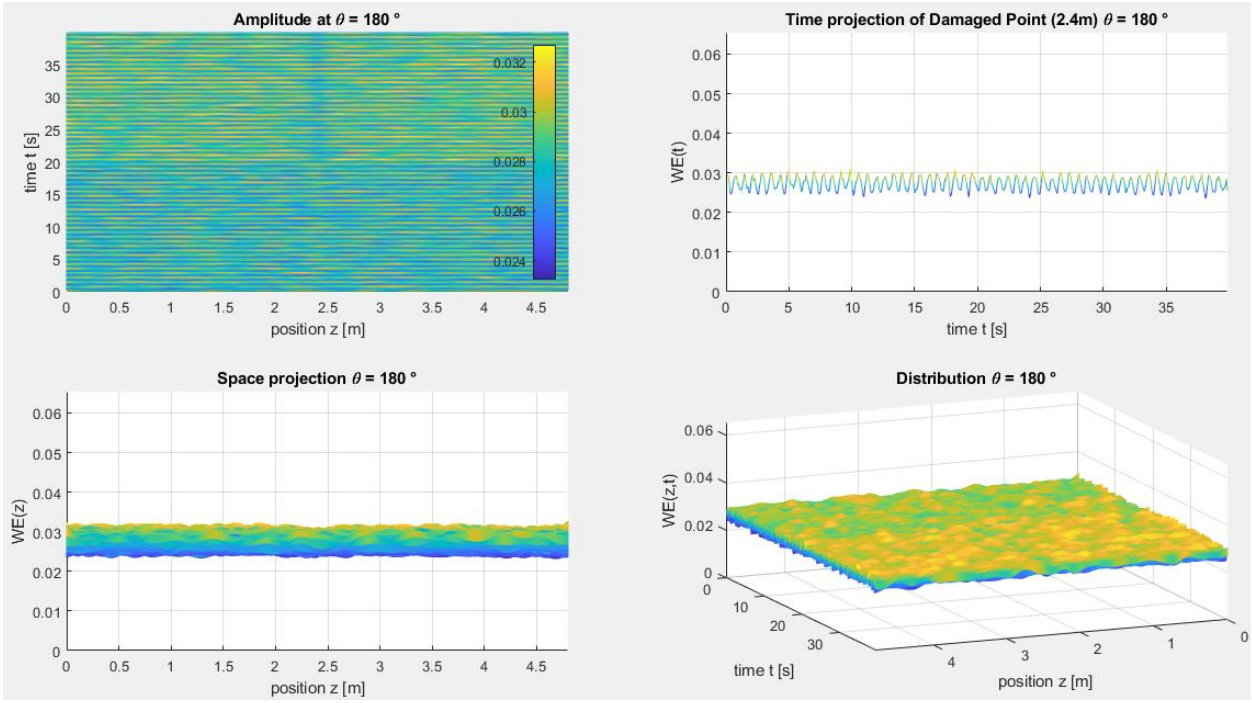

Figure 6.3 Comparison of 180° results (WE) for undamaged- and 5% damaged- cross section with 5% white noise

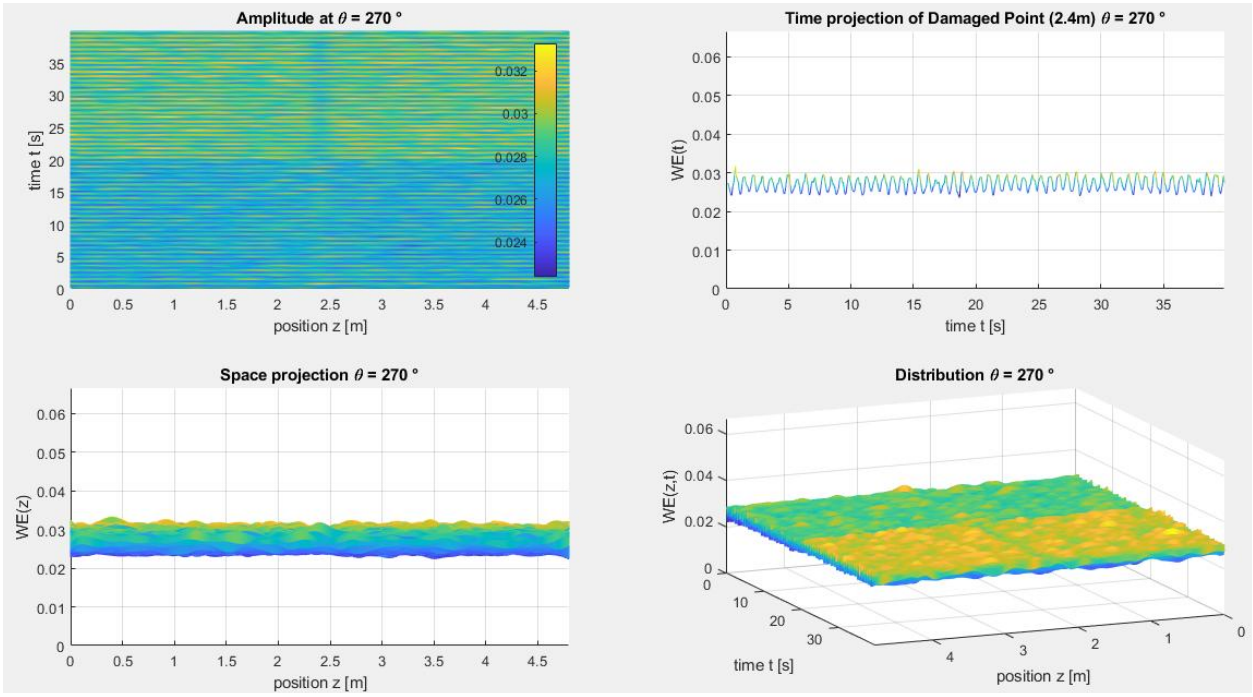

Figure 6.4 Comparison of 270° results (WE) for undamaged- and 5% damaged- cross section with 5% white noise

The graphs above do not show any useful results. Since the noise inside the signal tends to flatten the spectrum, an additional white noise of 15% is applied, reaching a total of 20%.

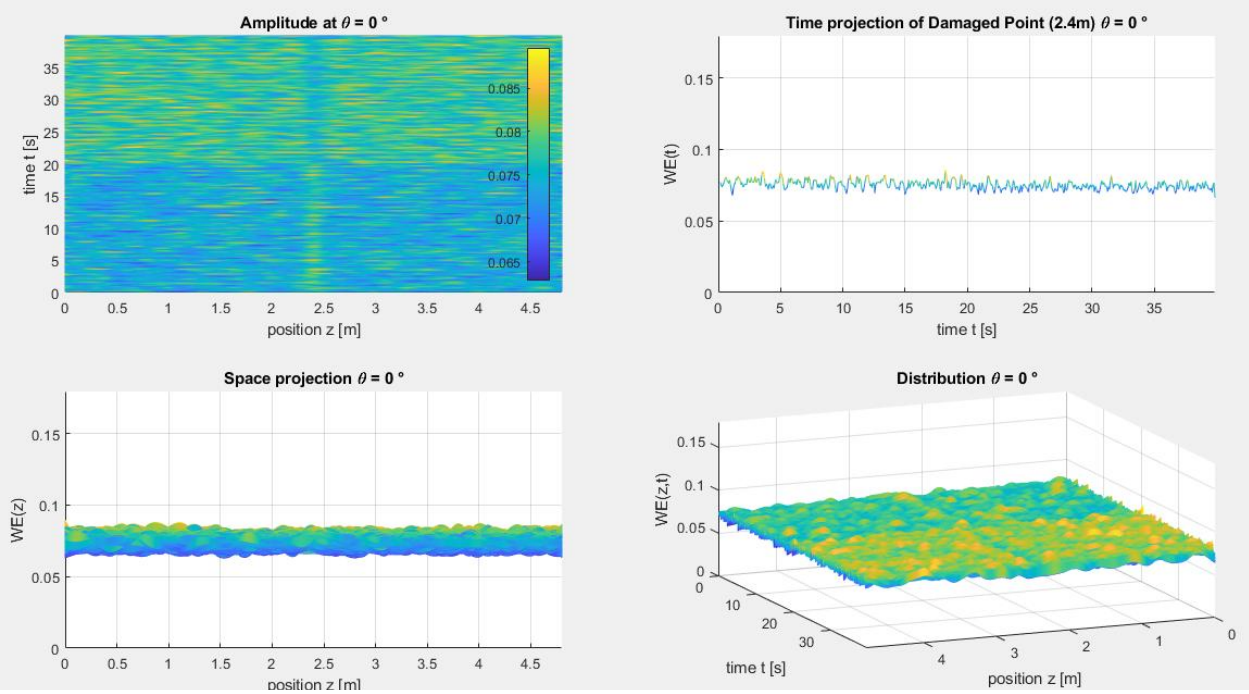

Figure 6.5 Comparison of 0° results(WE) for undamaged- and 5% damaged- cross section with 20% white noise

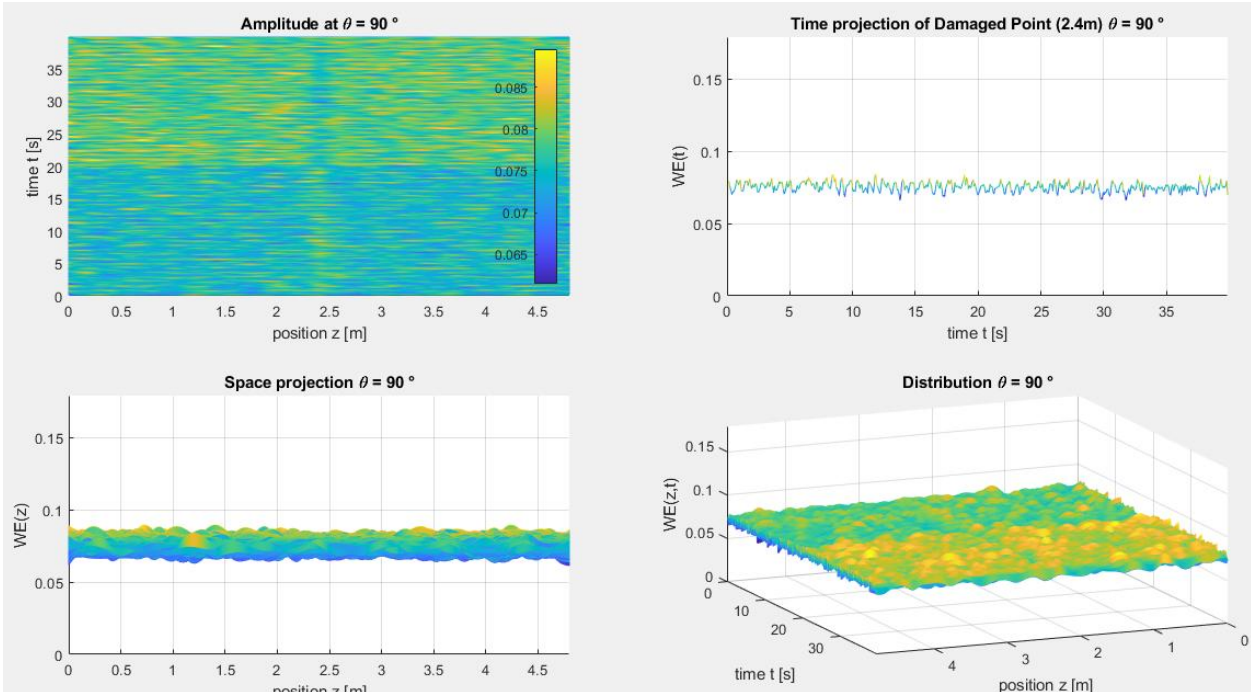

Figure 6.6 Comparison of 90° results (WE) for undamaged- and 5% damaged- cross section with 20% white noise

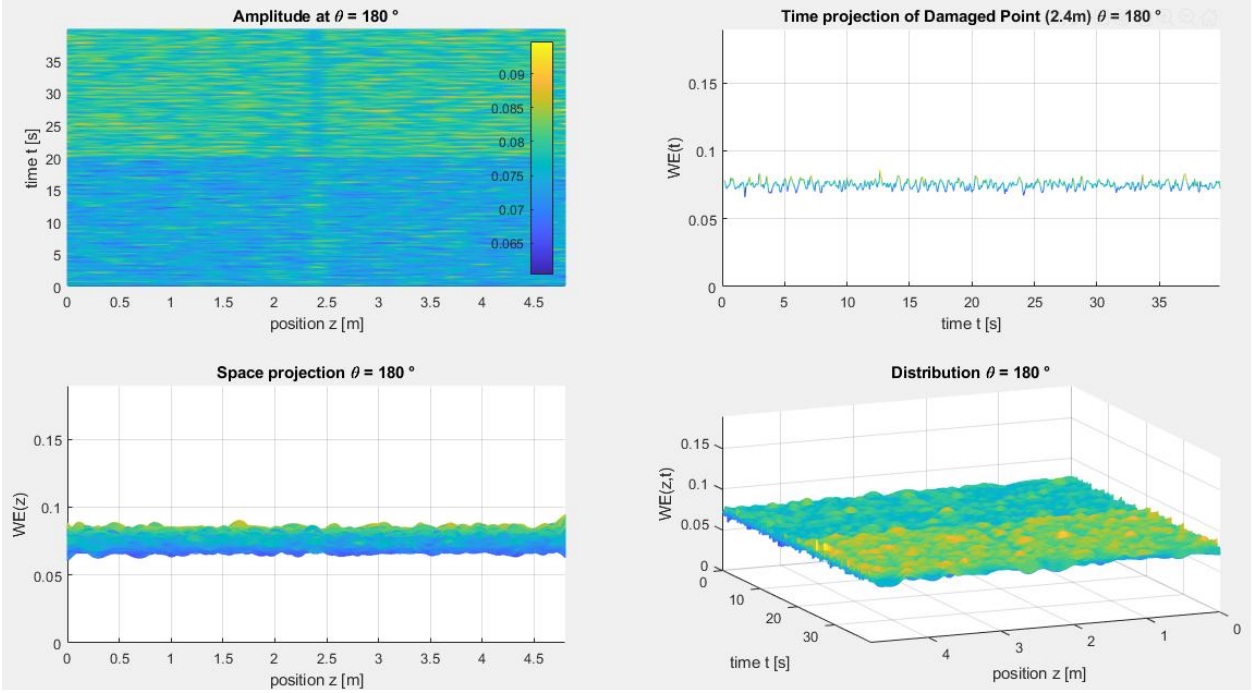

Figure 6.7 Comparison of 180° results (WE) for undamaged- and 5% damaged- cross section with 20% white noise

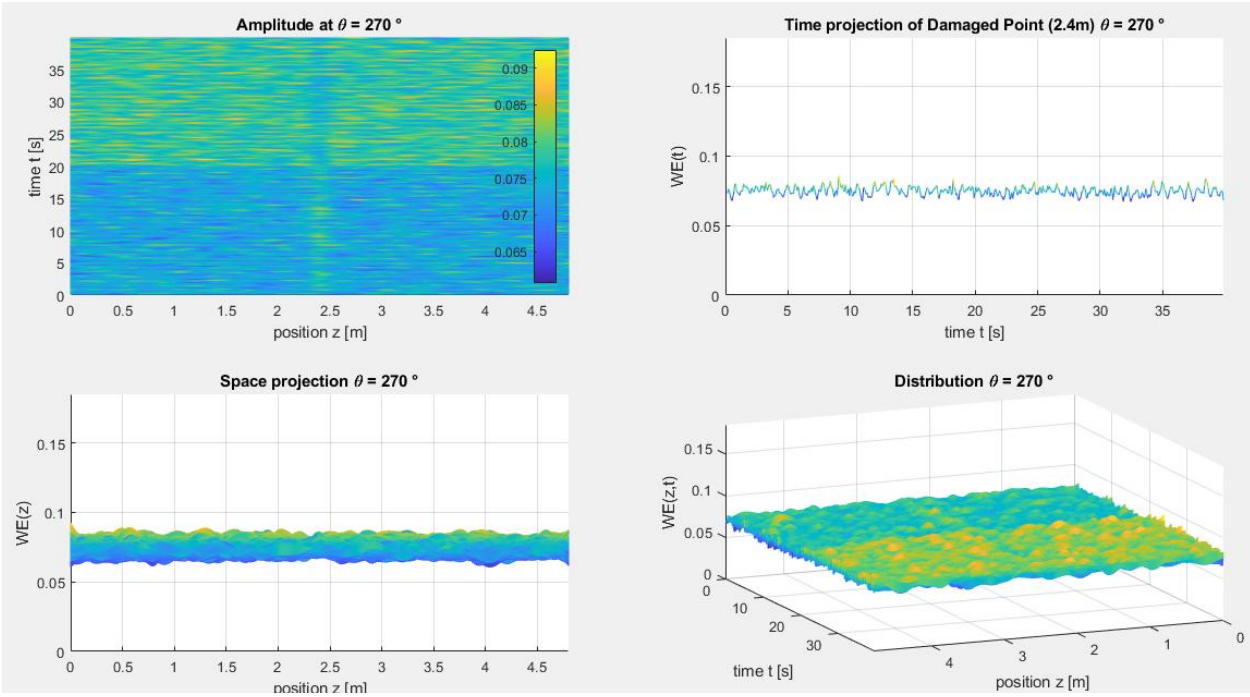

Figure 6.8 Comparison of 270° results (WE) for undamaged- and 5% damaged- cross section with 20% white noise

From the graphs referred to 20% of noise it can be seen how "dirtying" the signal serves to make the results entropy variations more evident. In particular, it is noticeable a decrease of entropy in the damaged area (centered at 2.4m) after the 20th second of the signal (after the application of the damage). In any case, the results obtained with a 5% reduction of section stiffness cannot be considered satisfactory as it is a form of damage too mild.

6.1.2. 20% Stiffness Reduction

At this point an attempt is made to identify a form of damage stronger than the previous one, in particular a stiffness reduction in the cross section of 20% compared to the intact material is studied.

Given the congruence of the results obtained for the 4 optical fibers (we are studying a problem that equally involves the persistence zones of the sensors) we limit to show the graphs concerning the data extrapolated from the 90° point. The considerations consequential the observations of these results can also be associated to the other monitored positions (0 °; 180 °; 270 °).

Also in this case, several graphs are defined, for the same damage scenario, which differ for the percentage quantity of Gaussian white noise introduced inside the signal.

Now, also the graphs concerning the normalized entropy compared to the initial conditions at time 0 (before the energy is administered to the structure) are introduced. With these graphs it is possible to establish the variation of entropy, in percentage, due to the presence of the damage.

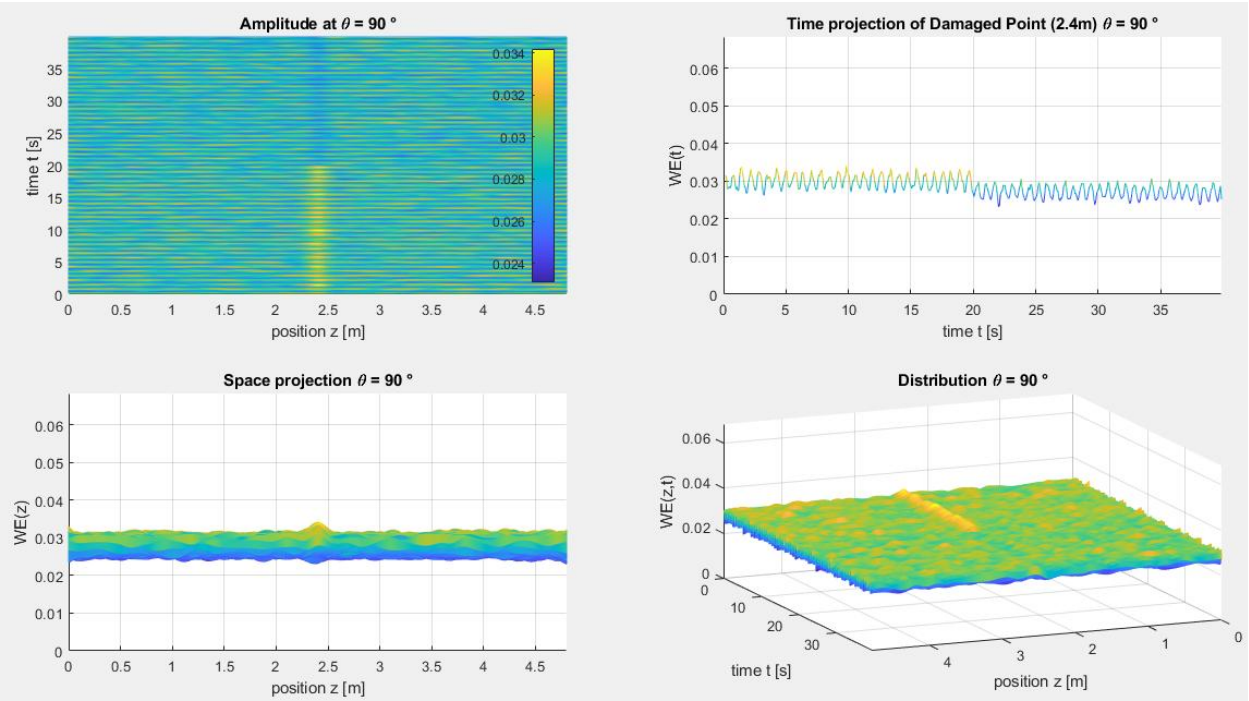

Figure 6.9 Comparison of 90° results (WE) for undamaged- and 20% damaged- cross section with 5% white noise

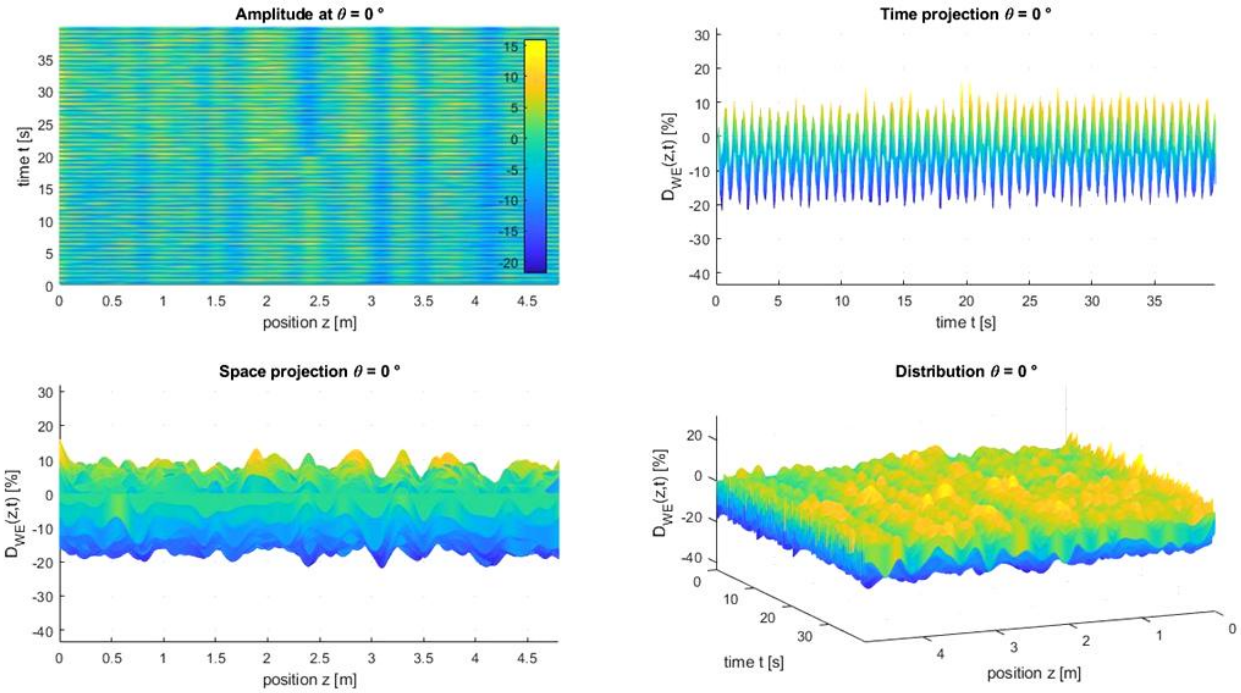

Figure 6.10 Comparison of 90° normalized results (WE) for undamaged- and 20% damaged- cross section with 5% white noise

The results in *Figure 6.9* show a more marked variation of entropy in the damaged area than in the previous case, even though the signal is still quite "clean" with only 5% of white noise.
Wanting to highlight the result even more, as before, 15% noise is added to the signal.

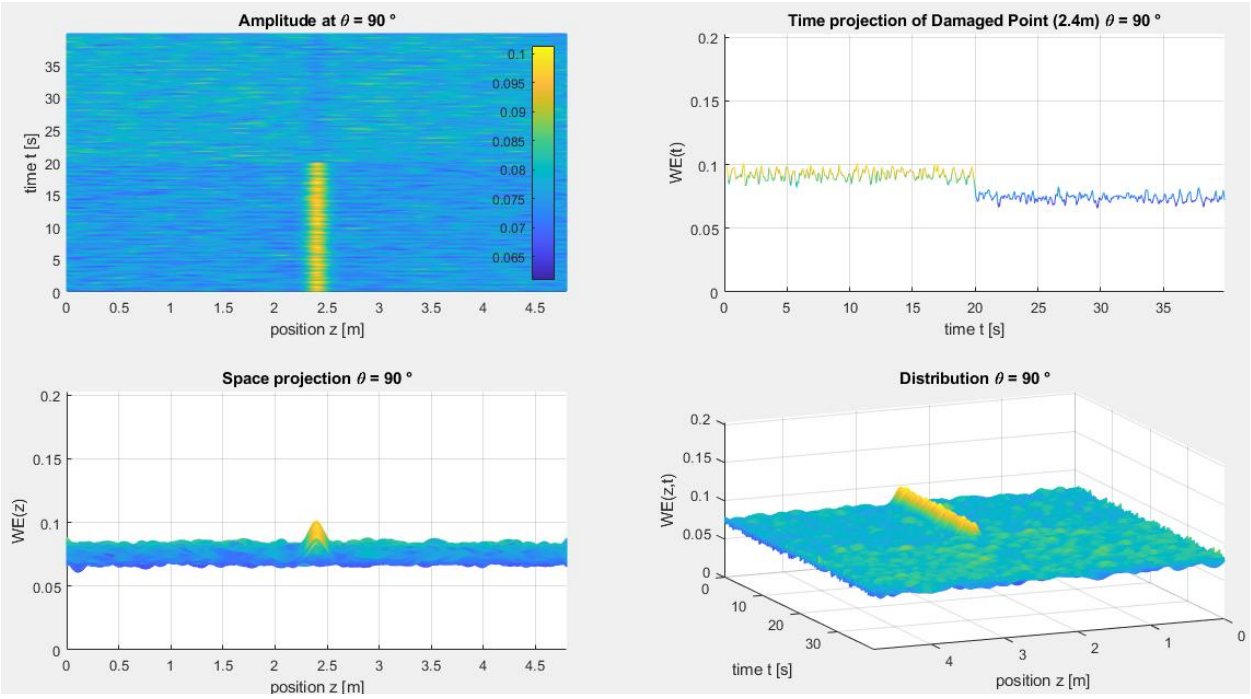

Figure 6.11 Comparison of 90° results (WE) for undamaged- and 20% damaged- cross section with 20% white noise

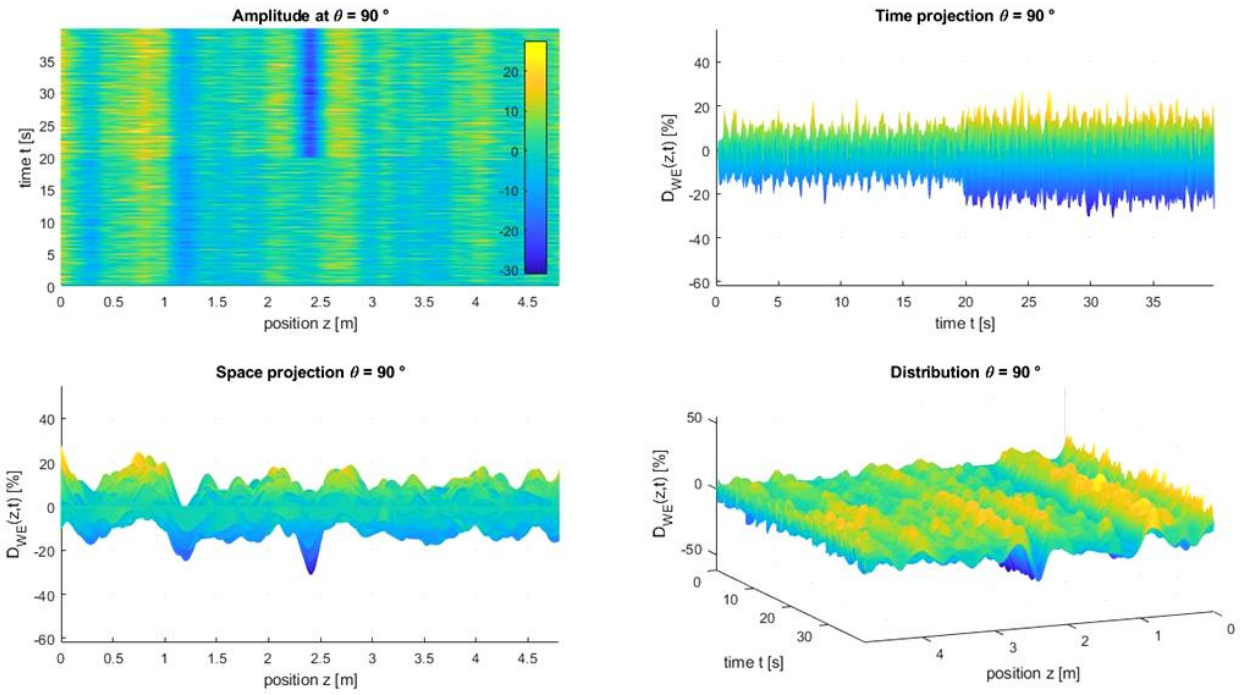

Figure 6.12 Comparison of 90° normalized results (WE) for undamaged- and 20% damaged- cross section with 20% white noise

This is the first time that the area affected by stiffness degradation is clearly highlighted. Moreover, it is possible to notice (from the graph on the top right of *Figure 6.12*) how the global entropy of the system, after the damage occurred, tends to increase in range and decrease in absolute value with respect to the measure referred to the intact structure.

6.1.3. 50% Stiffness Reduction

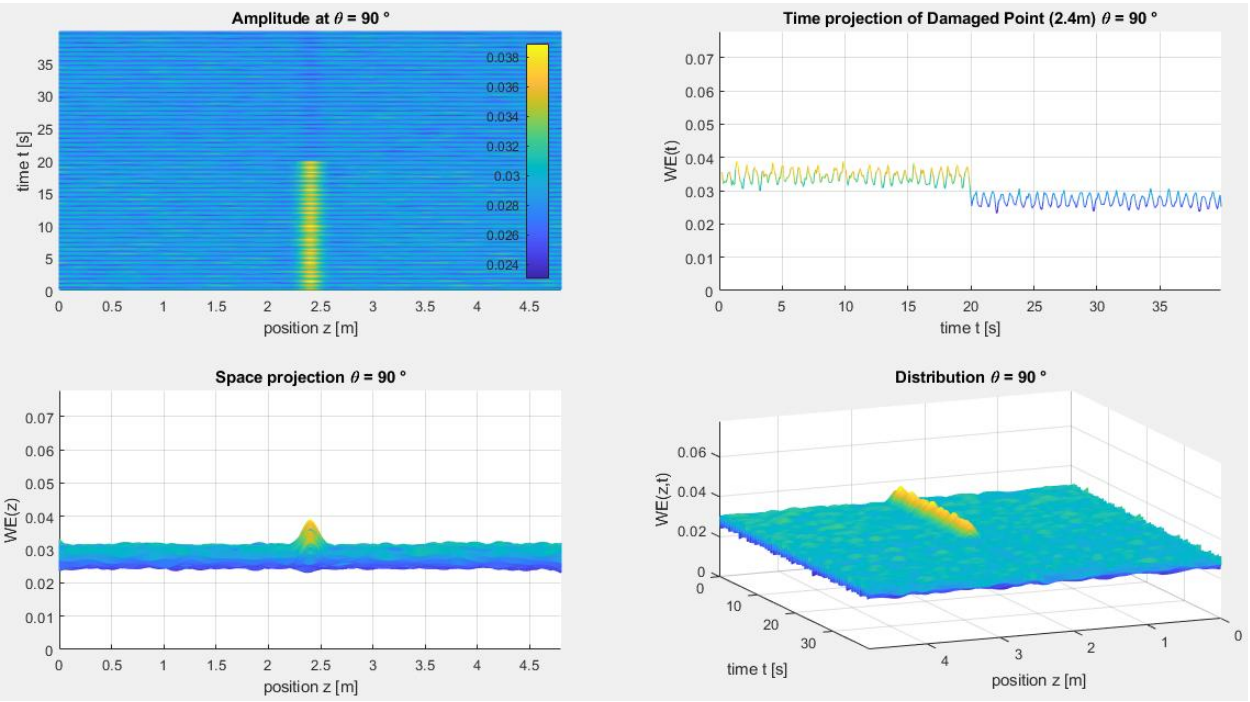

Figure 6.13 Comparison of 90° results (WE) for undamaged- and 50% damaged- cross section with 5% white noise

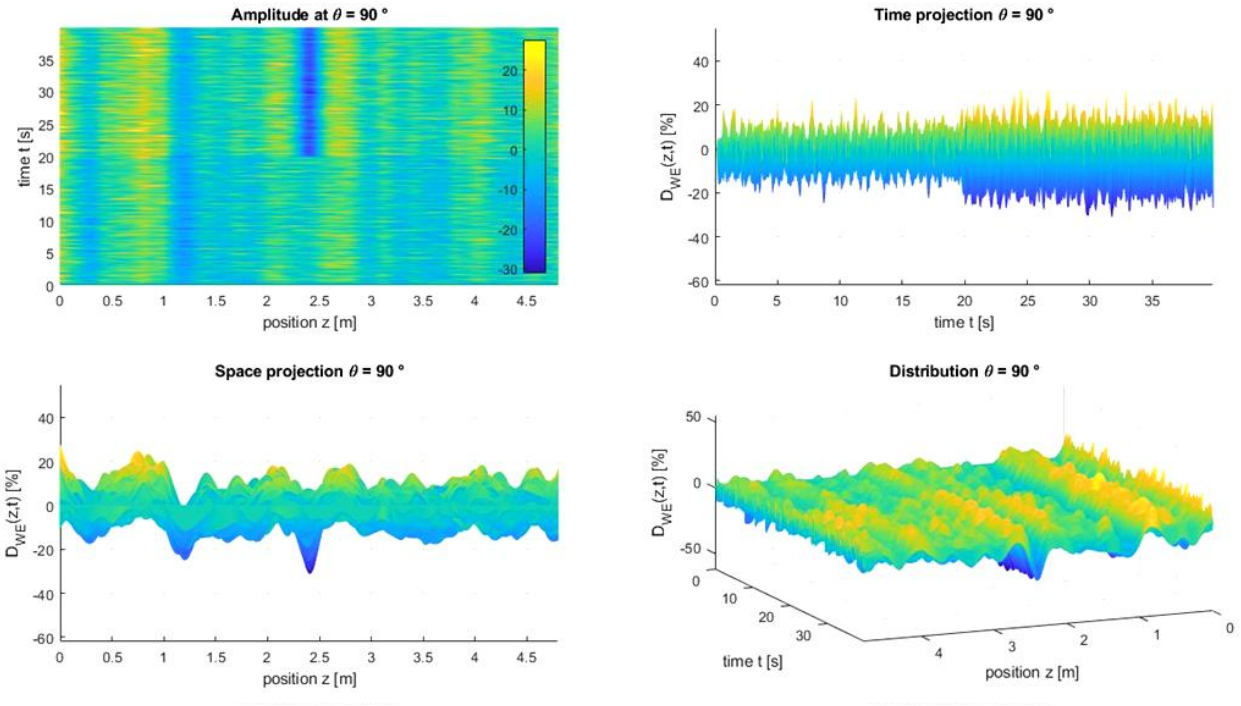

Figure 6.14 Comparison of 90° normalized results (WE) for undamaged- and 50% damaged- cross section with 5% white noise

50% damage with a 5% dirty signal, without having to add additional white noise to locate the area affected by degradation. Then, the 50% stiffness reduction is easily identifiable by applying the concepts of entropy to the pure signal, without having to further modify it.

6.1.4. 70% Stiffness Reduction

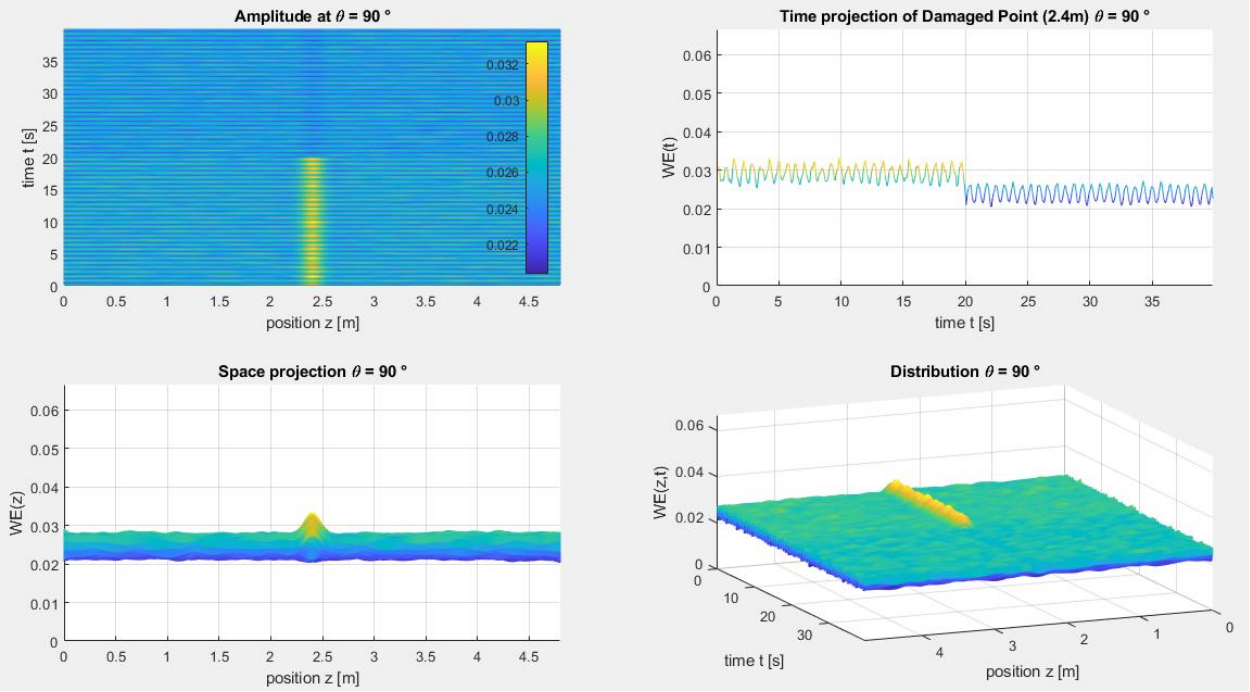

Figure 6.15 Comparison of 90° results (WE) for undamaged- and 70% damaged- cross section with 3% white noise

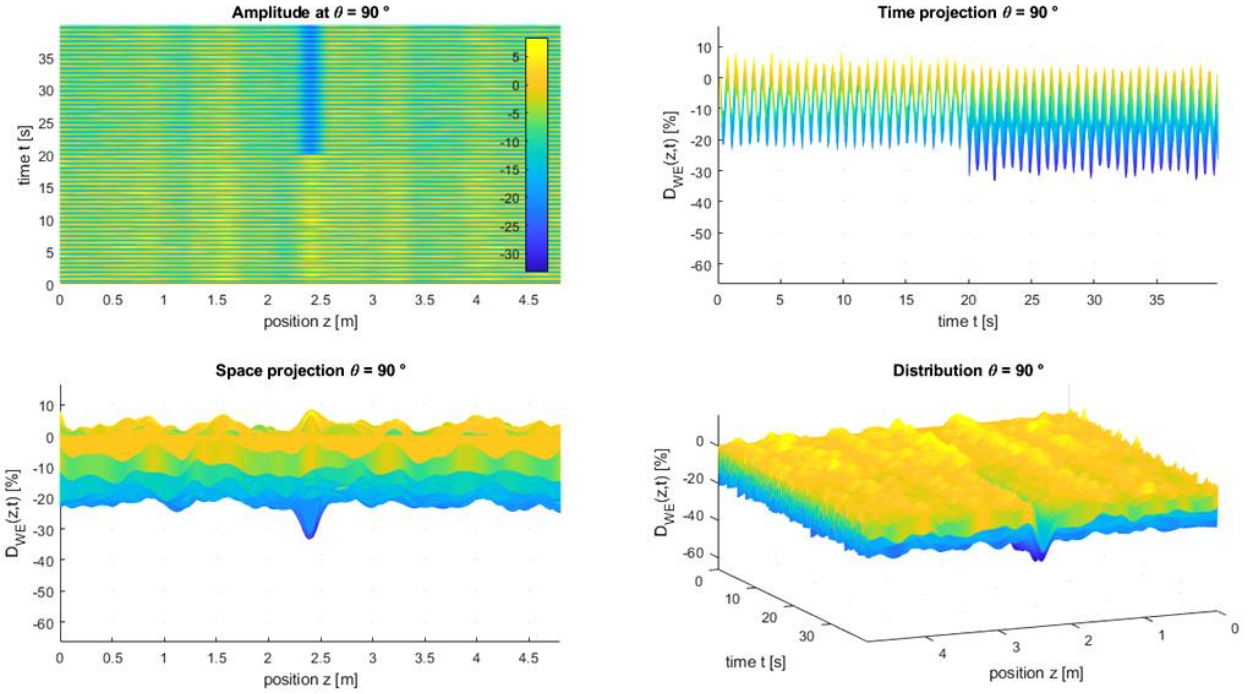

Figure 6.16 Comparison of 90° normalized results (WE) for undamaged- and 70% damaged- cross section with 3% white noise

In the case of damage equal to 70%, damage detection and position are possible even with cleaner signals than those built on data extrapolated from real sensors.

6.2 Single Element Damaged

Once the previous damage case, which presumably represents the most easily identifiable scenario (a totally damaged cross section defines a definitely greater increase in deformability than in the case of a partially damaged portion), has been studied, we try to analyze milder conditions of change in system condition in order to understand what is the applicability and sensitivity of Wiener Entropy as Damage-Sensitive Feature.

In particular, we choose to simulate a pitting corrosion condition, in which the analytically applied damage affects a single finite element 0.087m x 0.1m positioned at 2.4m of the pipeline.

In this first study of pitting corrosion, the damaged element is placed at the 90° point of the cross section, just below the "up" optical fiber.

The percentages of stiffness reduction studied below are only those at 20% and 50% because the Wiener Entropy is too insensitive to sufficiently highlight a variation of the system conditions equal to 5% on a very small geometry and, on the other hand, the 70% damage condition is certainly identifiable if those at 20% and 50% are too.

6.2.1. 20% Stiffness Reduction

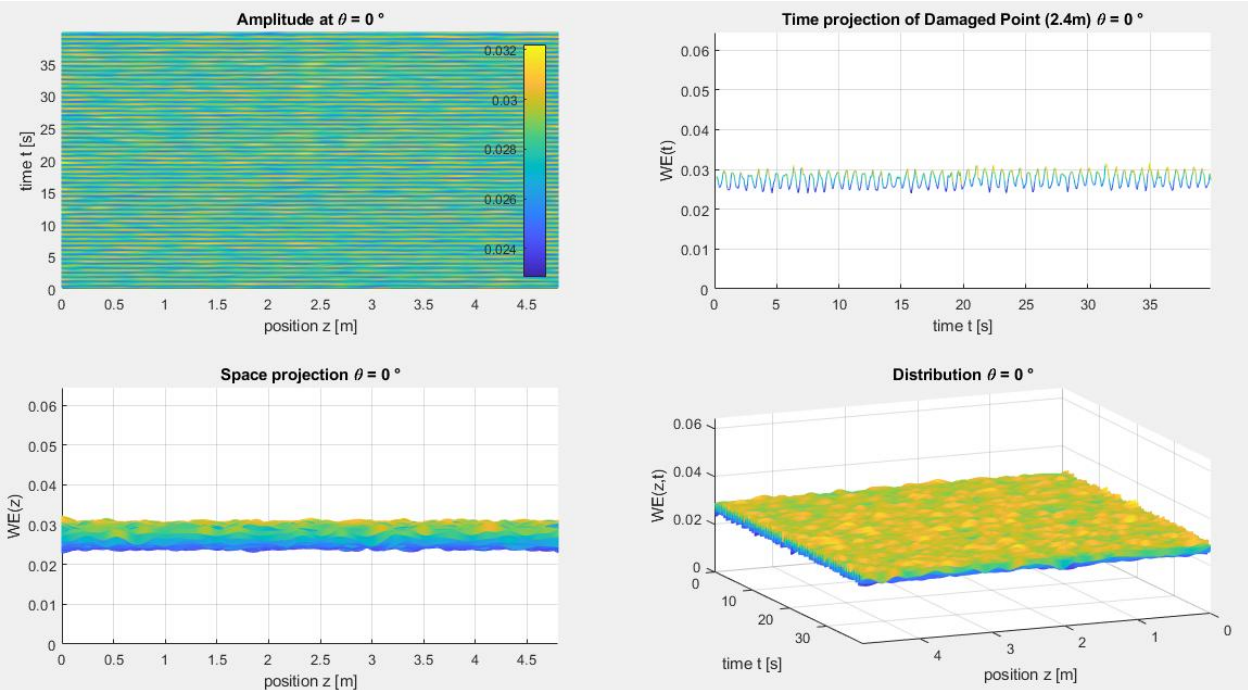

Figure 6.17 Comparison of 0° results (WE) for undamaged- and 20% damaged- single element with 5% white noise

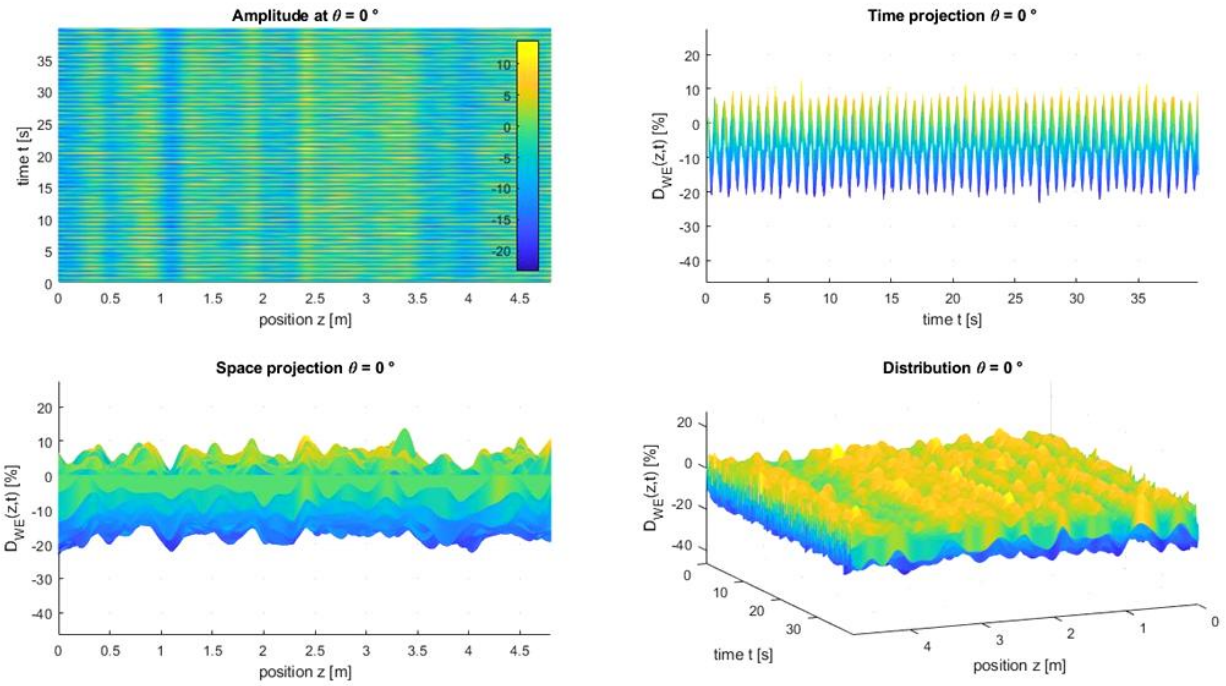

Figure 6.18 Comparison of 0° normalized results (WE) for undamaged- and 20% damaged- single element with 5% white noise

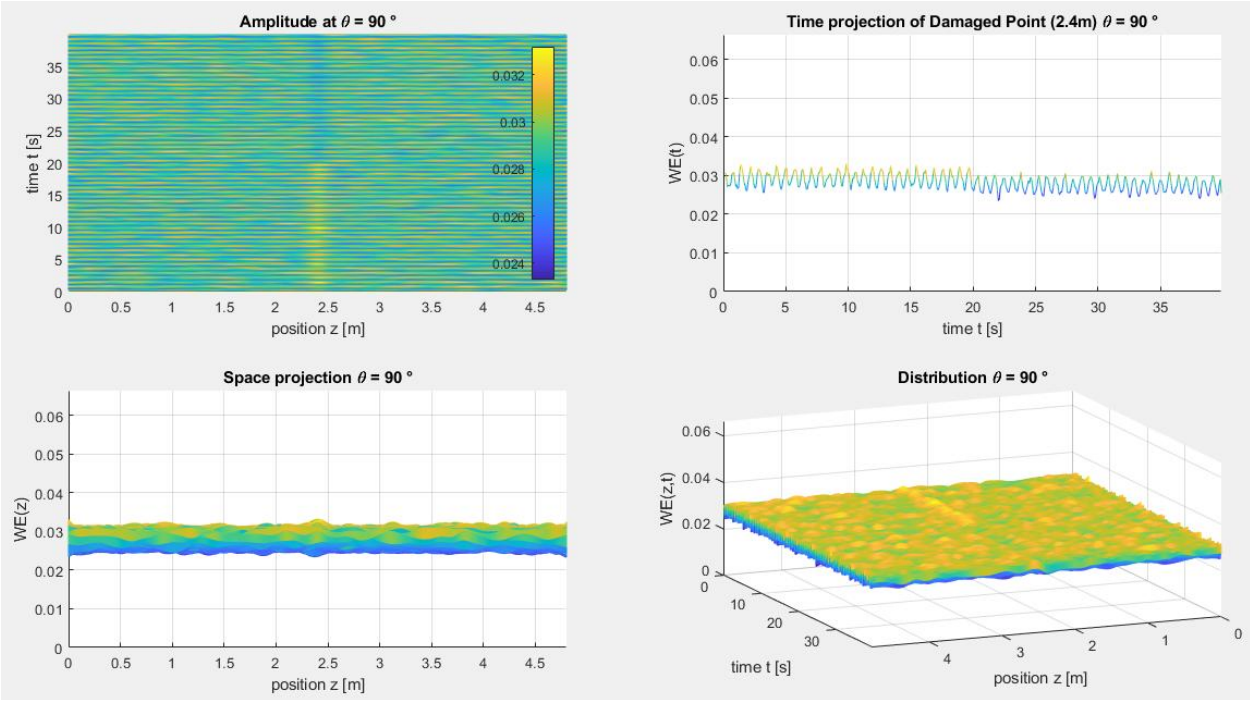

Figure 6.19 Comparison of 90° results (WE) for undamaged- and 20% damaged- single element with 5% white noise

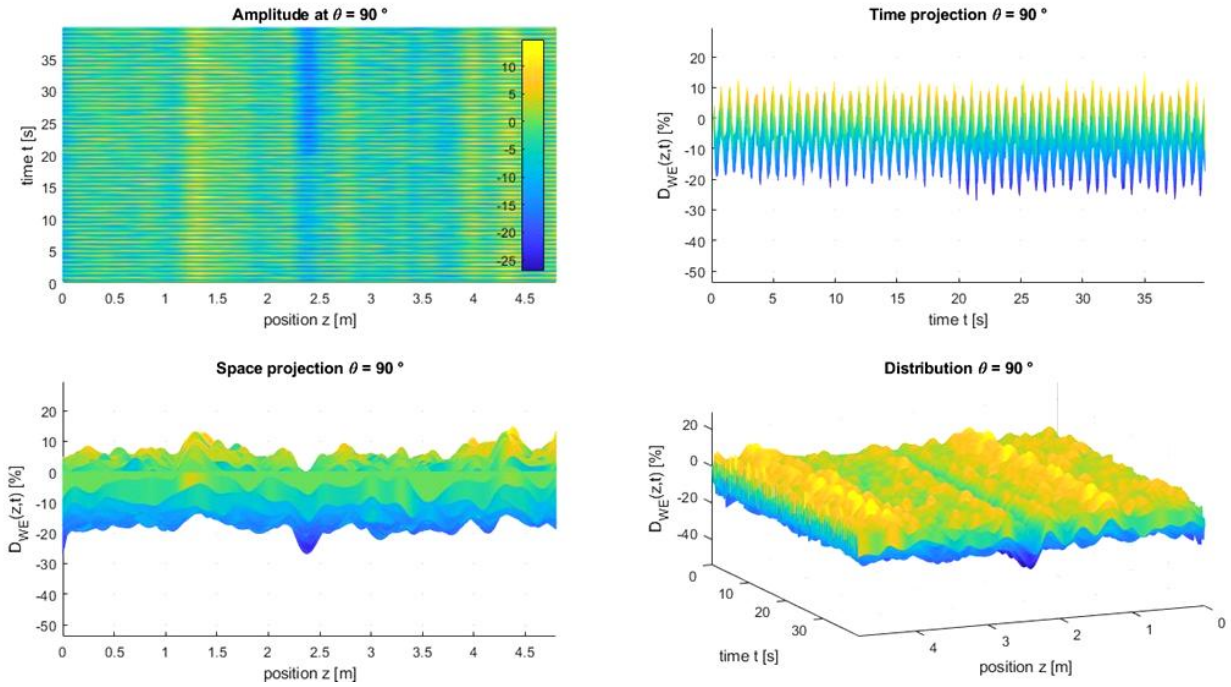

Figure 6.20 Comparison of 90° normalized results (WE) for undamaged- and 20% damaged- element with 5% white noise

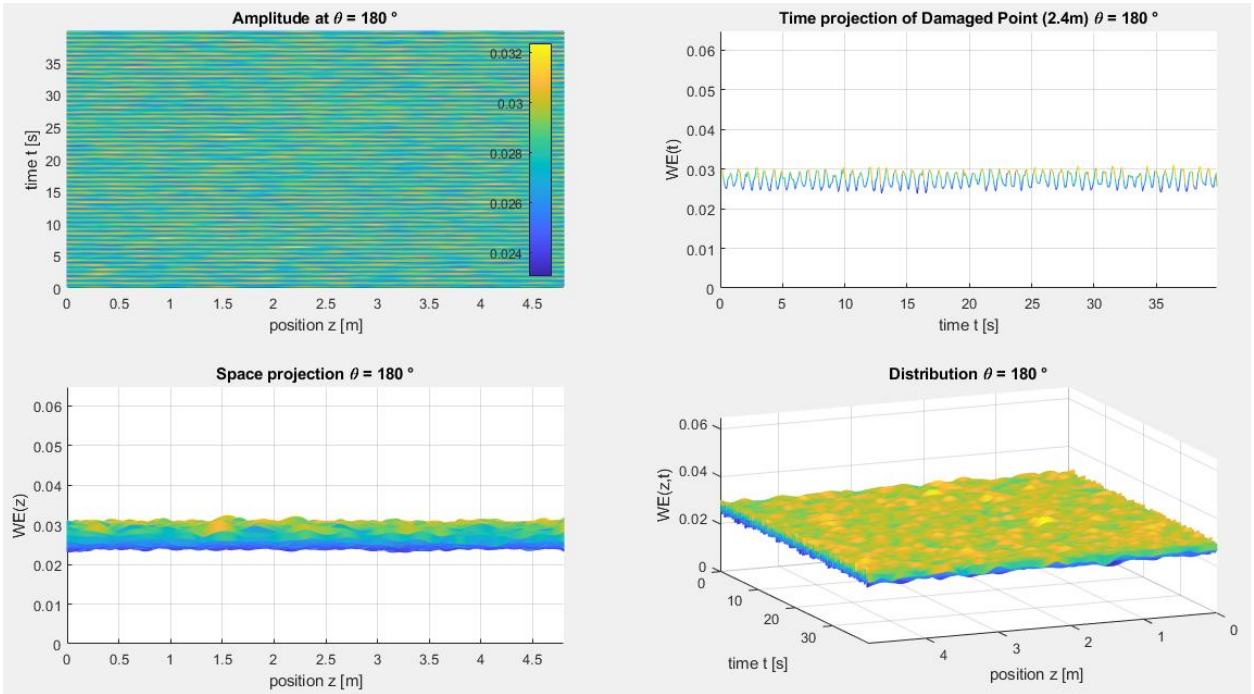

Figure 6.21 Comparison of 180° results (WE) for undamaged- and 20% damaged- single element with 5% white noise.

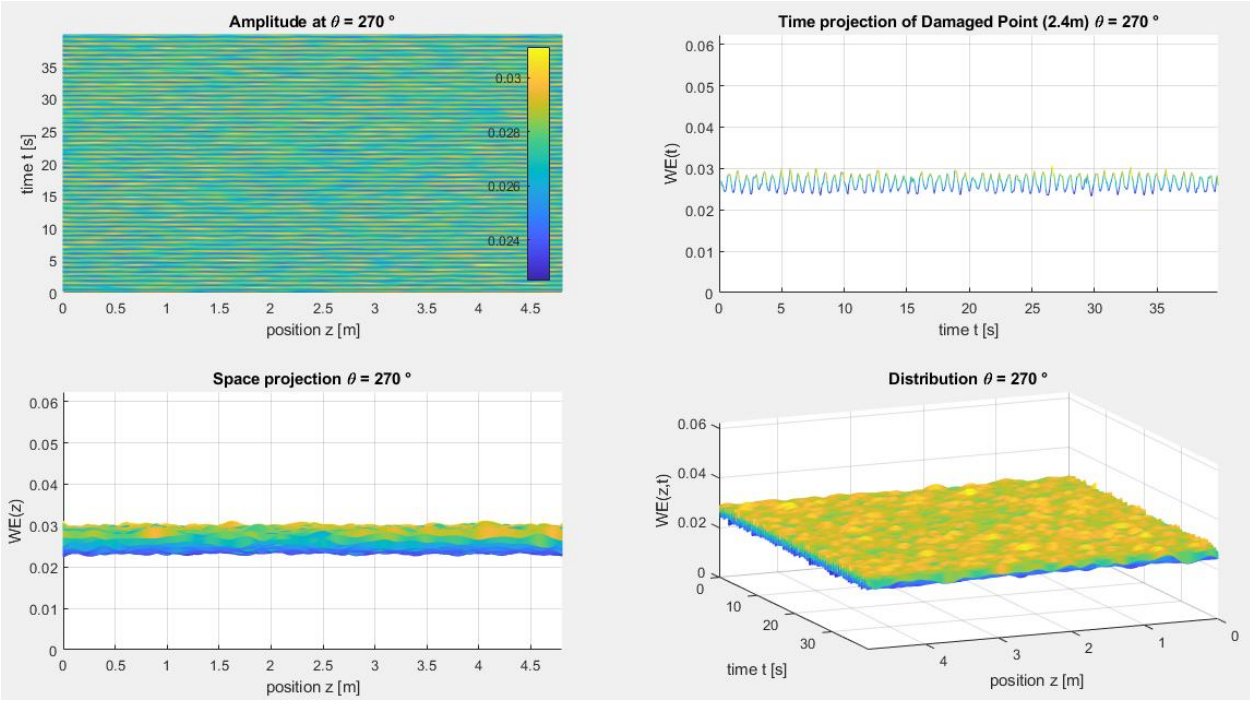

Figure 6.22 Comparison of 270° results (WE) for undamaged- and 20% damaged- single element with 5% white noise

The graphs with the normalized results of the points at 180 ° and 270 ° are omitted because they are congruent to the one shown in *Figure 6.18* for the 0° point.

The results show an absence of entropy variation from the undamaged to the damaged condition in points "far" from the damaged element.

As regards the results in *Figure 6.19* of the points located at 90 ° of the cross section (just where the reduction of stiffness has been placed), it is perceived an entropy decrease after 20 seconds of monitoring at 2.4m of the longitudinal direction (where the damage persists).

In the top right graph of *Figure 6.20*, on the other hand, the descending "step" of entropy due to the application of the damage is highlighted.

Below are inserted the same results with a signal soiled with 20% of white noise to better highlight the variation of entropy at 90° and understand if there are anomalies also in other points.

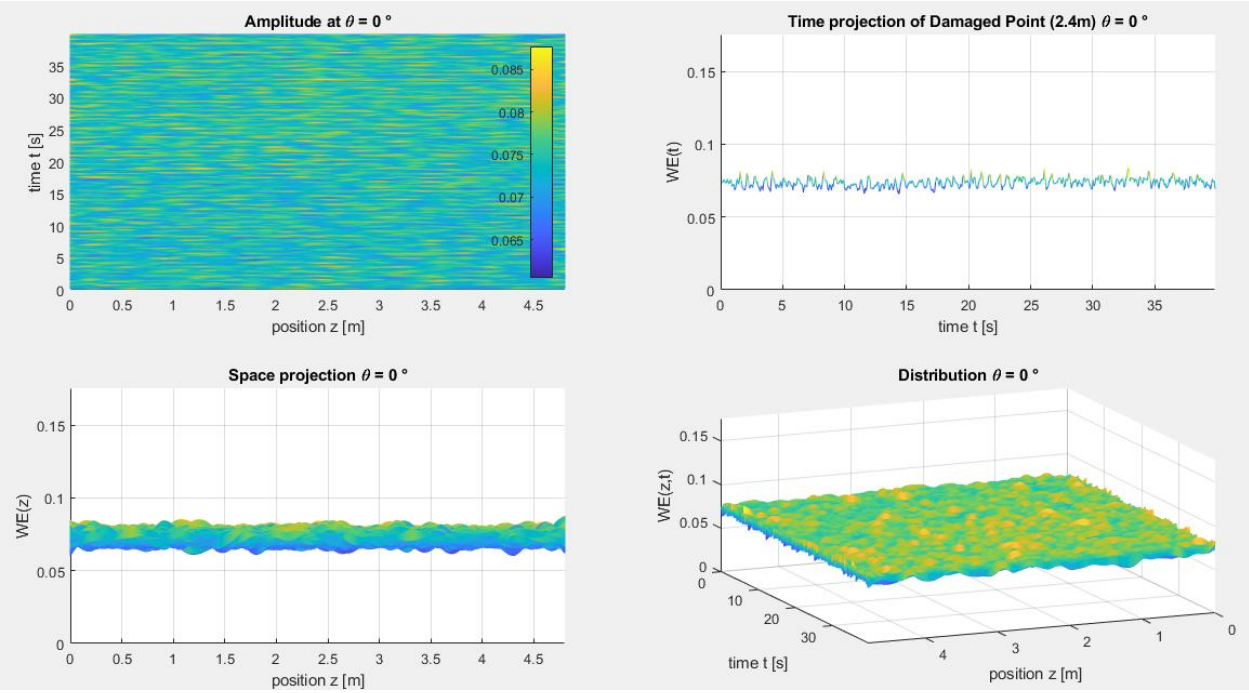

Figure 6.23 Comparison of 0° results (WE) for undamaged- and 20% damaged- single element with 20% white noise

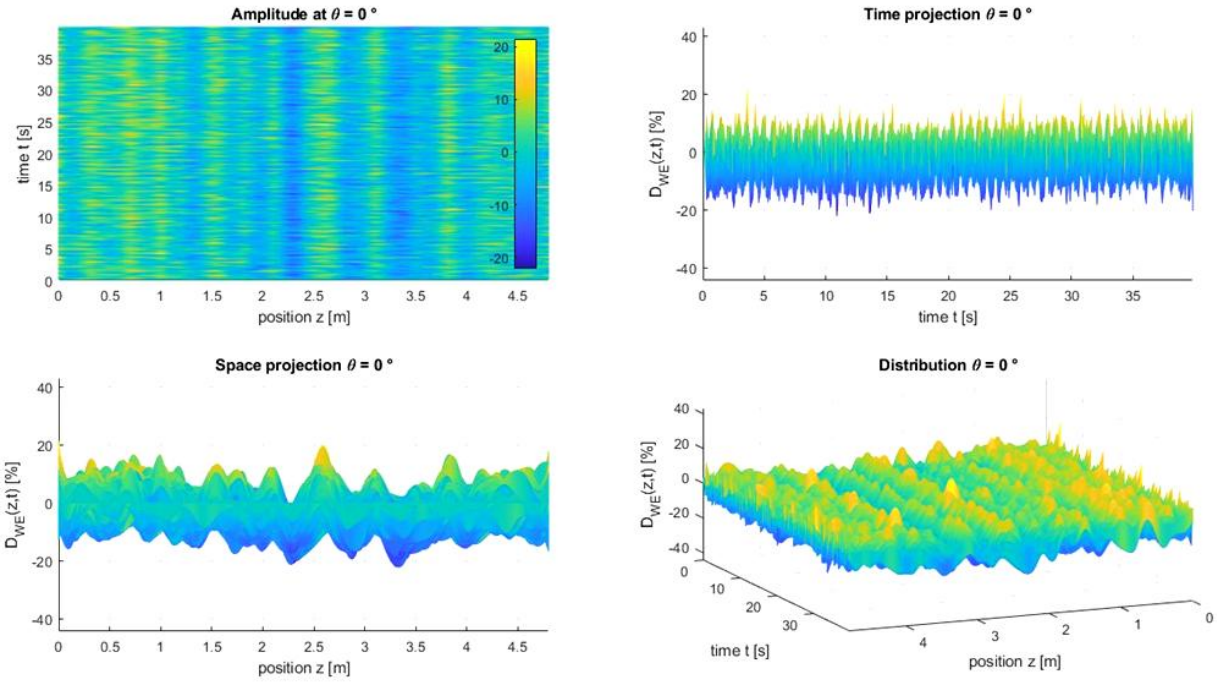

Figure 6.24 Comparison of 0° normalized results (WE) for undamaged- and 20% damaged- element with 20% white noise

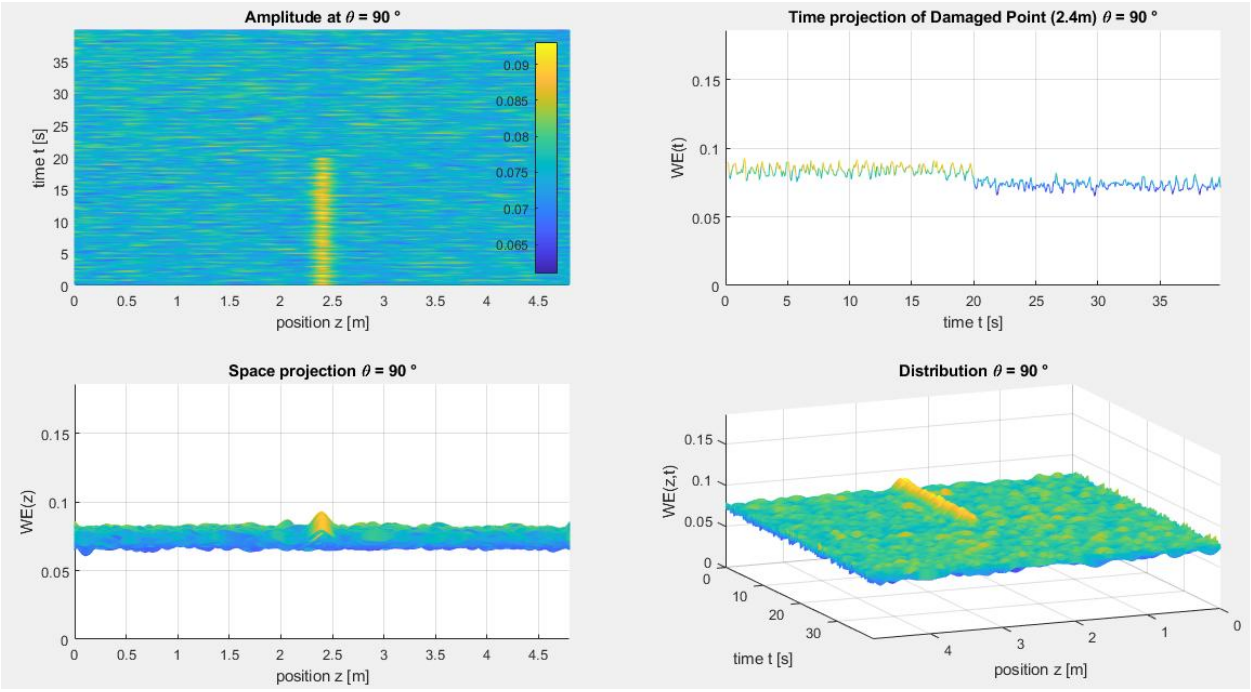

Figure 6.25 Comparison of 90° results (WE) for undamaged- and 20% damaged- single element with 20% white noise

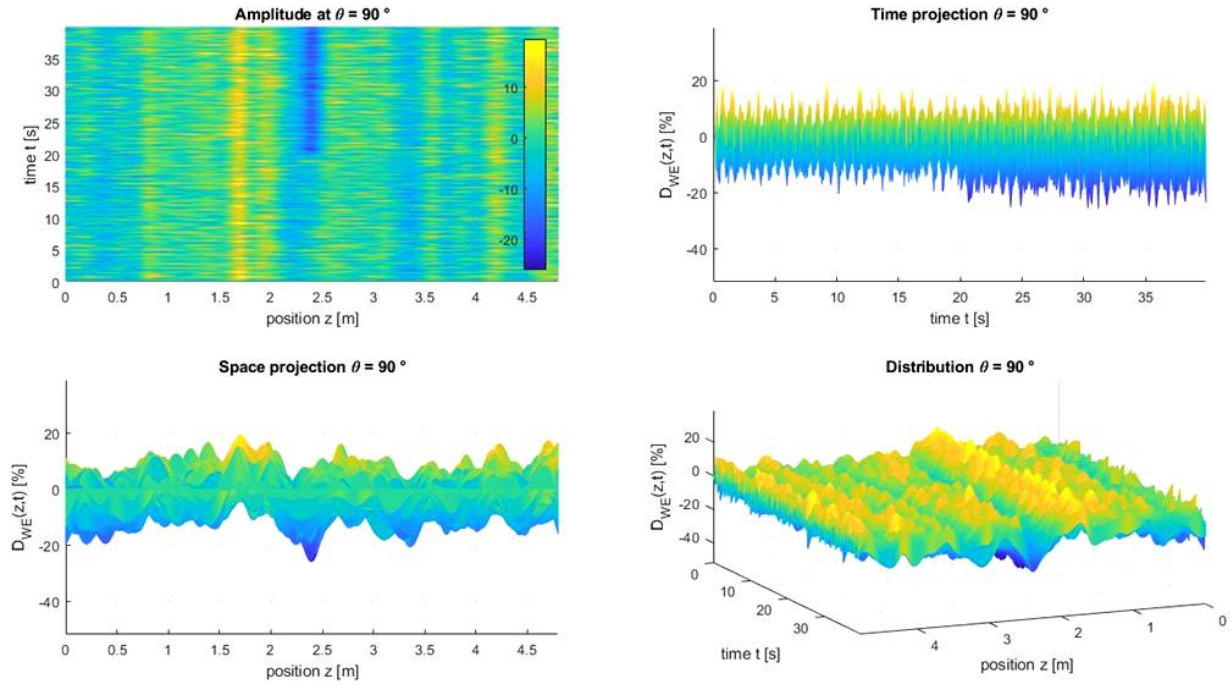

Figure 6.26 Comparison of 90° normalized results (WE) for undamaged- and 20% damaged- element with 20% white noise

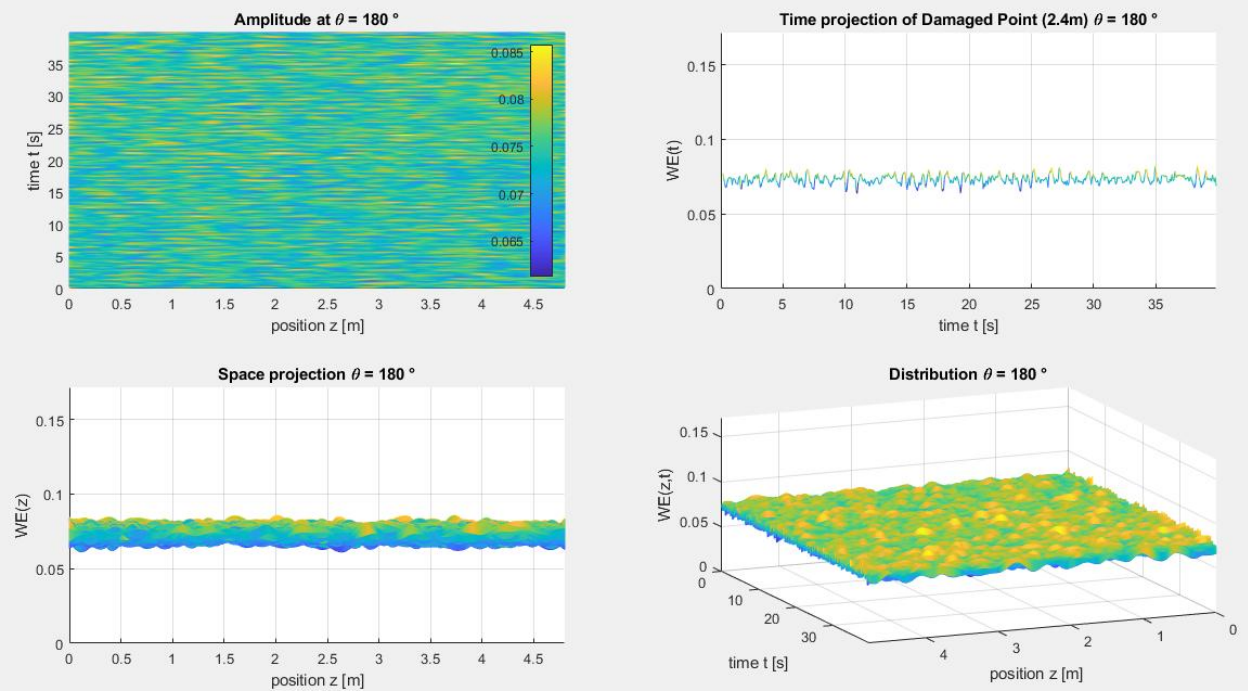

Figure 6.27 Comparison of 180° results (WE) for undamaged- and 20% damaged- single element with 20% white noise

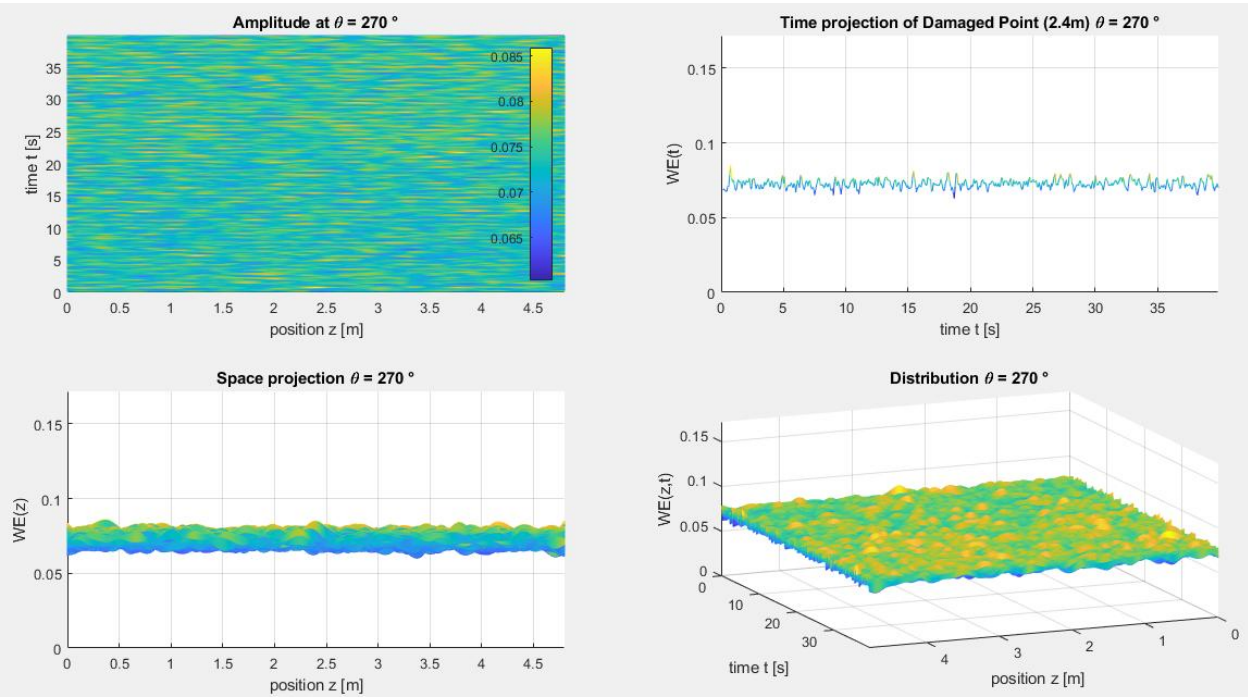

Figure 6.28 Comparison of 270° results (WE) for undamaged- and 20% damaged- single element with 20% white noise

Even increasing the noise inside the signal, the results remain substantially the same: no symptoms of damage in the sensors far from the degradation while the entropy variation on the sensor in correspondence of the decreased stiffness element is accentuated even more.

6.2.2. 50% Stiffness Reduction

Comparing the results obtained with the 50% damage to the previous one, the "crest" of entropy is quite evident limiting the white noise to the 10% of the signal. A substantial difference occurs with the case of the totally damaged cross-section: with the same percentage of damage and white noise applied, the entropy variations for large damage geometries are greater than those obtained for smaller damage dimensions.

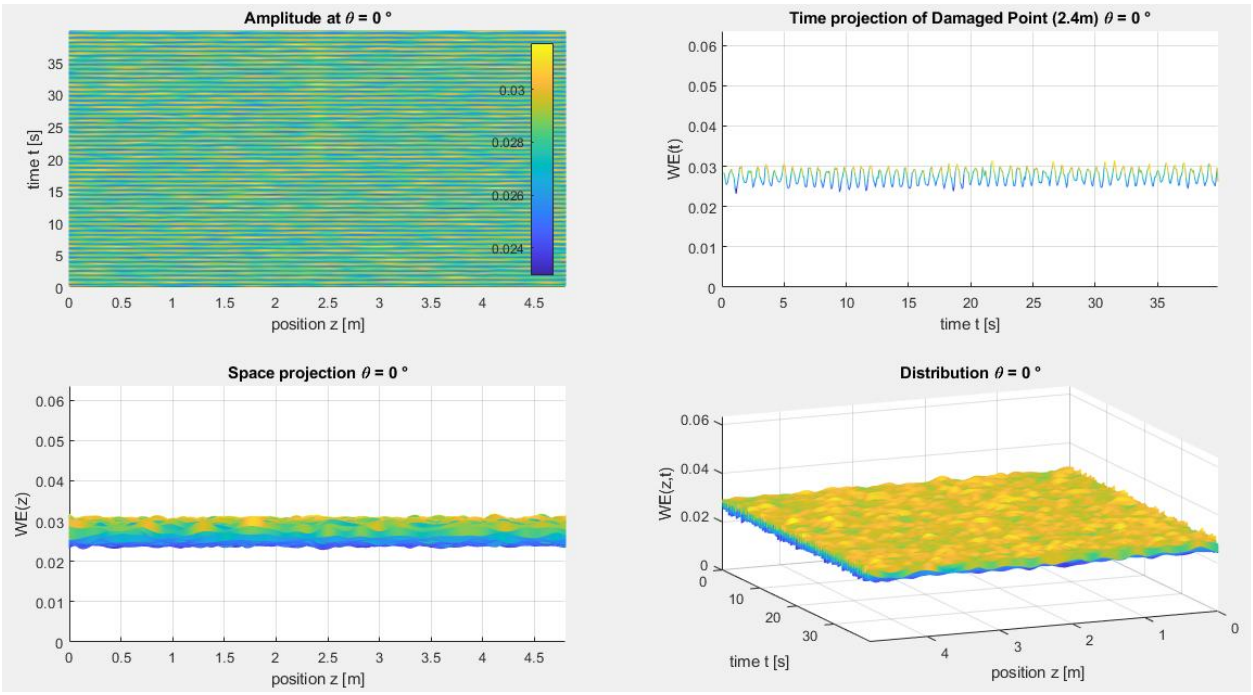

Figure 6.29 Comparison of 0° results (WE) for undamaged- and 50% damaged- single element with 5% white noise

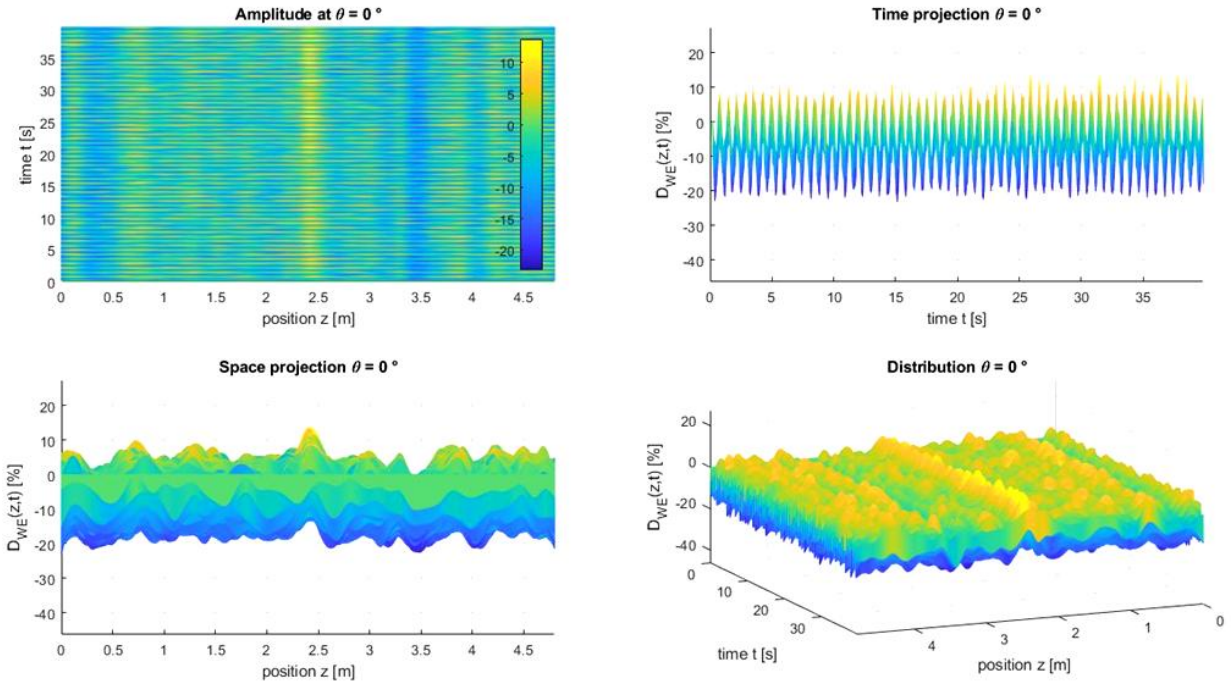

Figure 6.30 Comparison of 0° normalized results (WE) for undamaged- and 50% damaged- single element with 5% white noise

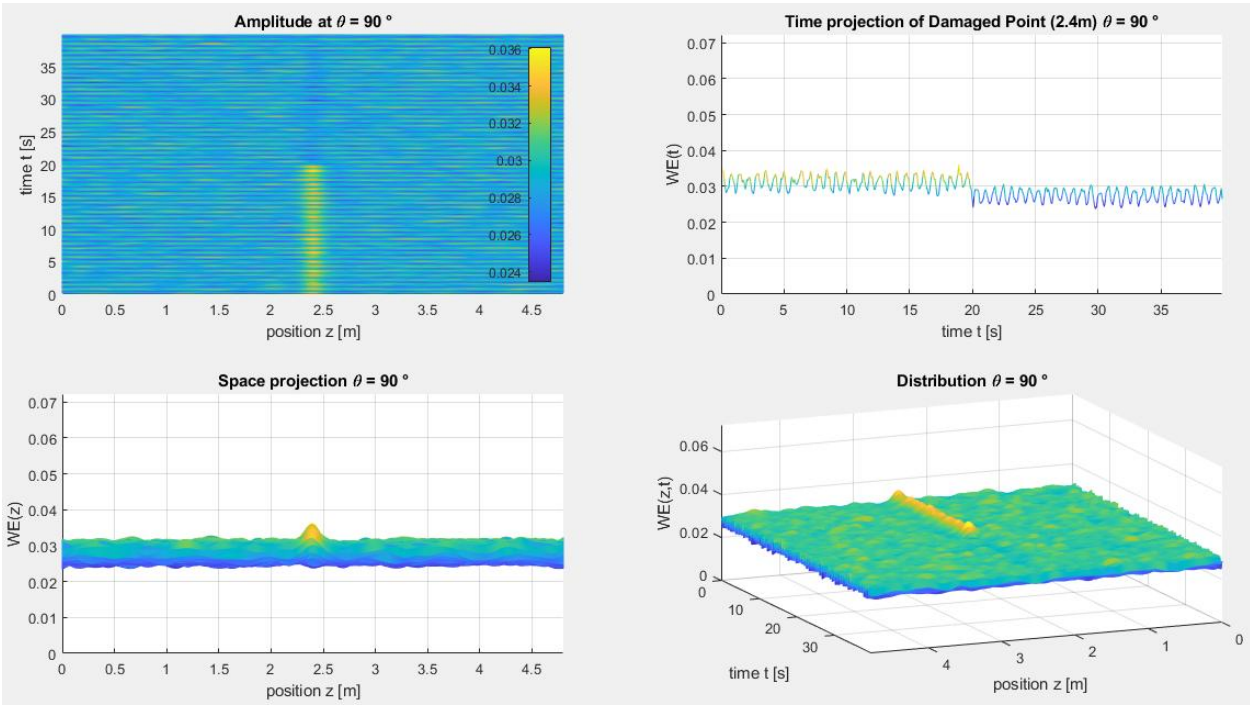

Figure 6.31 Comparison of 90° results (WE) for undamaged- and 50% damaged- single element with 5% white noise

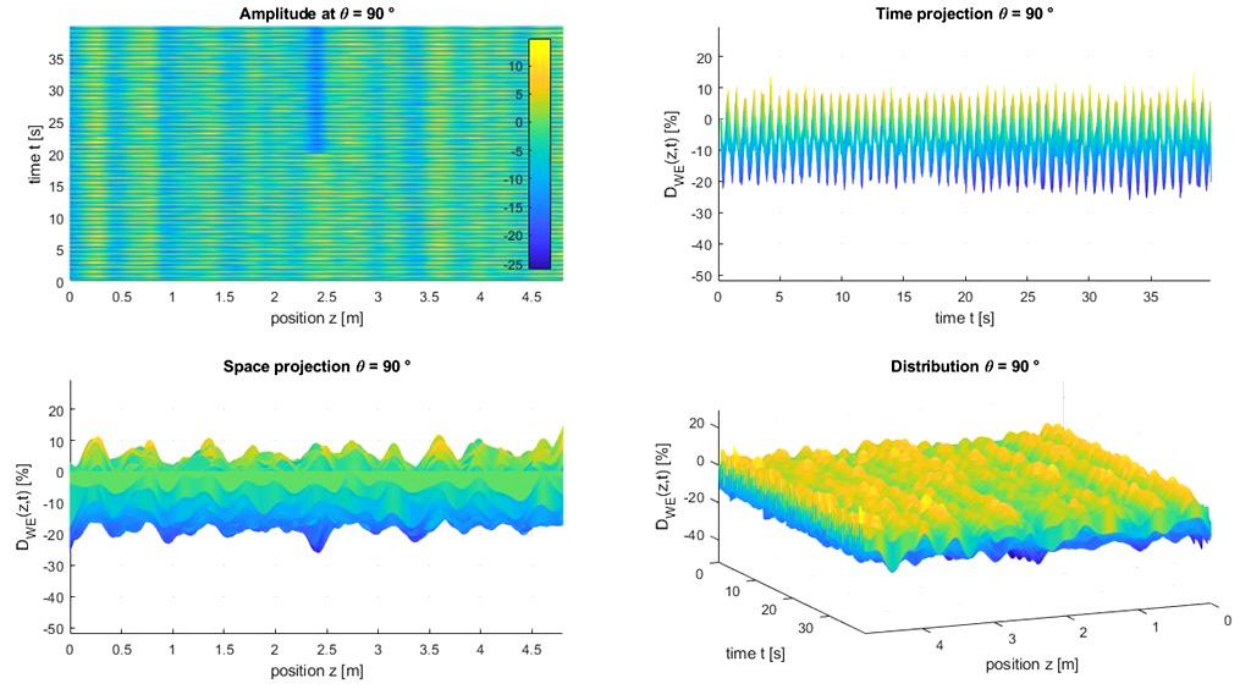

Figure 6.32 Comparison of 90° results (WE) for undamaged- and 50% damaged- single element with 5% white noise

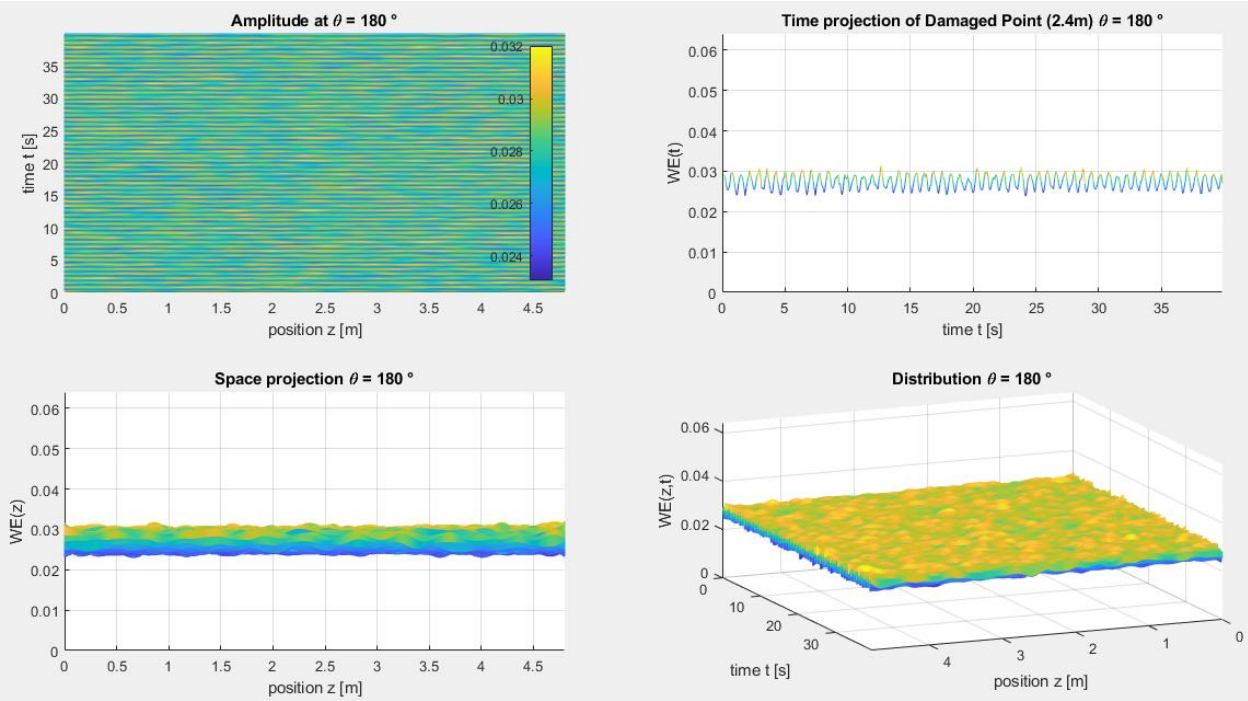

Figure 6.33 Comparison of 180° results (WE) for undamaged- and 50% damaged- single element with 5% white noise

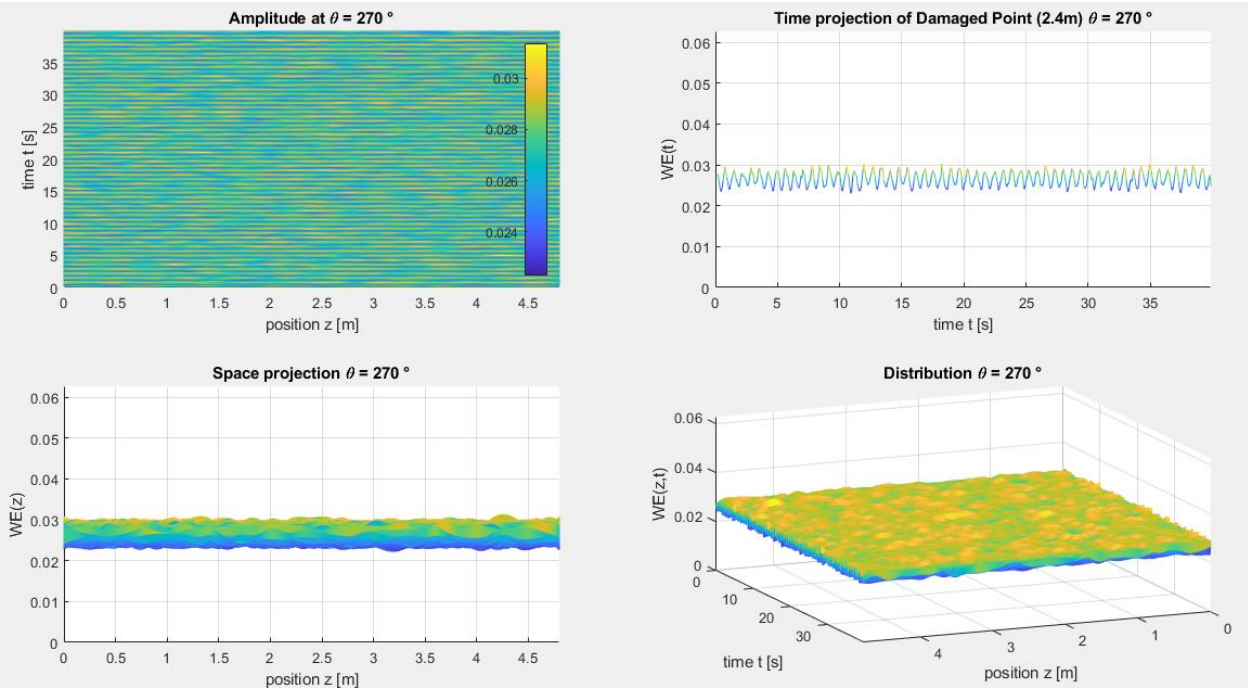

Figure 6.34 Comparison of 270° results (WE) for undamaged- and 50% damaged- single element with 5% white noise

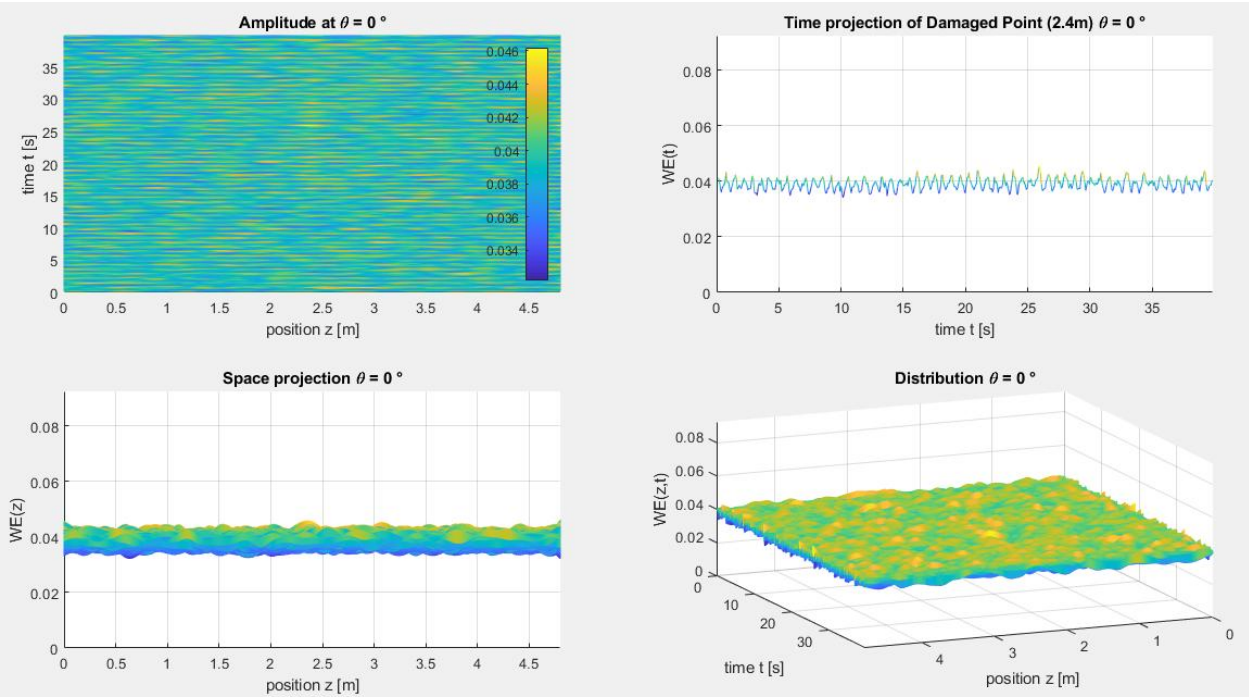

Figure 6.35 Comparison of 0° results (WE) for undamaged- and 50% damaged- single element with 10% white noise

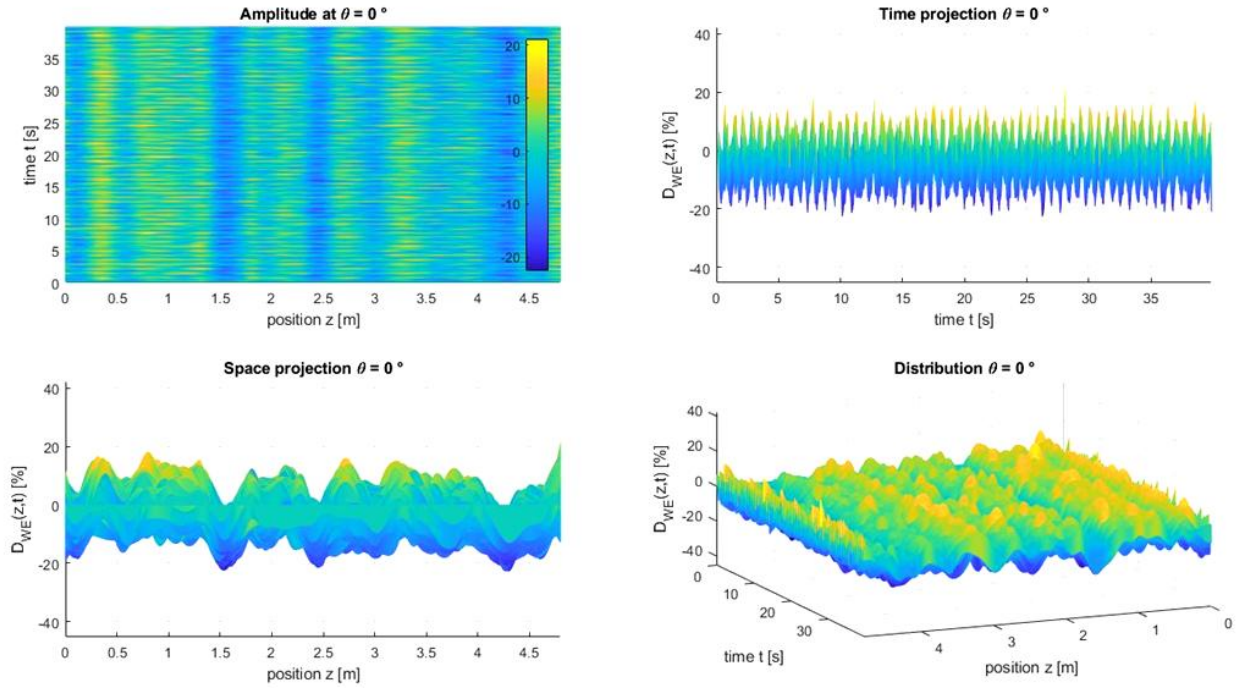

Figure 6.36 Comparison of 0° normalized results (WE) for undamaged- and 50% damaged- element with 10% white noise

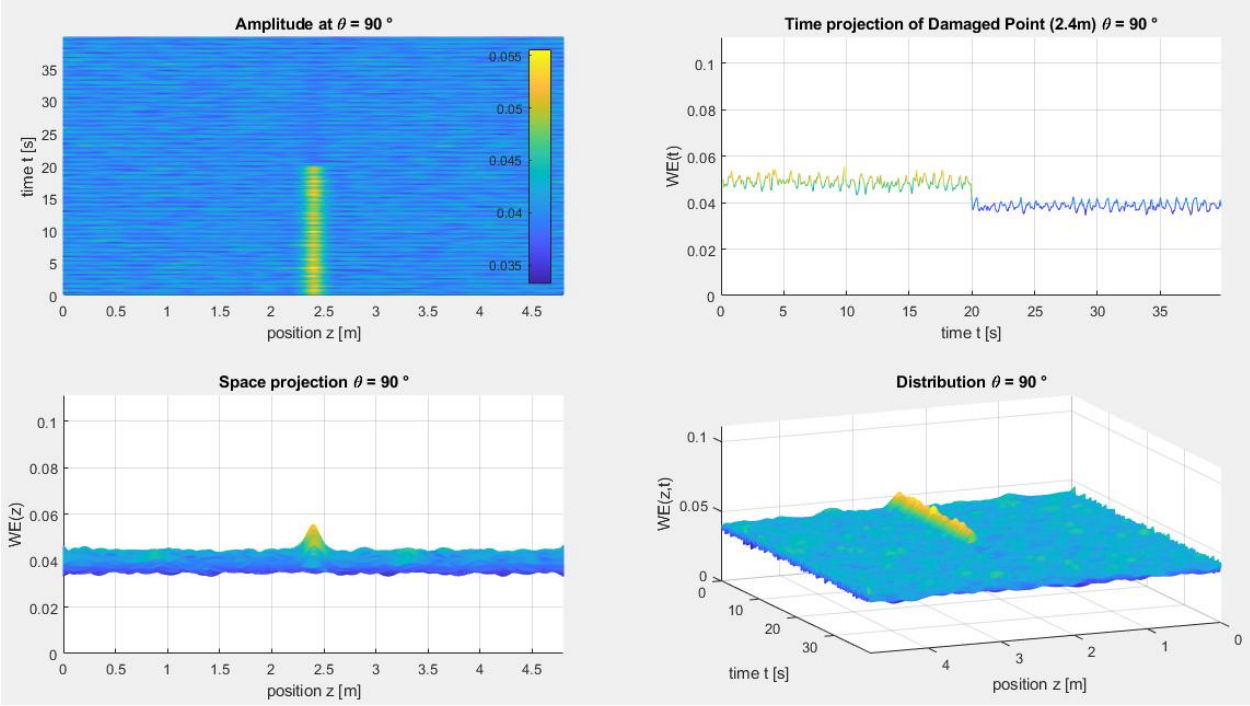

Figure 6.37 Comparison of 90° results (WE) for undamaged- and 50% damaged- single element with 10% white noise

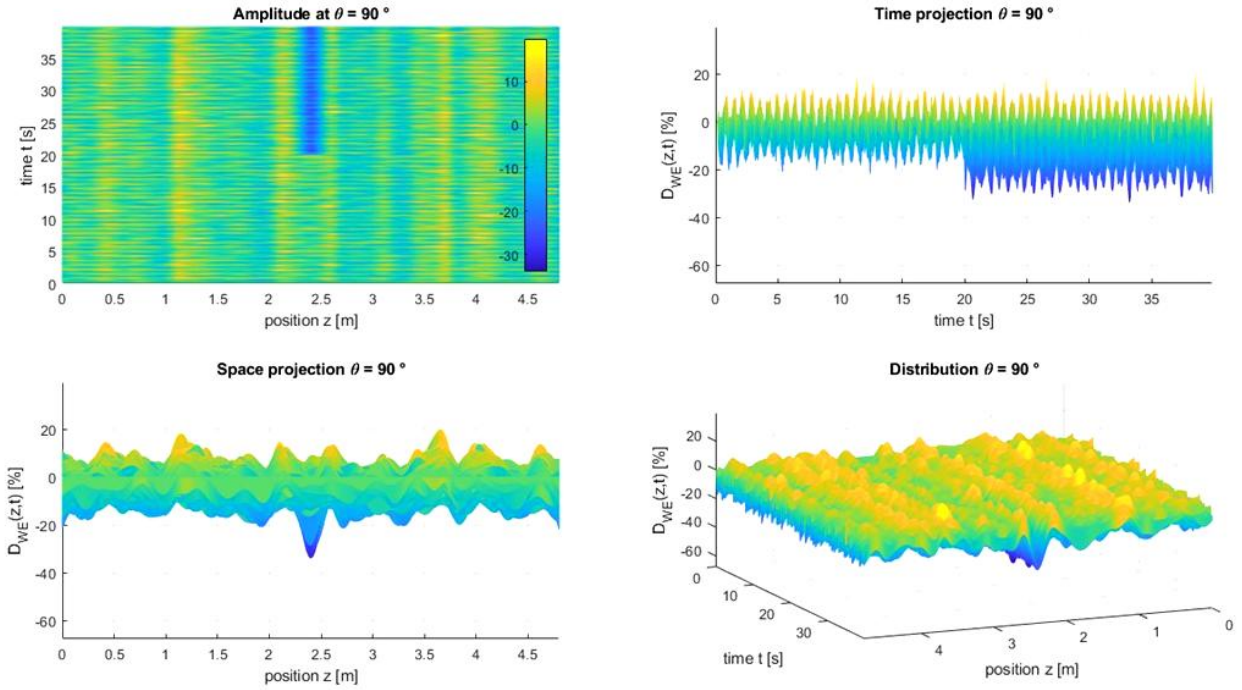

Figure 6.38 Comparison of 90° normalized results (WE) for undamaged- and 50% damaged- element with 10% white noise

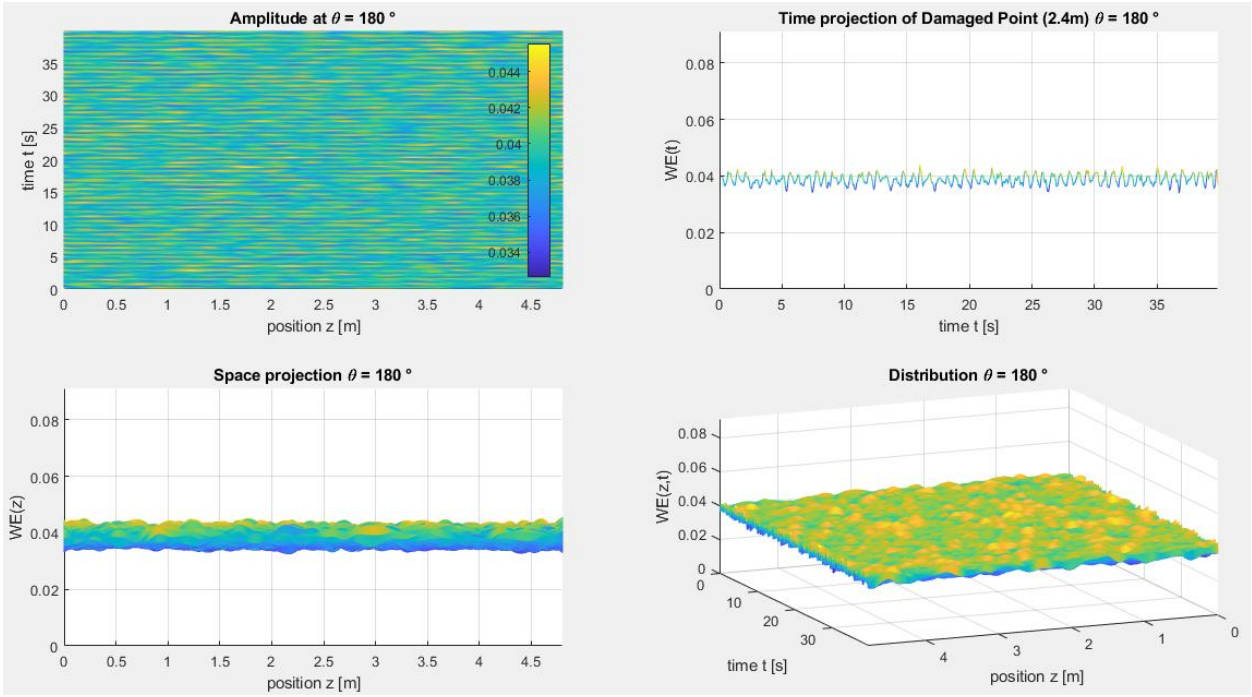

Figure 6.39 Comparison of 180° results (WE) for undamaged- and 50% damaged- single element with 10% white noise

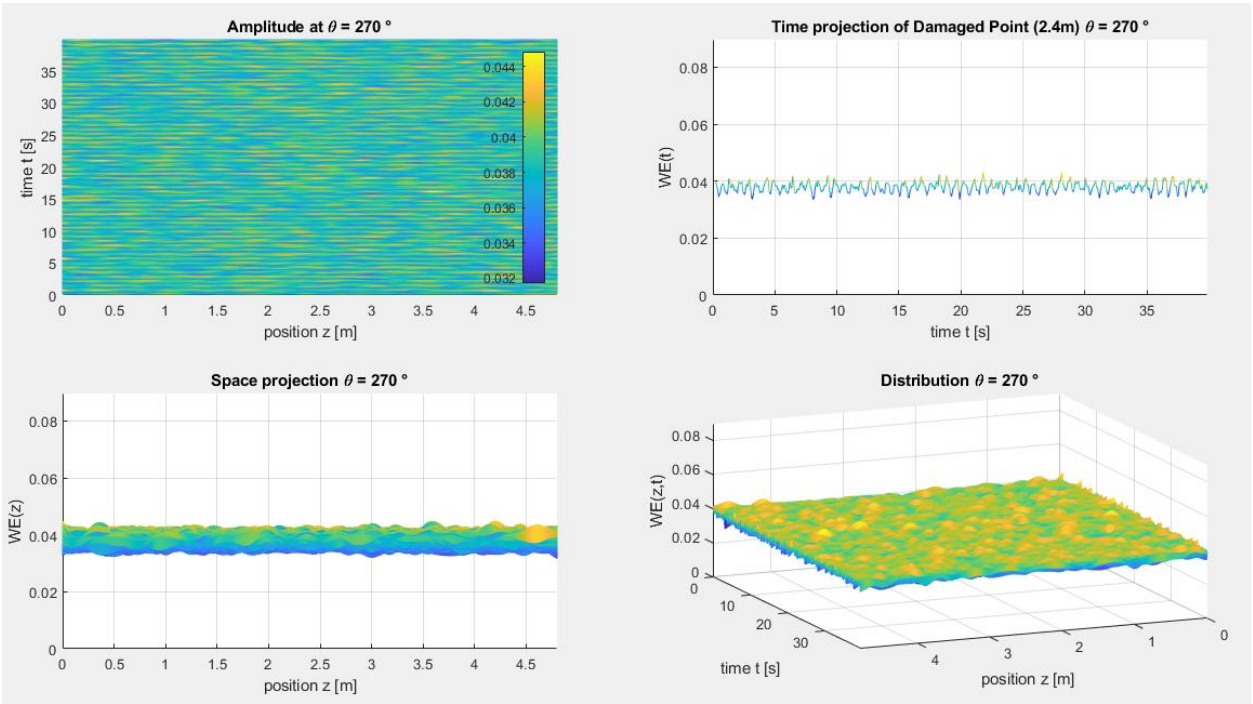

Figure 6.40 Comparison of 270° results (WE) for undamaged- and 50% damaged- single element with 10% white noise

6.3 Single Element Damaged between two sensors

The last case studied is that in which pitting corrosion affects an area between two sensors.
In particular, the damage phenomenon is analytically simulated by reducing the stiffness of the finished element 0.087m x 0.1m located at 45 ° of the cross section (corrosion affects the point between the sensors at 0° and 90°).
This can be considered the most difficult damage scenario to identify due to its reduced geometry and maximum distance from all sensors placed on the pipeline.

6.3.1. 20% Stiffness Reduction

This paragraph shows the results relating to the sensors placed at 90° and 270° because they are comparable respectively to those at 0° and 180°.
The following figures demonstrate how the 5% of white noise does not allow a sufficiently accentuated identification of the 20% damage located between two sensors.
For this reason it is chosen to "dirty" the signal, as in the previous cases, up to obtaining a 20% of total noise. In any case, this operation does not allows to identify with great certainty the presence and position of the system alteration studied.

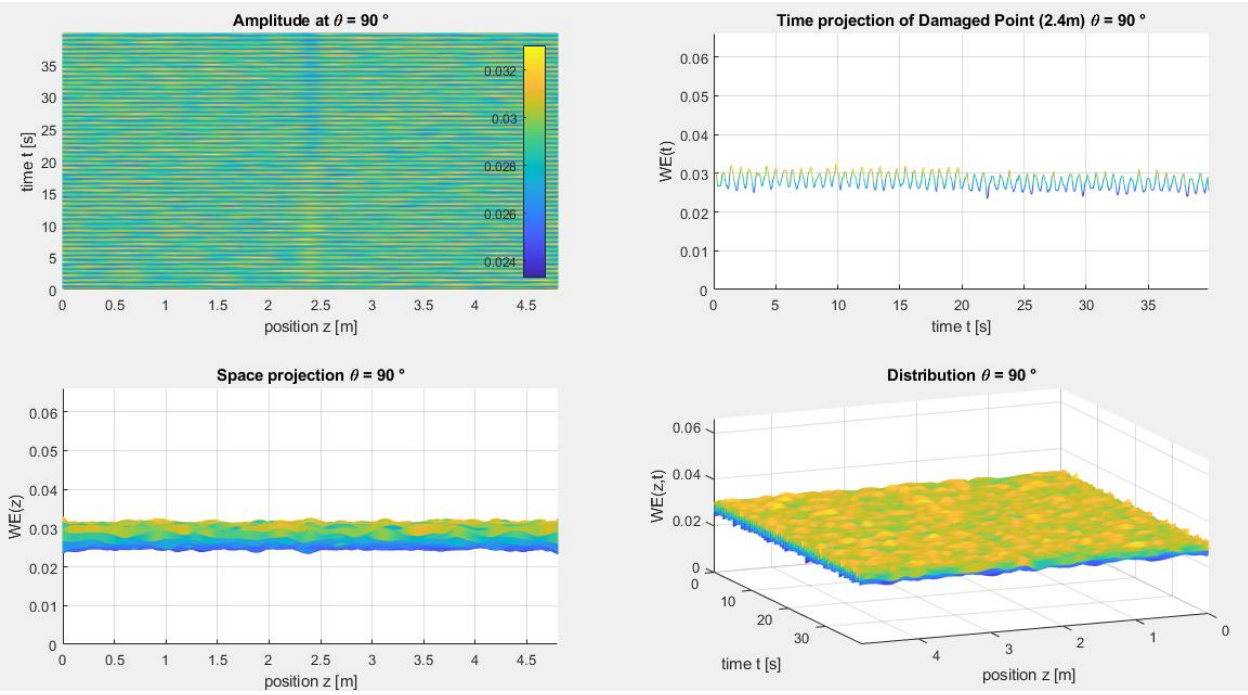

Figure 6.41 Comparison of 90° results (WE) for undamaged- and 20% damaged- element at 45° with 5% white noise

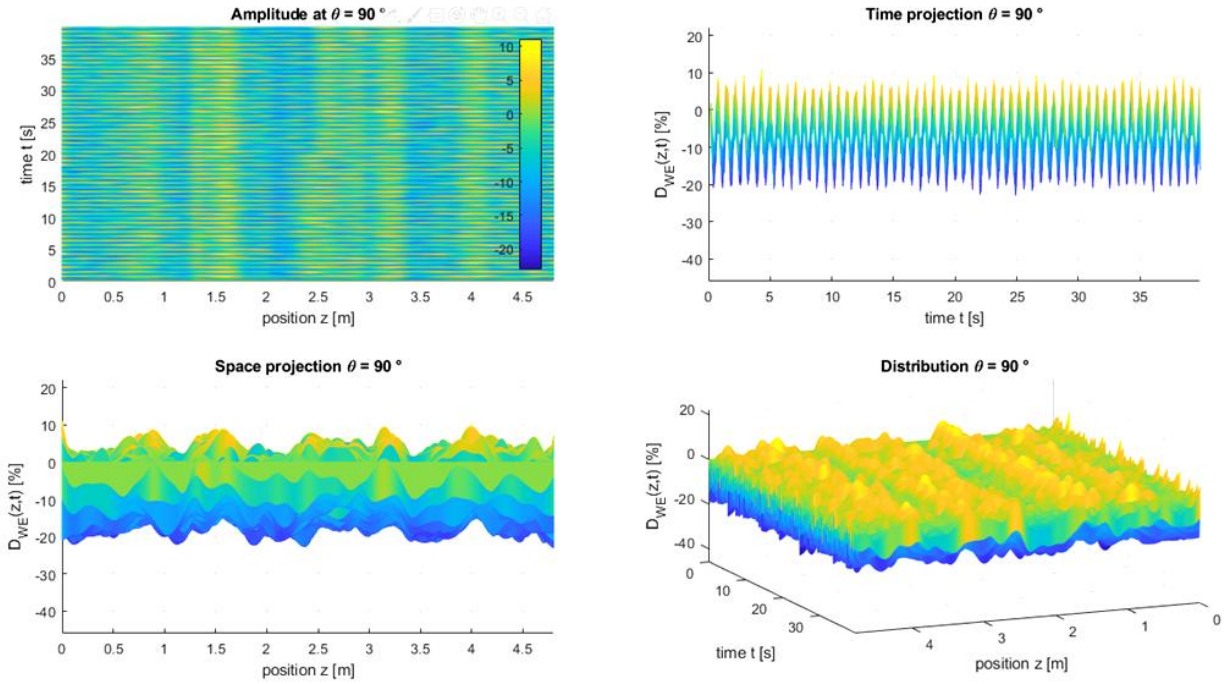

Figure 6.42 Comparison of 90° normalized results (WE) for undamaged- and 20% damaged- element at 45° with 5% white noise

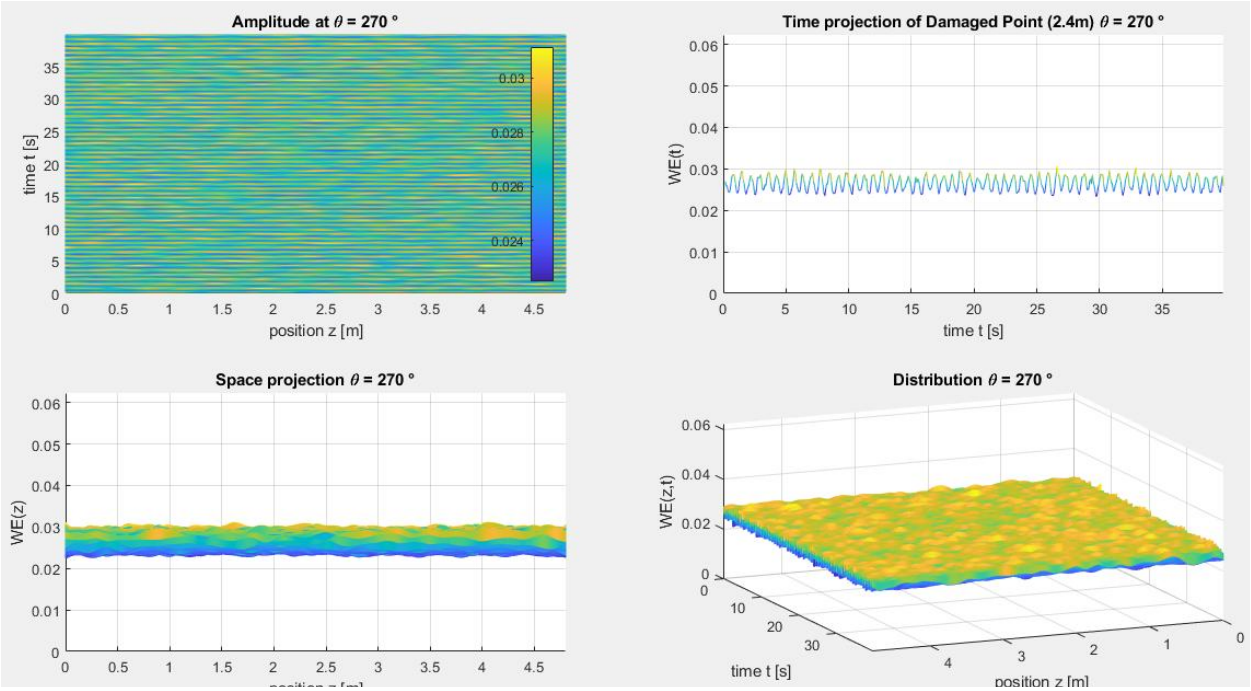

Figure 6.43 Comparison of 270° results (WE) for undamaged- and 20% damaged- element at 45° with 5% white noise

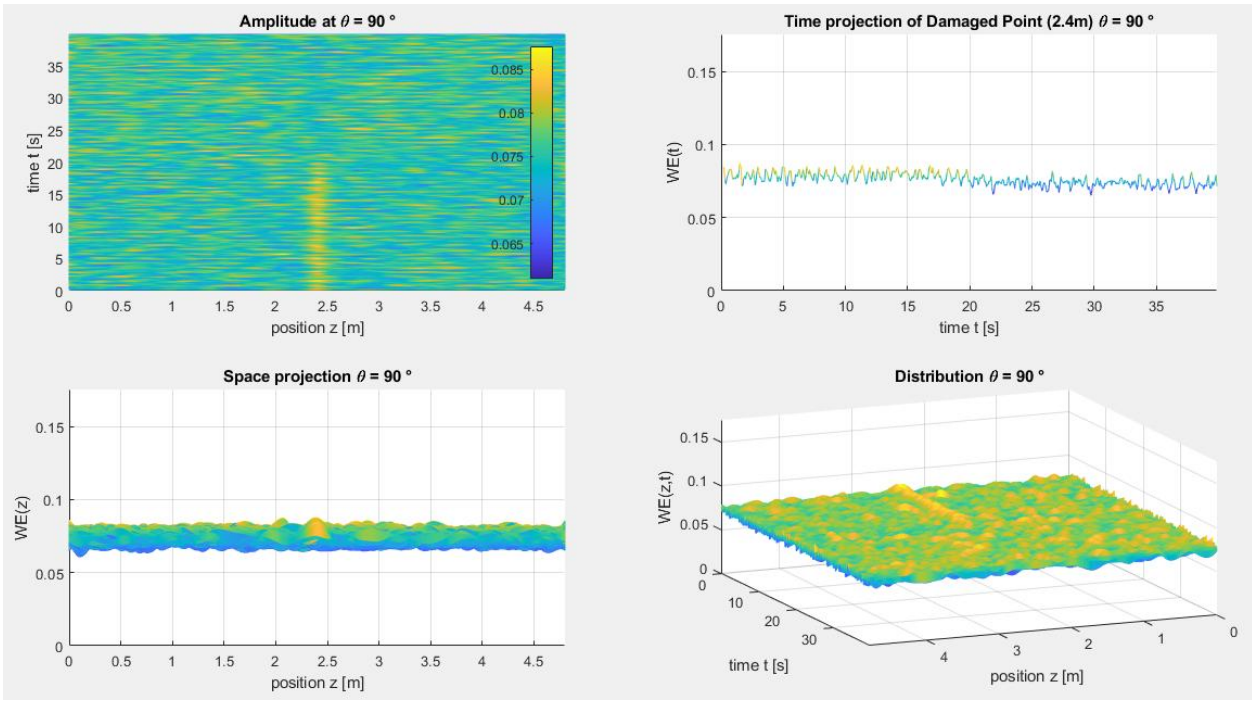

Figure 6.44 Comparison of 90° results (WE) for undamaged- and 20% damaged- element at 45° with 20% white noise

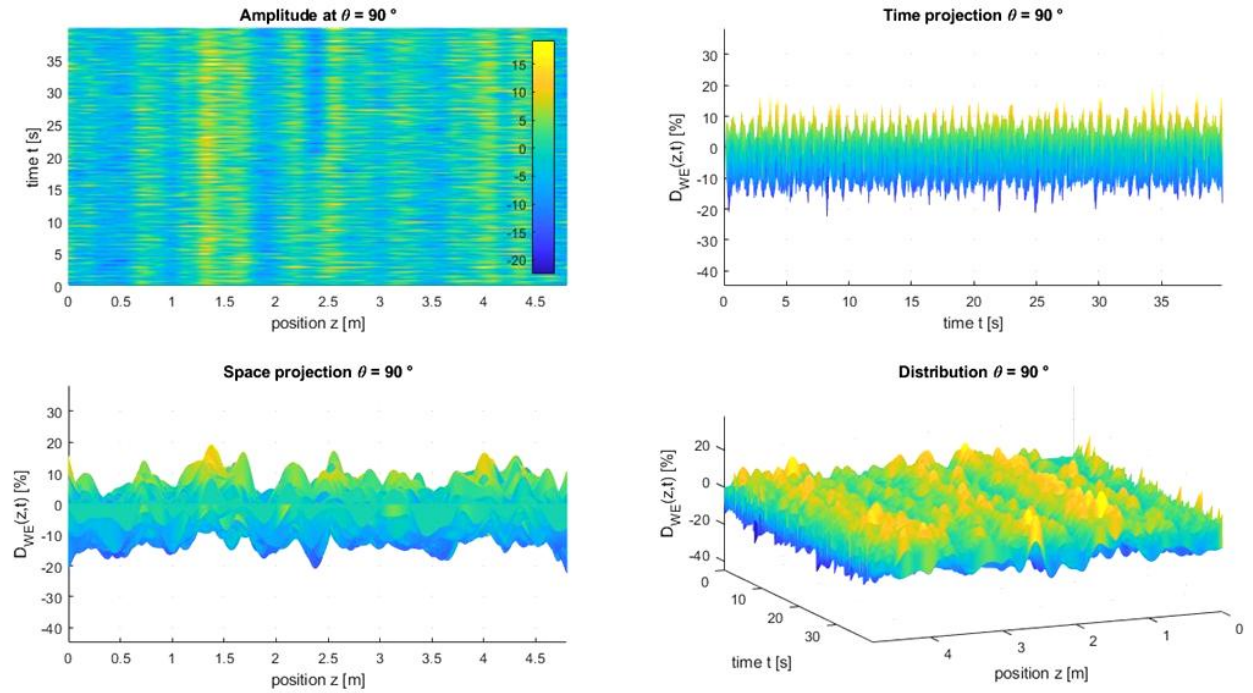

Figure 6.45 Comparison of 90° normalized results (WE) for undamaged- and 20% damaged- element at 45° with 20% white noise

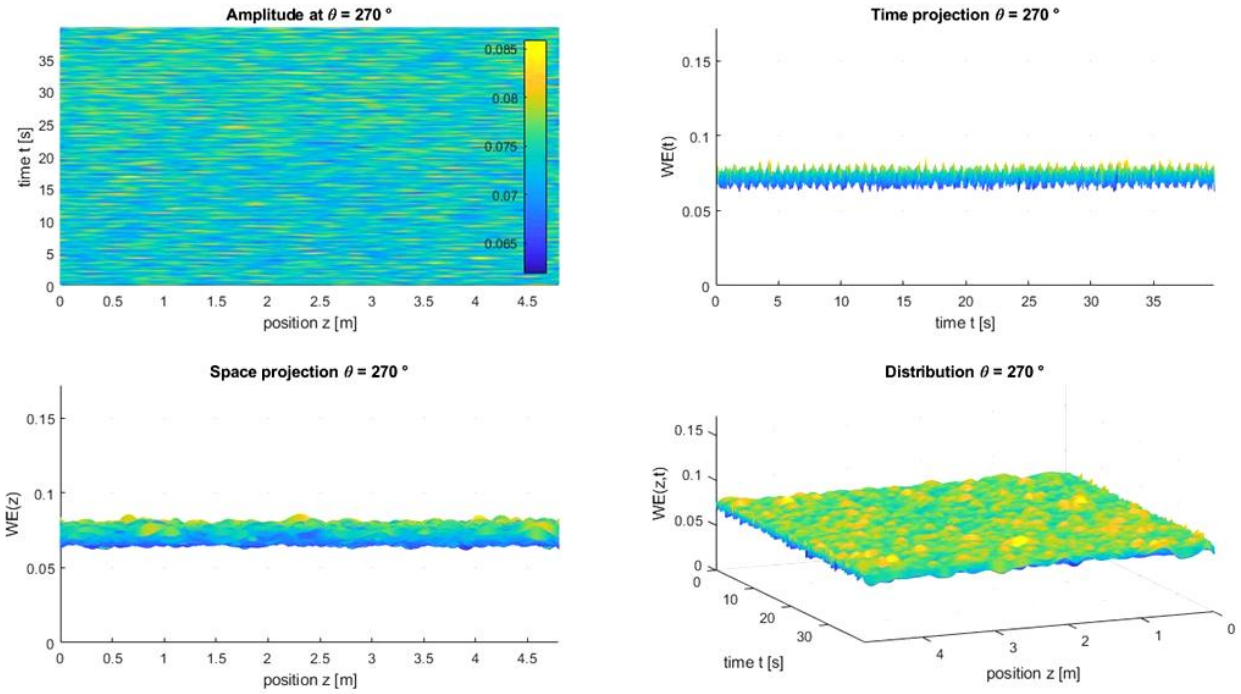

Figure 6.46 Comparison of 270° results (WE) for undamaged- and 20% damaged- element at 45° with 20% white noise

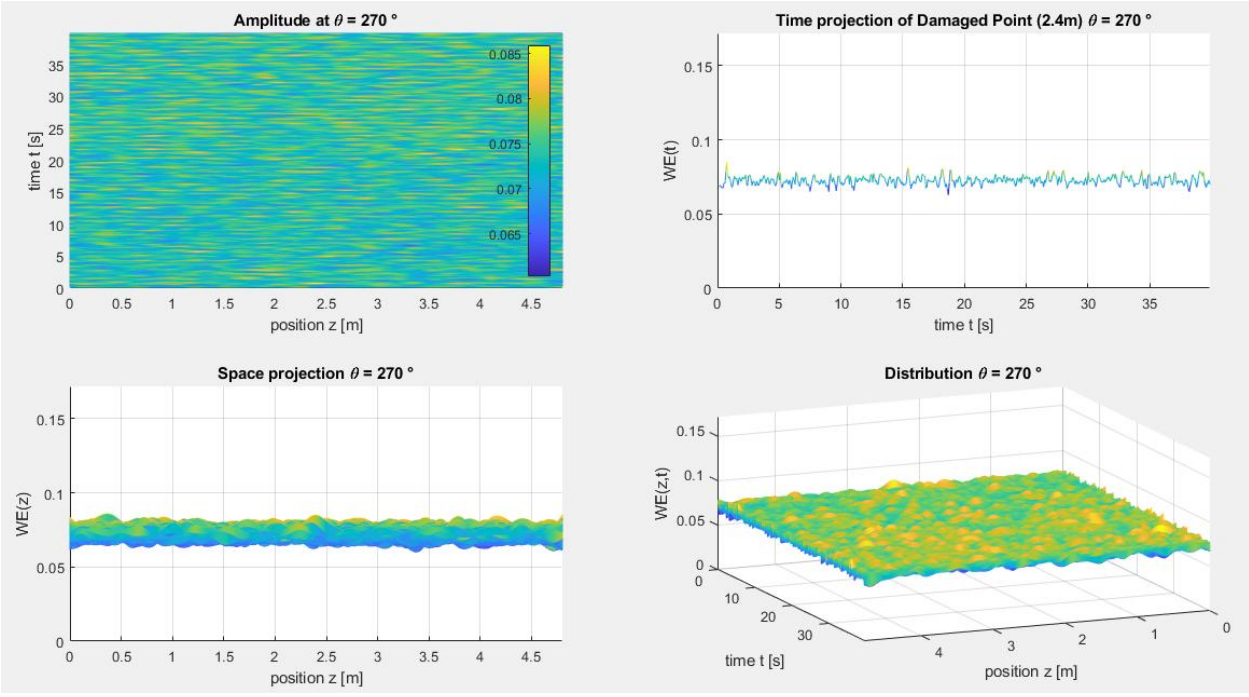

Figure 6.47 Comparison of 270° normalized results (WE) for undamaged- and 20% damaged- element at 45° with 20% white noise

6.3.2. 50% Stiffness Reduction

Also in this case, but only for 5% of noise, the results at 90° and 270° are shown, because they can be considered representative also of those at 0° and 180° respectively. This choice is made because with 5% of noise it is not possible to identify the damage with certainty, but it is achieved with 20% of white noise. In the latter case, the results related to all monitored points are shown.

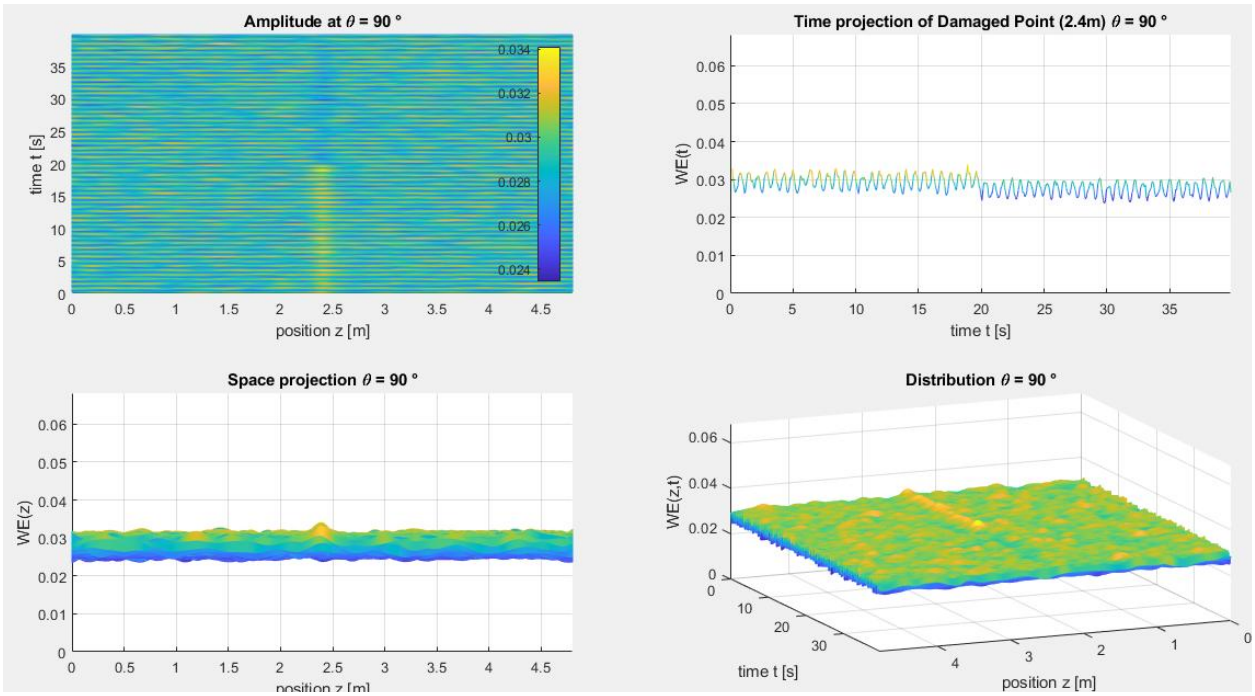

Figure 6.48 Comparison of 90° results (WE) for undamaged- and 50% damaged- single element at 45° with 5% white noise

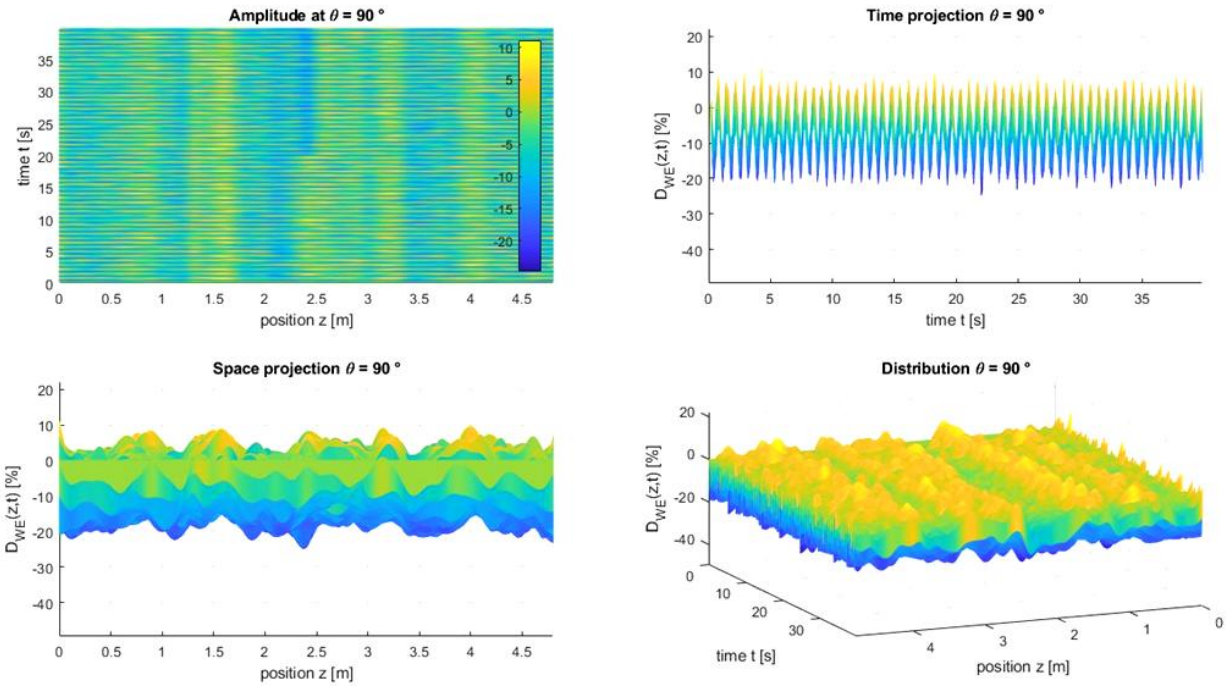

Figure 6.49 Comparison of 90° normalized results (WE) for undamaged- and 50% damaged- element at 45° with 5% white noise.

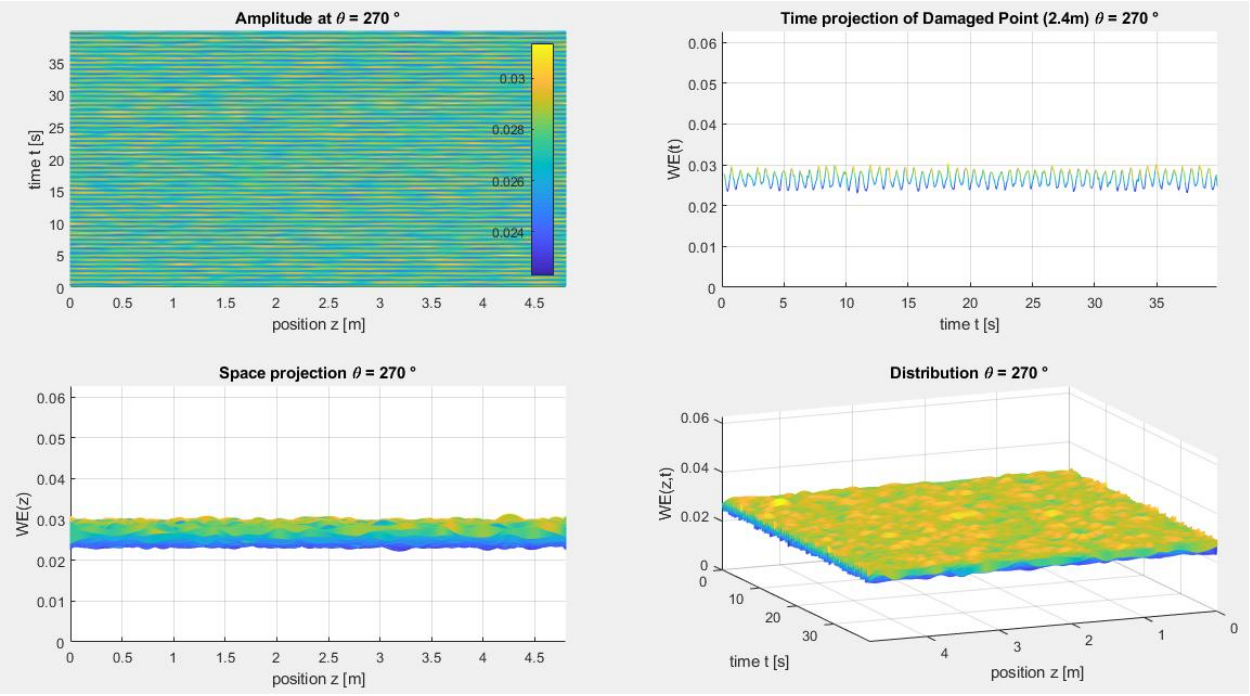

Figure 6.50 Comparison of 270° results (WE) for undamaged- and 50% damaged- single element at 45° with 5% white noise

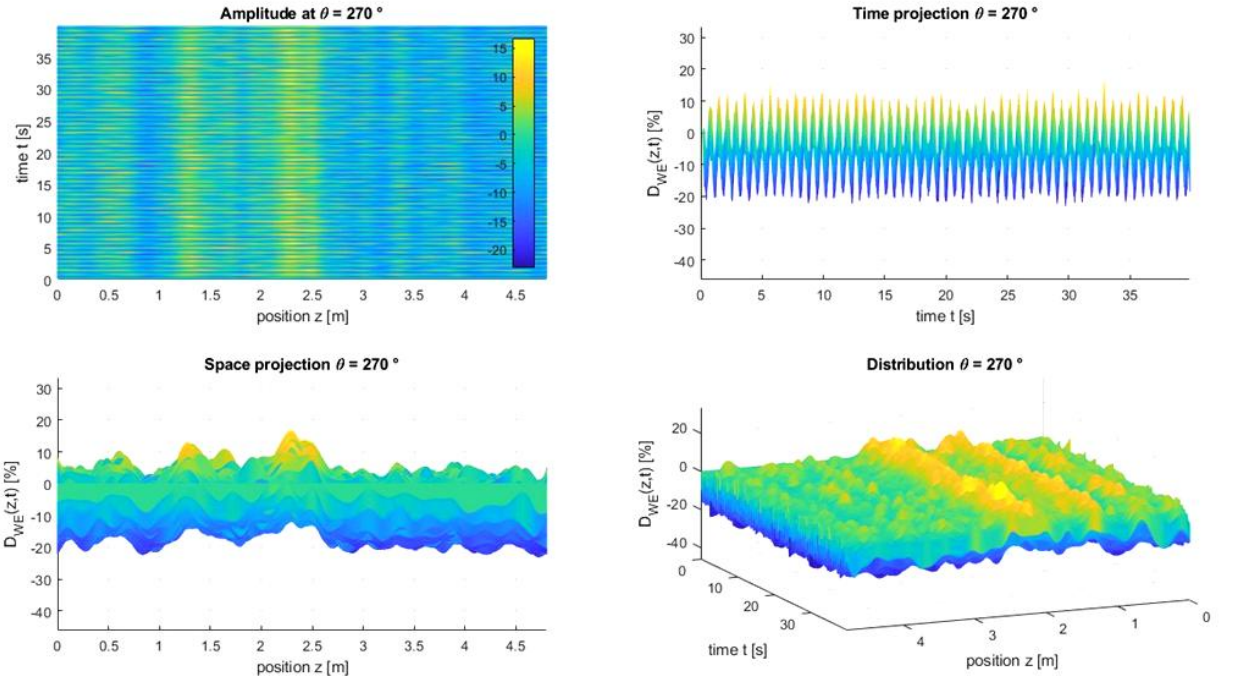

Figure 6.51 Comparison of 270° normalized results (WE) for undamaged- and 50% damaged- element at 45° with 5% white noise

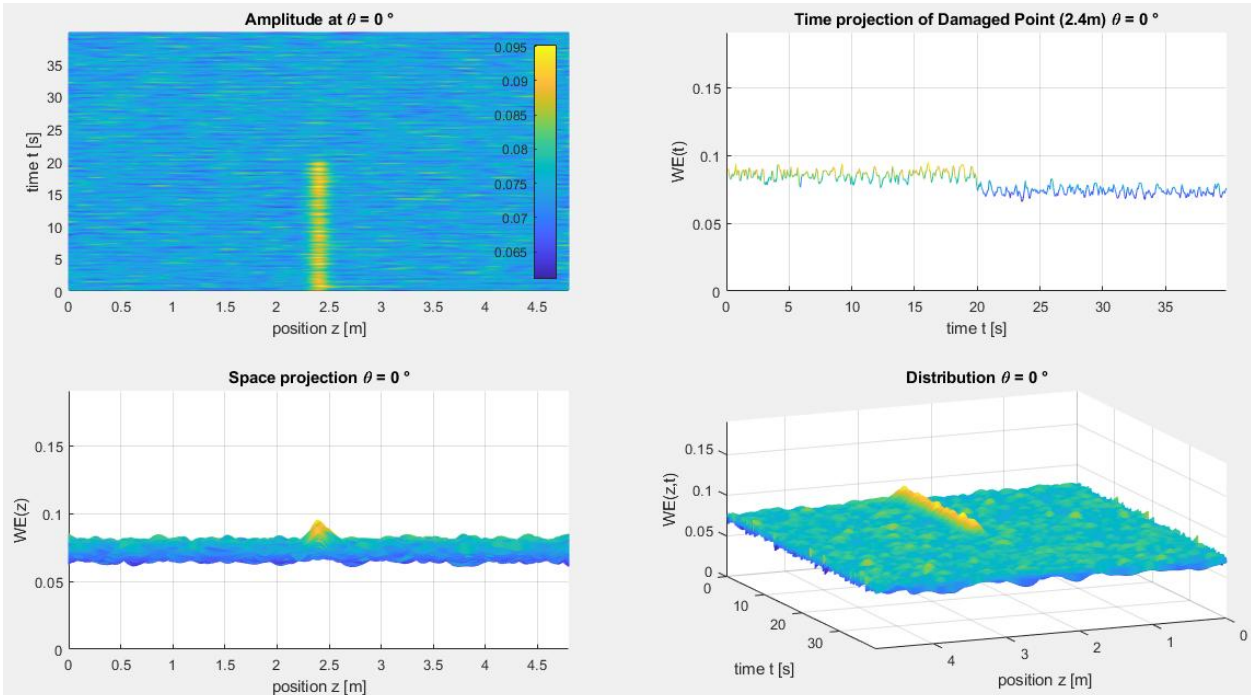

Figure 6.52 Comparison of 0° results (WE) for undamaged- and 50% damaged- single element at 45° with 20% white noise

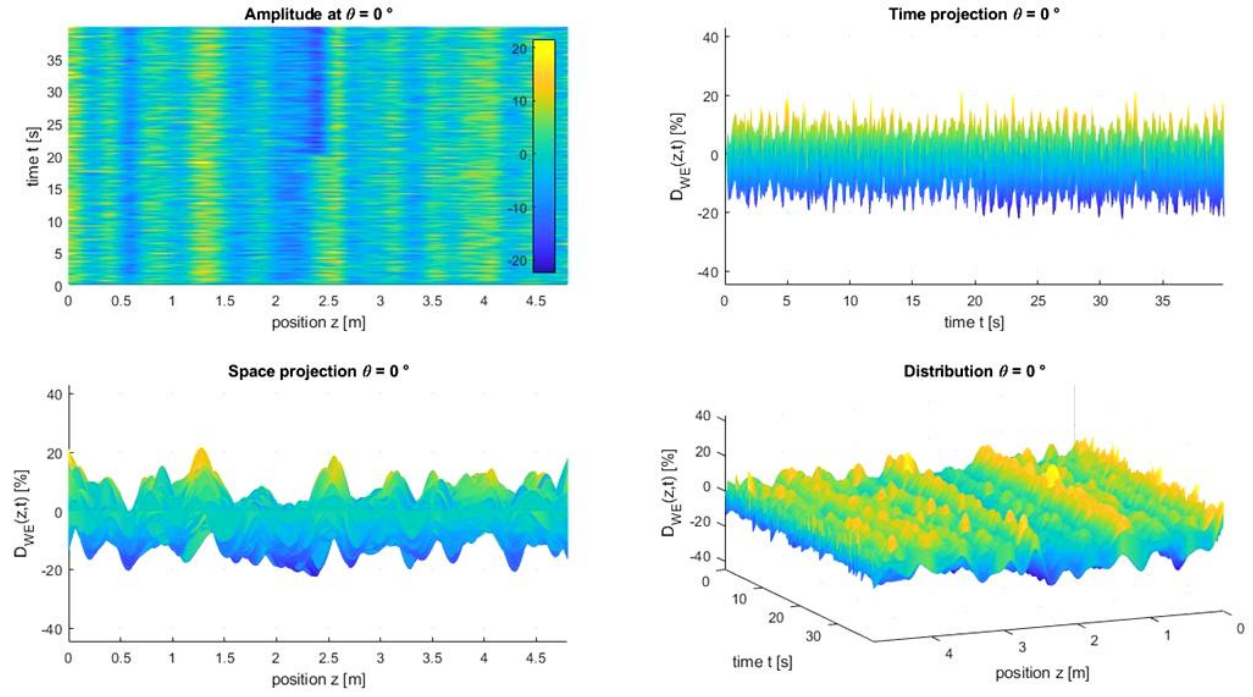

Figure 6.53 Comparison of 0° normalized results (WE) for undamaged- and 50% damaged-element at 45° with 20% white noise

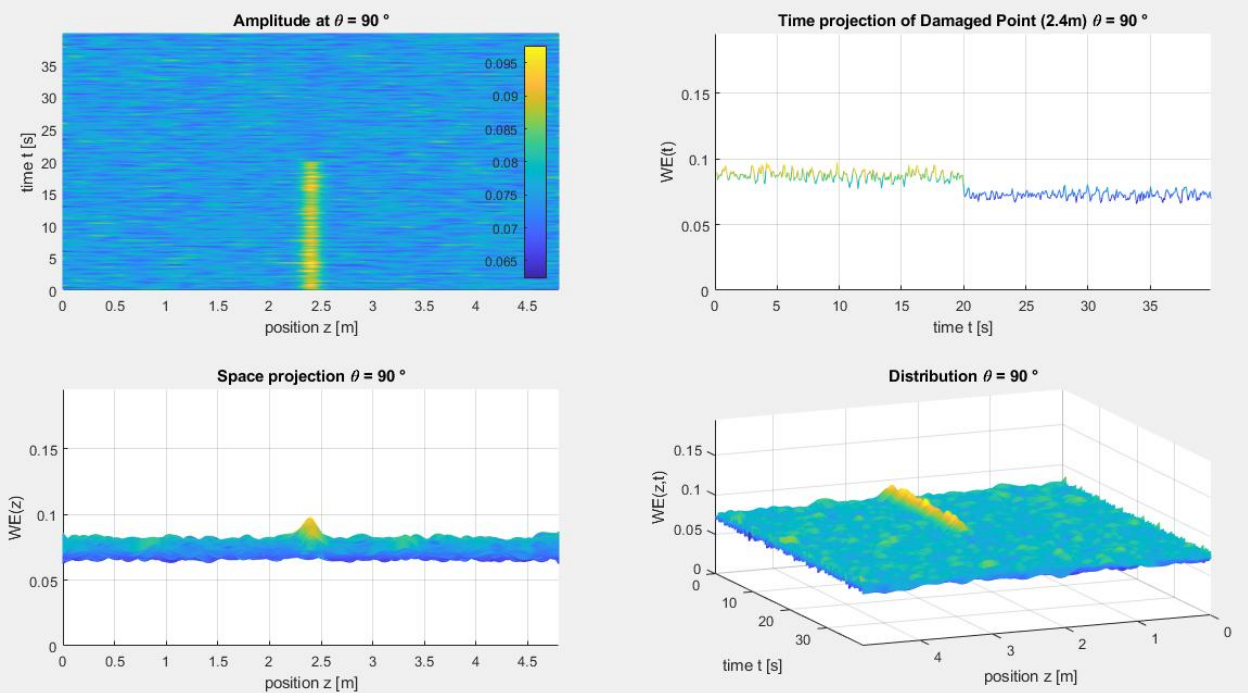

Figure 6.54 Comparison of 90° results (WE) for undamaged- and 50% damaged- single element at 45° with 20% white noise

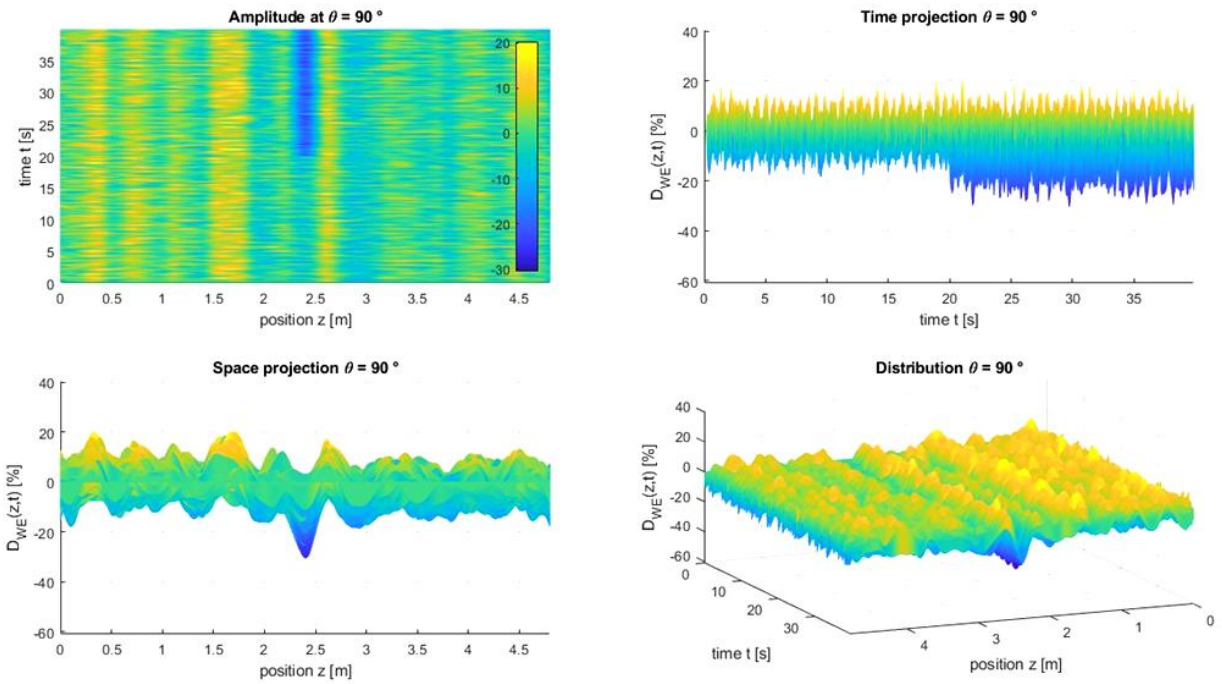

Figure 6.55 Comparison of 90° normalized results (WE) for undamaged- and 50% damaged- element at 45° with 20% white noise

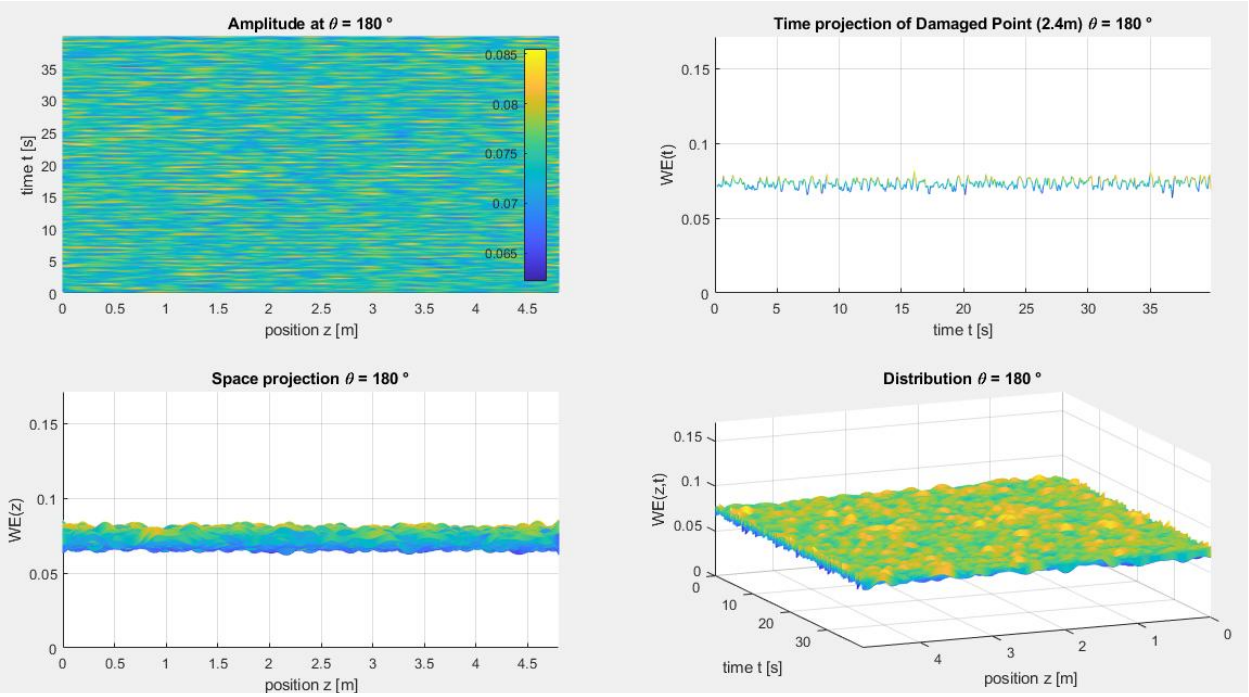

Figure 6.56 Comparison of 180° results (WE) for undamaged- and 50% damaged- single element at 45° with 20% white noise

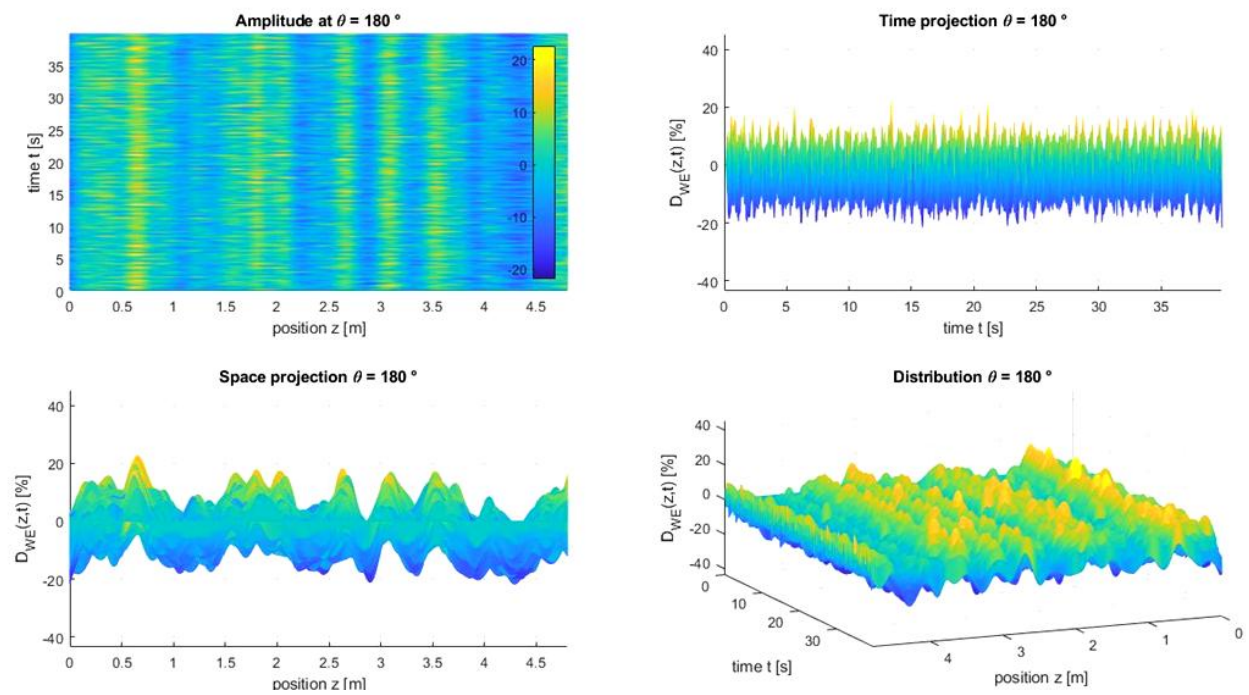

Figure 6.57 Comparison of 180° normalized results (WE) for undamaged- and 50% damaged-element at 45° with 20% white noise

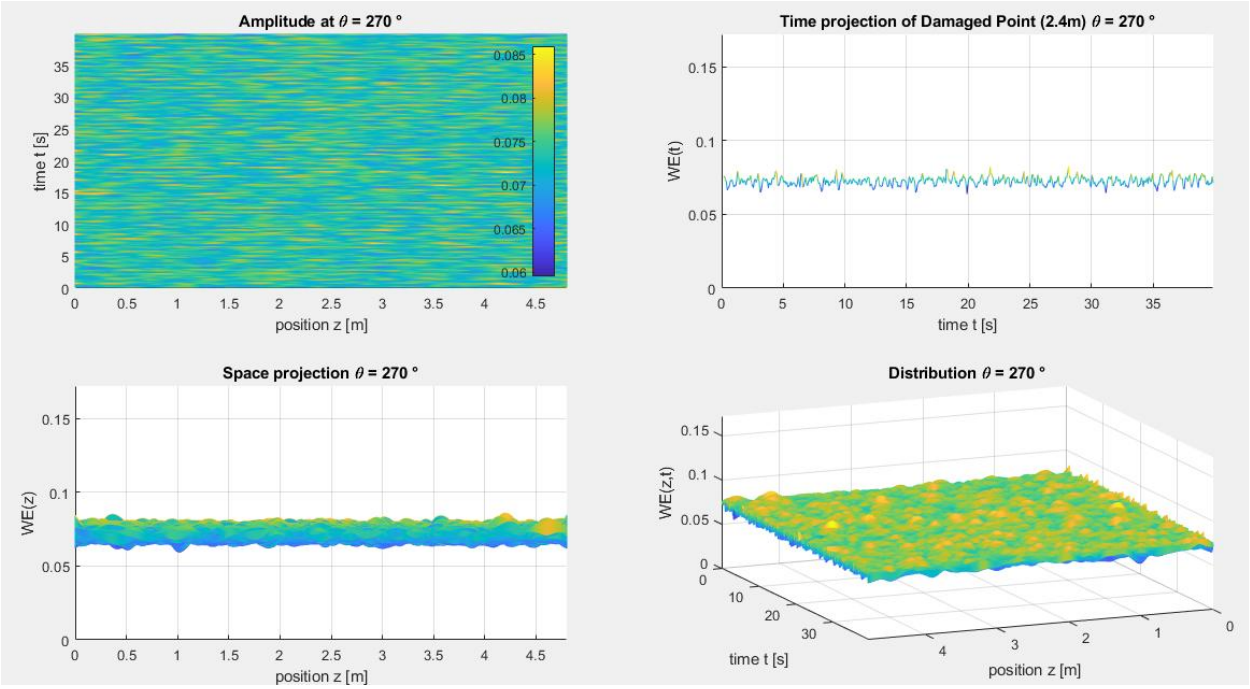

Figure 6.58 Comparison of 270° results (WE) for undamaged- and 50% damaged- single element at 45° with 20% white noise

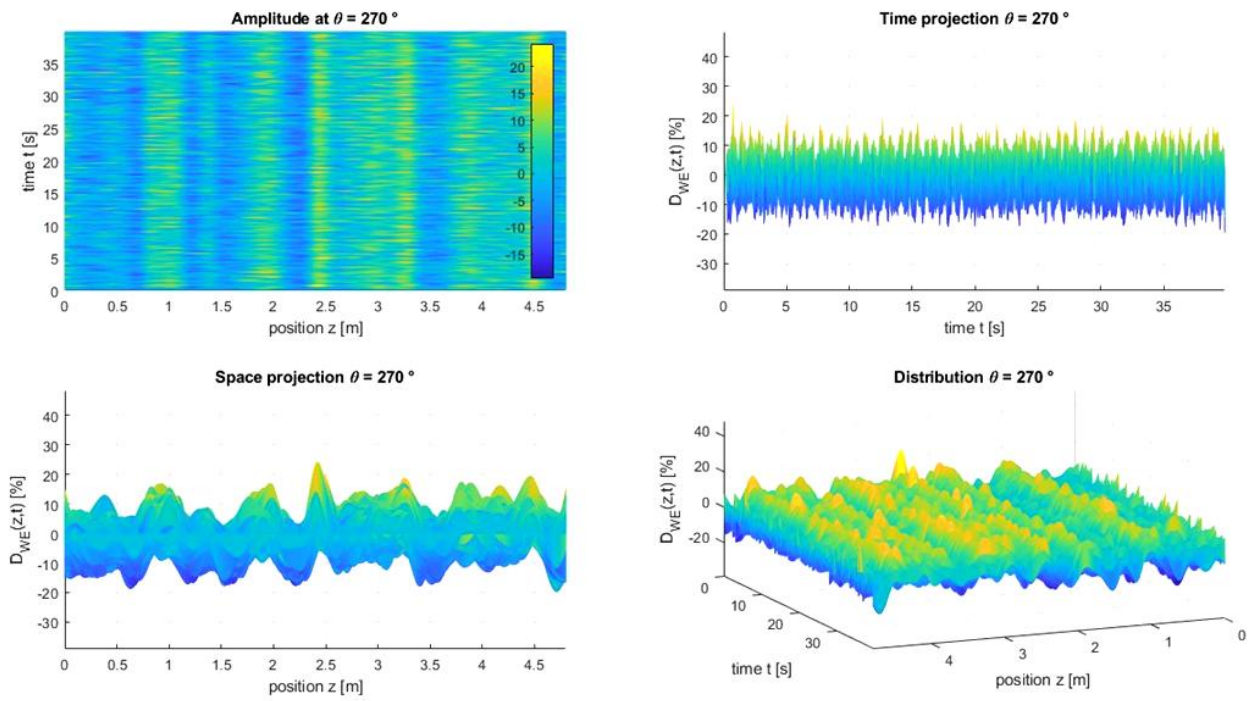

Figure 6.59 Comparison of 270° normalized results (WE) for undamaged- and 50% damaged-element at 45° with 20% white noise

6.4. Evolution of the Damage

At this point, in order to complete the study, the various percentages of damage are concatenated along the time axis in order to show, in an approximate way, how a progressive and rapid evolution of the damage would appear. The results that are considered are those relating to chapter *6.1 Cross Section Completely Damaged*

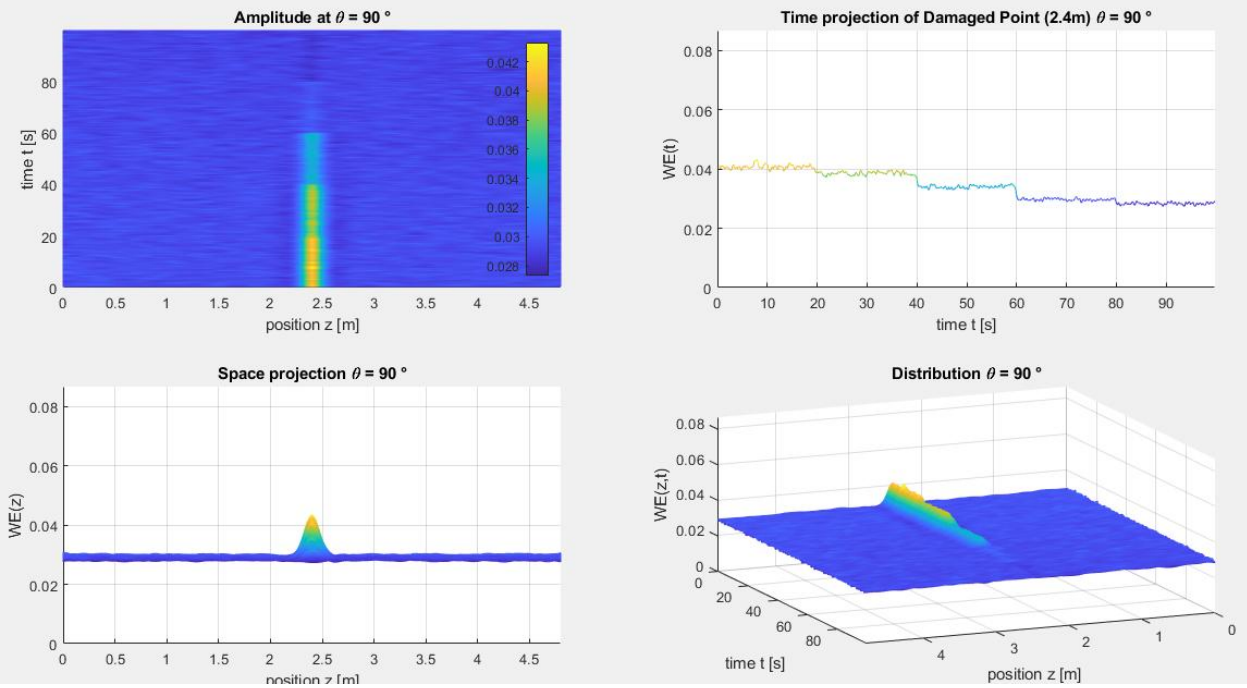

Figure 6.60 Evolution of 90° results (WE) for damaged cross section (from 0% to 70% of damage) with 5% white noise

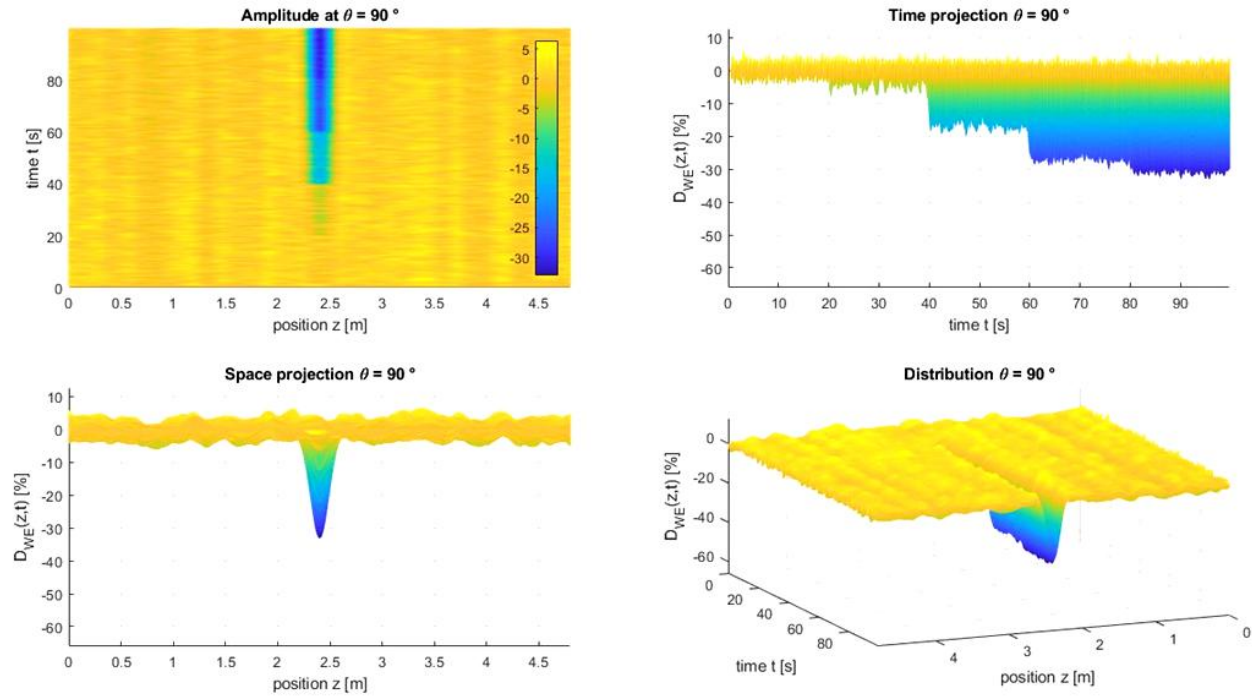

Figure 6.61 Evolution of 90° normalized results (WE) for damaged cross section (from 0% to 70% of damage) with 5% white noise

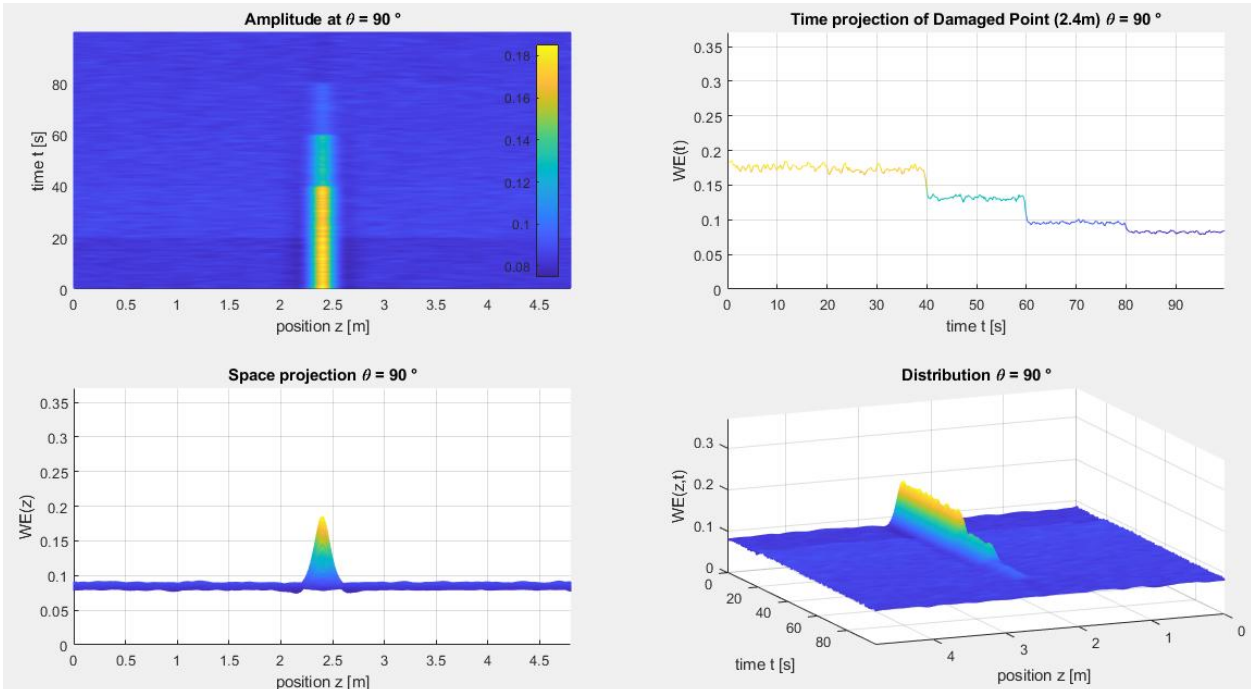

Figure 6.62 Evolution of 90° results (WE) for damaged cross section (from 0% to 70% of damage) with 20% white noise

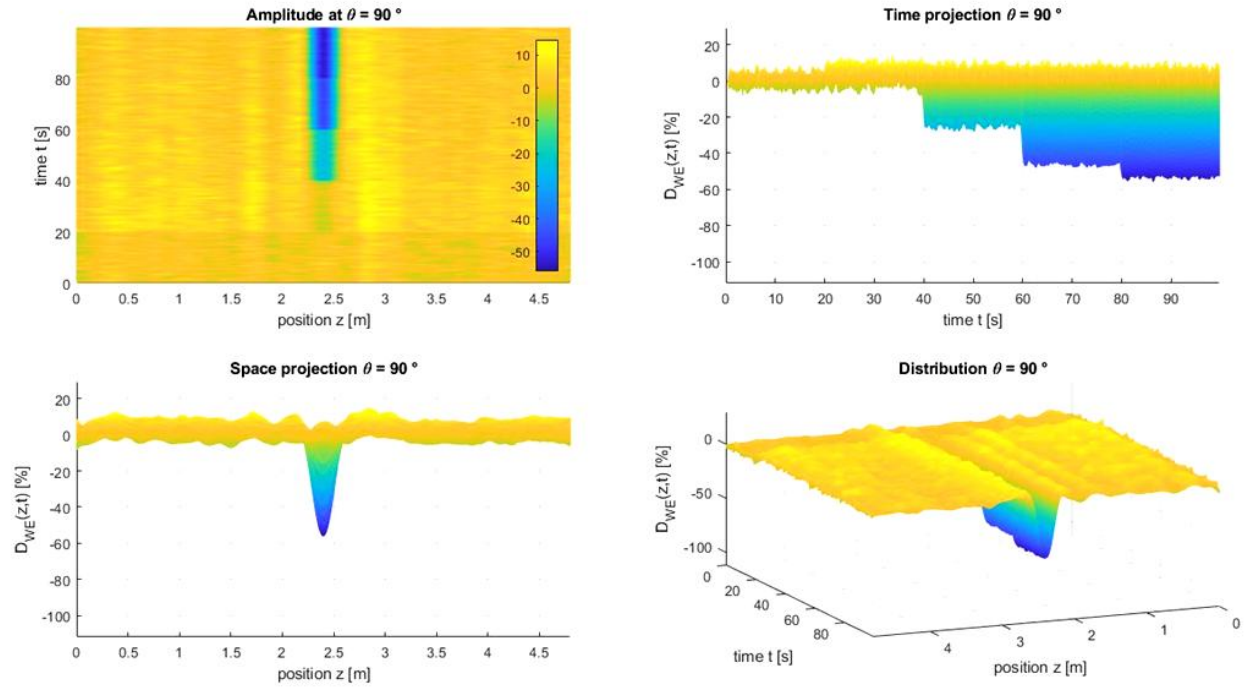

Figure 6.61 Evolution of 90° normalized results (WE) for damaged cross section (from 0% to 70% of damage) with 20% white

From the results shown above, it is evident that the entropy, in correspondence of the stiffness reduction area, progressively decreases as the severity of the damage increases.

7. Discussion

At this point the results obtained are summarized. For this purpose, reference is made to *Table 7.1; 7.2 and 7.3* which indicates whether the results obtained allow to objectively define a Damage Identification , depending on the damage geometry, severity of the damage and white noise of the signal.

In particular, the table results are highlighted with 3 colours:

- Red: the result does not allow the identification of the damage;
- Yellow: the identification of the damage is not evident enough to be considered uniquely valid;
- Green: the result allows to objectively define the presence and location of the damage.

Cross Section Completely Damaged				
	White Noise [%]			
	5	10	15	20
5% Damage				
20% Damage				
50% Damage				
70% Damage				

Table 7.1 Results summary for Completely Damaged Cross Section.

Single Element Damaged				
	White Noise [%]			
	5	10	15	20
5% Damage				
20% Damage				
50% Damage				
70% Damage				

Table 7.2 Results summary for Damaged Single Element.

Single Element Damaged between two sensors				
	White Noise [%]			
	5	10	15	20
5% Damage				
20% Damage				
50% Damage				
70% Damage				

Table 7.3 Results summary for Damaged Single Element between two sensors.

8. Conclusions

The approach based on the use of Wiener Entropy as damage-sensitive feature for the monitoring of Steel Pipelines seems to be a valid alternative to the common Structural Health Monitoring techniques in the field of civil engineering such as Vibration Based Investigation (never been applied to Pipeline structures) or to those currently used in Pipeline Integrity Management.
In fact, it has been found that the Wiener Entropy identified from strain measures, being highly sensitive to structural condition changes, is able to identify even slight states of degradation inside the Steel Pipes.

In particular, from the analysis conducted on a progressive complexity from the point of view of damage identification, it is found that, in the worst case, it is possible to detect a degradation equal to 50% of the loss of stiffness on reduced extension areas.
Then, this study, the first in-depth on this topic, has shown how a Structural Health Monitoring, based on the use of distributed optical fiber sensors as monitoring tool and the Wiener Entropy as damage-sensitive feature, is able to easily reach the first two levels of the Rytter hierarchy: the damage detection and position are identifiable according to the areas in which the Wiener Entropy tends to vary and, in particular, to decrease in value.

Unfortunately, the work was not able to answer the question concerning the severity of the damage: the percentage variations of entropy value depend not only to the level of degradation reached but also on the position with respect to the sensors, on the geometry of the damaged area and also on the noise of the input signal.
Although these limitations have been noted, it is not excluded that the development of more in-depth studies may also respond to the need to grasp the degree of damage achieved by the Steel Pipes structures.
Other interesting insights regarding this work could concern the effects that the internal pressure of the transported fluids have on the damage identification process.